TECHNISCHE
UNIVERSITÄT
WIEN
Vienna University of Technology

DIPLOMARBEIT

NEW LEAD- TELLURIUM OXO COMPOUNDS: STRUCTURE DETERMINATION AND THERMAL BEHAVIOUR

ausgeführt am Institut für

Chemische Technologien und Analytik

Bereich Strukturchemie

der Technischen Universität Wien

unter der Anleitung von

Ao.Univ.Prof. Dipl.-Chem. Dr.rer.nat. Matthias Weil

durch

CHRISTINE ARTNER

Dr. Ponzaunerstraße 11

2263 Dürnkrut

Wien, am 6. September 2010

Danksagung

Der größte Dank gilt meinem Betreuer Prof. Matthias Weil für die interessante Problemstellung, die große Bereitschaft mit der er mir die Welt der Strukturchemie vertraut machte und das offene Ohr welches er immer für meine Fragen und Probleme hatte.

Ebenso sehr möchte ich Berthold Stöger danken, dafür dass er einen Teil seines großen Wissens und seiner Erfahrung mit mir geteilt hat, sowie der überaus angenehmen Bürogemeinschaft.

Die zahlreichen Versuche wären nicht ohne die große Unterstützung von Matthias Czakler und Miriam Singer möglich gewesen.

Prof. Erich Zobetz danke ich für die Hilfe bei kristallographischen Problemen und Fragestellungen.

Bei Dr. Erich Halwax und Prof. Kurt Mereiter möchte ich mich für die Betreuung der Messgeräte bedanken und für die Hilfe bei der Auswertung der Daten..

Gerhard Wieser danke ich für die fürsorgliche Pflege der zahlreichen Apparaturen und Gerätschaften.

Prof. Frank Kubel danke ich für die Bemühungen um unseren Fachbereich, Angelika Graumann für die hervorragende und rasche Erledigung der administrativen Angelegenheiten und Mariana Pantazi für die Bemühungen das Labor und die Chemikalien in gutem Zustand zu halten.

Allen Kollegen der Strukturchemie möchte ich außerdem für die angenehme und produktive Arbeitsatmosphäre danken.

Bei meinem Kollegen Georg Mühlbauer möchte ich mich für die EDX Analysen bedanken.

Den (ehemaligen) Kollegen der Materialchemie danke ich für die netten Grillabende, und besonders Bernhard Feichtenschlager für die langjährige Freundschaft.

Ein besonderer Dank gilt Matthias Gartler für den persönlichen Beistand und Korrekturlesen der Arbeit.

Weiters möchte ich all meinen Freunden für das Verständnis danken, dass ich sie in letzter Zeit allzu oft vertrösten musste.

Ein großer Dank gilt meinen Eltern für die finanzielle und persönliche Unterstützung, ohne die das ganze Studium nicht möglich gewesen wäre.

Kurzfassung

Verbindungen welche zweiwertiges Blei enthalten, zeigen aufgrund der stereochemischen Aktivität des freien $6s^2$-Elektronenpaars oft interessante elektrochemische Eigenschaften. Einige dieser Verbindungen zählen zur Strukturfamilie der Perowskite, welche ebenfalls für ihr ferroelektrisches und supraleitendes Verhalten bekannt sind. Anwendungen einiger dieser Verbindungen sind weit verbreiten, wie zum Beispiel $Pb(Zr,Ti)O_3$ als keramischer Leiter. Das Te^{6+}- Kation kann durch die Ausbildung eines sehr stabilen Netzwerkes aus $[TeO_6]$- Oktaedern diese Eigenschaften unterstützen. In den 1970ern wurden einiger Blei-Telluroxide mit perowskitähnlicher Struktur auf ihre elektrischen und magnetischen Eigenschaften untersucht.

Das Ziel dieser Arbeit war es, neue Blei-Tellur-Sauerstoffverbindungen zu synthetisieren und die Struktur dieser anschließend mit Einkristallröntgendiffraktion zu untersuchen. Einige weitere - bereits literaturbekannte - Verbindungen wurden, aufgrund zum Teil fragwürdiger Strukturmodelle, neu bestimmt. Unter besonderer Beobachtung stand dabei das freie Elektronenpaar des Pb^{2+}- Kations und der Einfluss, welchen es auf die untersuchten Strukturen besitzt, unter anderem in Anwesenheit weiterer zweiwertiger Kationen.

Der zweite Teil der Arbeit beschäftigt sich mit dem thermischen Verhalten einiger zuvor synthetisierter Verbindungen. Phasenreine mikrokristalline Proben wurden mittels DSC, TG und temperaturabhängiger XRPD gemessen. XRPD bei Raumtemperatur wurde als Standardanalysemethode für alle Proben verwendet. Einige wenige kristalline Proben wurden außerdem mittels EDX untersucht.

Zur theoretischen Untersuchung der zuvor ermittelten Strukturen wurde das Bindungs-Valenz Modell angewendet. Für die perowskitähnlichen Strukturen wurden des Weiteren die Oktaederverkippungen berechnet.

Es war möglich, sechs neue Verbindungen zu synthetisieren und die Struktur dieser zu bestimmen. Das war einerseits die Pb-reiche ternäre Verbindung Pb_5TeO_8, die beiden quaternären Verbindungen Pb_6CdTeO_{10} und $Pb_6Co_9Te_5O_{30}$, sowie die zwei in einer verzerrten Doppelperowskitstruktur kristallisierenden Verbindungen Pb_2CaTeO_6 und Pb_2CdTeO_6. Die Struktur von $PbAl_8Ca_2O_{15}$ wird ebenfalls beschrieben, diese Verbindung fiel als Nebenprodukt bei der Synthese in Korrundtiegeln an.

Die Struktur von Pb_2TeO_5 wurde neu bestimmt und ergab eine andere Raumgruppe als in der Literatur beschrieben wurde. Dasselbe gilt für Pb_2CoTeO_6 und Pb_2MnTeO_6, welche beide in der unverzerrten Doppelperowskitstruktur kristallisieren und nicht, wie behauptet, in einer tetragonalen verzerrten Doppelperowskitstruktur, beziehungsweise der einfachen Perowskitstruktur.

Vier weitere Verbindungen konnten synthetisiert werden, wobei aufgrund einiger Unstimmigkeiten nur vorläufige Strukturmodelle beschrieben werden können . Diese sind die Chiolithähnliche Struktur von $PbCa_4Te_3O_{14}$, eine neue kupferhaltige Verbindung $PbCuTeO_5$, welche deutliche Jahn-Teller Verzerrung der Cu-O Koordinationspolyeder zeigt. Des Weiteren wird die Struktur von $Pb_{22}Te_7AlO_{44.5}$ beschrieben, sowie einige analoge Al-freie Strukturen dieser Verbindung, beziehungsweise Verbindungen in denen Al durch ein anderes zweiwertiges Kation ersetzt wurde.

Die Stereoaktivität des Pb^{2+} $6s^2$ Elektronenpaares machte sich bei fast allen untersuchten Strukturen bemerkbar, führte allerdings nur in einem Fall zu einer nicht-zentrosymmetrischen Struktur (Pb_6CdTeO_{10}). Für Pb^{2+} wurden Koordinationszahlen zwischen 4 und 12 ermittelt, im Gegensatz zum Te^{6+} Kation, welches immer oktaedrische Koordinationspolyeder mit Sauerstoff ausbildet. Die Koordinationspolyeder der anderen zweiwertigen Kationen waren zumeist stark verzerrt, wobei eine Koordinationszahl von 6 am häufigsten zu finden war.

Die Untersuchung am thermischen Verhalten von Pb_5TeO_8, Pb_6CdTeO_{10} und den beiden

Doppelperowskitstrukturen Pb_2CaTeO_6 und Pb_2CdTeO_6 zeigte eine Zersetzung aller Proben ab etwa 830°C. Die beiden Doppelperowskitverbindungen zeigten außerdem umkehrbare Phasenübergänge bei 235°C und 281°C. Diese Phasenübergänge wurden anschließend mittels Temperaturabhängiger XRPD genauer untersucht, wobei die Hochtemperaturphase beider Verbindungen kubische Metrik zeigte. Pb_6CdTeO_{10} zeigte keine Phasenübergänge im untersuchten Temperaturbereich.

Abstract

Compounds containing Pb^{2+} cations can bear interesting electric properties, due to the stereoactive $6s^2$ electron lone pair. Some of these structures adapt to the perovskite family, which is also known for its ferroelectric and superconducting properties. Applications are widely found, for example for $Pb(Zr,Ti)O_3$ as a ceramic conductor. The Te^{6+} cation can support these properties by building a very stable octahedral coordination sphere with oxygen. In the 1970s some lead/tellurium oxide compounds with a perovskite-related structure were studied concerning their electric and magnetic behaviour.

The aim of this work was to synthesise new lead- tellurium oxo compounds and determine their structure with single-crystal X-ray diffraction. Other already known compounds were reinvestigated due to questionable reported structures. A focus was laid upon the role of the Pb $6s^2$ electron lone pair on its effect on the structures, also in the presence of other divalent cations.

The second part of this work deals with the thermal behaviour of some of the synthesised compounds. Phase-pure microcrystalline samples were measured with DSC, TG and temperature-dependent XRPD. XRPD at room temperature was used as a routine analysis for all samples. Few crystalline samples were also analysed by EDX.

The bond valence model was applied to discuss the final structure results, and octahedral tilt calculations were performed for the perovskite-related structures.

It was possible to synthesise and solve the structures of six new compounds. The ternary Pb-rich compound Pb_5TeO_8, the two quaternary compounds Pb_6CdTeO_{10} and $Pb_6Co_9Te_5O_{30}$, as well as two compounds, Pb_2CaTeO_6 and Pb_2CdTeO_6, crystallising in a distorted double-perovskite structure. The structure of $PbAl_8Ca_2O_{15}$ is also reported, this compound was obtained as a by-product when corundum crucibles were used for solid state synthesis.

The structure of Pb_2TeO_5 was reinvestigated with a different result as described in the literature. The same counts for Pb_2CoTeO_6 and Pb_2MnTeO_6, that are of the undistorted cubic 1:1 B-site ordered double-perovskite structure, in contrast to a tetragonal perovskite structure and simple perovskite structure, respectively, as previously reported. Pb_2TeO_5 crystallises in a different space group than described in literature.

The structures of four more compounds are provided as well, but their final structure models remain preliminary. These are the chiolith-like structure of $PbCa_4Te_3O_{14}$, a new copper-containing compound $PbCuTeO_5$ with serious Jahn-Teller distortion of the Cu-O coordination spheres, the structure of $Pb_{22}Te_7AlO_{44.5}$, as well as some of its derivatives not containing Al and other divalent cations, respectively.

The stereochemical activity of the Pb^{2+} $6s^2$ electron lone pair was observed for almost all structures, but resulted only in one case in a non-centrosymmetric structure (Pb_6CdTeO_{10}). Coordination numbers between 4 and 12 were determined for the Pb^{2+} cation, whereas the Te^{6+} cations always build up regular octahedral coordination spheres. The coordination spheres of the other divalent cations were often seriously distorted, commonly with a coordination number of 6.

The study of the thermal behaviour of Pb_5TeO_8, Pb_6CdTeO_{10} and the two double-perovskite compounds of Pb_2CaTeO_6 and Pb_2CdTeO_6 showed decomposition of all compounds above about 830°C. The two double-perovskite compounds additionally showed reversible phase transitions at 235°C and 281°C, respectively, which are analysed by temperature-dependent XRPD. Both compounds attend a cubic metric at high temperature. Pb_6CdTeO_{10} showed no phase transition in the investigated temperature range.

Contents

Part I

General

Chapter 1

General

1.1 Aim of this work

The aim of this work was to synthesise new oxide compounds containing Pb^{2+} and Te^{6+} cations and determine their crystal structures. This field was then expanded to quaternary structures with an additional divalent cation. A focus was laid on the role of the $6s^2$ lone pair of Pb^{2+} in terms of stereoactivity and formation of non-centrosymmetric structures.

These new compounds were then synthesised as pure phases, to examine their thermal properties, mainly using DSC, TG and non ambient XRPD.

Furthermore, possible errors in literature, described in the introduction, should be cleared, by reinvestigating these compounds.

1.2 Introduction

Compounds containing Pb^{2+} cations often exhibit significant structural distortion due to the stereoactive non-bonding $6s^2$ valence-shell electrons, commonly known as lone pairs. Pb^{2+}-containing compounds have been the subject of numerous investigations which eventually resulted in many applications, for example as sensors and capacitors [1]. However, due to legal requirements, the use of lead and its compounds in industry is restricted or even banned today. Nevertheless, these compounds, mostly derivatives of the perovskite structure family, have still one of the best characteristics with respect to ferroelectricity and piezoelectricity.

Perovskites are one of the most important inorganic structure families, due to their ability to incorporate a wide range of elements in their structures [2]. They are part of numerous research activities as some of them are ferroelectric, superconducting and charge ordering [3–6]. Even colossal magnetoresistance was reported for some manganese containing perovskites [7–9]. Some of these properties were also detected for Pb-containing compounds, a well-known example is $Pb(Zr,Ti)O_3$ [10–12]. This compound is a ferroelectric relaxor and widely used as a ceramic conductor [12,13].

Tellurium in its highest oxidation state $TeVI$ can be ferroelectrically active due to its small size and high charge [14]. In oxide compounds it usually bonds to six oxygen atoms, in an octahedral coordination sphere. In most compounds these octahedra are very rigid and stable.

The synthesis of some lead/ tellurium oxide compounds with a perovskite structure was first described in 1963 by Bayer [15]. He also mentioned that they might be ferroelectric. In the 1970's Politova and others investigated dielectric properties of some of these compounds [16,17]. Most of these were found to be antiferroelectric [18]. They also gave information on the structure

3

type and cell parameters and found that Pb_2MTeO_6 where $M =$ Mg, Co, Mn, Ni, Zn are cubic with a cell parameter $a \approx 8$ Å and $M =$ Ca, Cd have a monoclinic cell.

The synthesis and unit cell determination of Pb_3TeO_6 was also reported by Politova et al [19]. They state that this compound is monoclinic and undergoes a phase transition at 490 K to a ferroelectric state.

A lot of research was performed on Pb_2MgTeO_6 [20, 21], for which two incommensurately modulated phases below 194 K and 142 K respectively were reported [22]. At room temperature is has a cubic structure, but studies were only performed on powder samples, due to a lack of successfully grown single crystals. This compound is an insulator and antiferromagnetic due to a large band gap [23, 24], in contrast to the W analogue Pb_2MgWO_6 which is paraelectric at higher temperatures [25, 26].

Until now, few other crystal structures of compounds containing Pb^{2+} and Te^{6+} were determined. These include the ternary compounds Pb_2TeO_5 [27] and Pb_3TeO_6 [19]. Wedel, Wulff and Müller-Buschbaum reported the structure of the two double-perovskites Pb_2CoTeO_6 and Pb_2MnTeO_6 [28] and [29], as well as other ternary compounds containing Ni, Cu and Fe: $Pb_6Ni_9Te_5O_{30}$ [30], $PbCu_3TeO_7$ [31] and $Pb_3Fe_2Te_2O_{12}$ [28].

Closer study of reports on Pb_2CoTeO_6 and Pb_2MnTeO_6 revealed some inconsistencies, as Pb_2CoTeO_6 was described as tetragonal but has actually cubic metrics and Pb_2MnTeO_6 was reported to crystallise in the simple perovskite structure with occupational disorder of the Mn and Te sites, but the ionic sizes of Mn and Te are not comparable. Question also arose when studying the report on Pb_3TeO_6, as different temperatures on the phase transitions are given.

1.3   Bond valence

The bond valence model describes in a very simply way the nature of ionic bonds, however it was proven to be a very useful concept in inorganic chemistry, especially when describing structures of inorganic compounds.

Theory and applications of the bond valence model were described by I.D. Brown in the monograph *The Chemical Bond in Inorganic Chemistry: The Bond Valence Model* [32]. Here only a very short comprehension of the most important equations and concepts is given. For further reading see Browns book and a review article [33].

1.3.1   Experimental bond valence

One important conclusion is the correlation of the bond length and its bond strength. An approximation of the experimental bond valence S_{ij} can be calculated by equations 1.1 and 1.2.

$$S_{ij} = e^{\frac{R_0 - R_{ij}}{B}} \tag{1.1}$$

$$S_{ij} = \left(\frac{R_{ij}}{R_0}\right)^{-N} \tag{1.2}$$

The unit of S_{ij} is vu (valence unit). R_{ij} is the bond length between the atoms i and j determined from structure analysis. R_0, B and N are parameters that have been calculated for a wide range of ions [34].

1.3.2 Network equations

The sum of the experimental bond valences of one ion is equal to its atomic valence V_i according to equation 1.3.

$$V_i = \sum_j S_{ij} \tag{1.3}$$

In most structures also equation 1.4 is fulfilled.

$$0 = \sum_{loop} S_{ij} \tag{1.4}$$

These two equations are also called the network equations.

1.3.3 Lattice induced strains

Structures that violate the network equations often affect lattice induced strain. This is also a powerful tool to determine errors in a structure. They are indicated by large values of the bond strain index (BSI) in equation 1.5 and the global instability index (GII) in 1.6. A BSI or GII value > 0.05 vu indicate a strained structure, whereas a structure with GII > 0.20 vu would be expected to be unstable.

$$BSI = \langle (S - s)^2 \rangle^{\frac{1}{2}} \tag{1.5}$$

$$GII = \left\langle \left(\sum_j S_{ij} - V_i \right)^2 \right\rangle^{\frac{1}{2}} \tag{1.6}$$

S is the experimental bond valence and s the theoretical bond valence. The angle brackets indicate a mean value over all bonds and atoms, respectively.

1.3.4 Brown's definition of a bond

Although many definitions of bonds are present, Brown also derived one in his book based on the bond valence:

> A bond exists between a cation and an anion if its experimental bond valence is larger than $0.04 \times$ the cation valence.

1.3.5 Effect of lone pairs

Cations with non-bonding valence- shell electrons, such as Pb^{2+} or Sn^{2+}, often induce distortion in structures [35]. This may lead to an irregular coordination sphere of these ions in crystals and is often indicated by a distribution in strong short bonds and weaker long bonds. Alcock [36] refers to those strong bonds as primary bonds and to the weaker ones as secondary bonds.

1.4 Experimental

All experiments and most of the measurements were carried out at the Vienna University of Technology, Institute for Chemical Technologies and Analytics, Department for Structural Chemistry from October 2009 to August 2010.

This section only provides the basic concepts on the preparation of the samples. For specific information on the synthesis of the compounds in detail see the corresponding chapters. All samples have been prepared by conventional solid state synthesis under atmospheric conditions.

1.4.1 Starting materials

All starting materials were purchased and were used without further purification. Starting materials were metal salts, mainly oxides, carbonates and hydroxides. They were weighted in stoichiometric amounts of the designated ratio in the compound. The used scale was a Mettler-Toledo AB 184 - A3.

A list of the used chemicals, as well as the supplier and their quality is given in Tab. 1.1.

Table 1.1: Source and quality of chemicals used

Chemical	Supplier	Quality
$CdCO_3$	Merck	p.a.
$CaCO_3$	Merck	p.a.
CaO	*unknown*	*unknown*
CdO	Fluka	p.a.
CuO	Aldrich	98%
H_6TeO_6	Aldrich	97.5%- 102.5%
$MnCO_3$	Aldrich	> 99.9%
MnO	*unknown*	*unknown*
$PbCO_3$	*unknown*	*unknown*
$2PbCO_3 \cdot Pb(OH)_2$	*unknown*	*unknown*
PbO	Merck	p.a.
TeO_2	Sigma- Aldrich	> 99%

Preliminary experiments were performed to study differences in tellurium sources. The salts examined were: TeO_2, H_6TeO_6 and TeO_3, gained from annealing of TeO_2 at 400° for 48 hours. No difference on the outcome of the experiments was observed. The oxygen in the air was sufficient to oxidise Te from Te^{IV} to Te^{VI}. TeO_2 was chosen for further experiments, as it was the most convenient to handle and of the highest purity.

A difference was noticed in the use of oxides and carbonates. Carbonates gave a better result, when synthesising phase-pure microcrystalline samples, whereas single crystals were more often grown when oxides were the source.

1.4.2 Crucible materials

Corundum was mainly used as crucible material, for fewer samples also platinum. If not declared otherwise, corundum was used in the experiment. The corundum crucibles were sometimes seriously attacked by the samples, which also led to new compounds containing aluminium, as for example $PbAl_8Ca_2O_{15}$. Still it was the best compromise, as platinum is also attacked by

many metal oxides, but is much more expensive, than corundum. At lower temperatures this effect was less often observed.

1.4.3 Temperature programs

Different temperature programs have been applied and are pictured in Figs. 1.1(a) to 1.1(f).
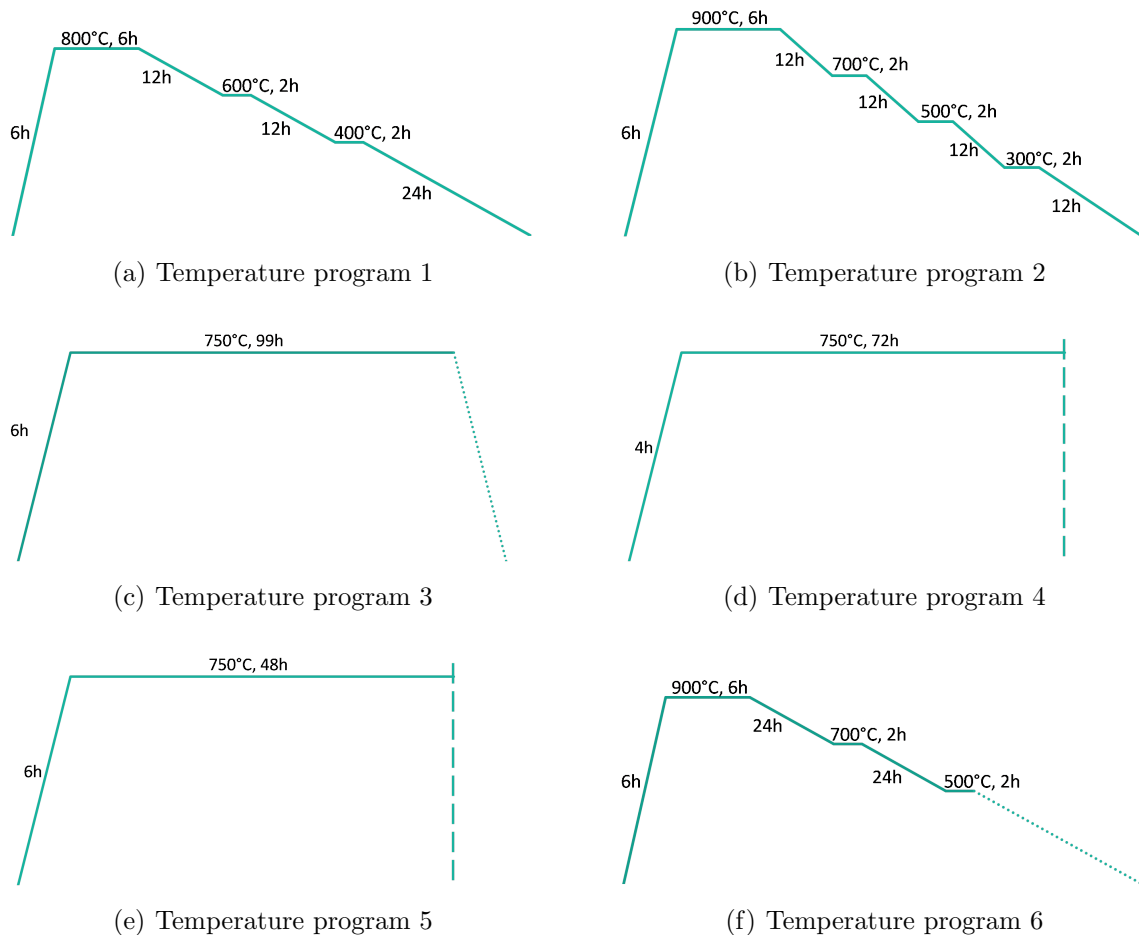
Figure 1.1: Different temperature programs used in the experiments. Dotted lines indicate cooling without a specific program, vertical dashed lines indicate quick cooling by taking the sample out of the hot furnace

Temperature program 3 was mainly used to prepare phase- pure microcrystalline samples, whereas crystals were best obtained with one of the other temperature programs.

A list of used muffle furnaces and their nominal maximum temperatures is given in Tab. 1.2.

1.4.4 Instruments, data collection strategies and analysis software

Single crystal X-ray diffraction

Single crystals were selected under a polarizing microscope and fixed on a glass or silica fibre with a cyanoacrylate based glue.

All measurements were performed under room temperature (RT) using MoKα (λ=0.71073 Å) radiation. Data was collected on a Bruker AXS SMART APEX II four- cir-

Table 1.2: Used furnaces and nominal maximum temperatures

Furnace	$T_{max}[°C]$
Heraeus KM 170	1150
Nabertherm L3/11/B170	1100
Nabertherm L3/11/S27	1100
Nabertherm LHT 04/16	1600
Nabertherm N11	1100

cle diffractometer with κ- geometry. To determine the orientation of the unit cell, a preliminary measurement was performed using the ω- scan technique. The data was collected in 3 runs with 20 images over 6°. With these informations, data collection strategy was then optimised to obtain full completeness and high redundancy. All data was measured with ϕ and ω- scans and 0.5° frame width.

SAINT PLUS software (Bruker Analytical X-ray Instruments Inc. Madison, WI, USA 2007) was used to integrate the frames. Absorption correction was done by using either the multi- scan approach implemented by SADABS [37] or by numerical methods implemented by HABITUS [38]. Crystal structure and refinement was performed using the SHELX software package [39]. Symmetry was then checked with the program PLATON [40]. Structures were drawn using the software ATOMS [41].

X-ray powder diffraction (XRPD)

All samples were measured on a Panalytical X'Pert Pro diffractometer with Bragg- Brentano geometry and CuK$\alpha_{1,2}$ radiation (1.54060 Å, 1.54439 Å). Reflections were detected either with an X'Celerator multi-channel detector with 2.546 ° scan length or a MINI-PROP counting tube. Data was usually collected in the 2θ range 5-67° in 15 minutes with rotation of 4s/U.

Data was evaluated using the X'Pert software package (PANanalytical 2009). Rietveld refinement and phase analysis was performed using the program TOPAS V2.1 and V4.1 (Bruker AXS 1999, 2008).

For the temperature-dependent XRPD measurements additionally an Anton- Paar TTK 450 was used.

Thermal analysis

Simultaneous thermogravimetry (TG)/different scanning calorimetry (DSC) experiments were performed on a NETZSCH STA 449 C Jupiter up to 1000°C in corundum crucibles. DSC measurements were performed on a NETZSCH DSC 200F3 with a heating and cooling rate of 10K/min in closed aluminium crucibles an N_2 flow. TG measurements were performed on a NETZSCH TG 209F3 with a heating rate of 20K/min in corundum crucibles. Data was evaluated with the program Proteus Analysis Version 4.8.5 (NETZSCH Gerätebau GmbH 1999-2008).

EDX

Energy-dispersive X-ray spectroscopy was performed on an FEI Quanta 200 with a tungsten filament and 20 kV accelerating voltage. Data was evaluated with the software program GENESIS spectrum (EDAX Inc.).

Part II

Structures of ternary compounds

Chapter 2

Pb_5TeO_8

2.1 Experimental

2.1.1 Preparation

Crystals of Pb_5TeO_8 were found in almost all samples, prepared at temperatures above 800° C. The reason is probably a local excess of PbO. Furthermore higher temperatures support the formation of Pb_5TeO_8.

A crystal for single crystal X- ray diffraction was obtained from a sample containing 1.35 g (6.0 mmol) PbO and 0.22 g (1.3 mmol) TeO_3, which were then heated according to the temperature program pictured in Fig. 2.1.

900°C, 1h

99h   700°C, 1h

6h

198h
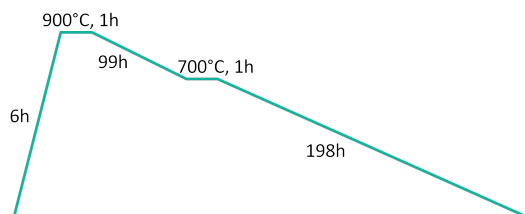
Figure 2.1: Temperature program for growth of single crystals of Pb_5TeO_8

Pure phase of the title compound was obtained by heating a well-ground and pressed mixture of 2.104 g (9.4 mmol) PbO and 0.289 g (1.8 mmol) TeO_2 according to temperature program 3 in Fig. 1.1(c).

The thermal behaviour of the compound is described in chapter 14.

2.1.2 Data collection and refinement

Data were collected based on a monoclinic cell in standard setting, with ω and ϕ scans in 9 runs. The data was then integrated and solved in space group $P2_1/c$. Parameters of the data collection and the refinement, as well as the crystal data are listed in Tab. C.1 in the appendix.

2.2 Structure

2.2.1 Structure solution

Pb_5TeO_8 is monoclinic, space group $P2_1/n$, with a monoclinic angle of $\beta = 91.0400(10)°$ and cell parameters $a = 7.4426(2)$ Å, $b = 12.0107(3)$ Å and $c = 10.6567(2)$ Å. The volume of the unit cell is $V = 952.45(4)$ Å^3. The atom positions are given in Tab. 2.1, selected bond lengths and angles in Tab. 2.2.

Table 2.1: List of atom positions and Wyckoff positions in Pb_5TeO_8

Atom	Wyckoff	x	y	z	U_{eq}
Pb1	4(e)	0.61455(2)	0.108600(16)	0.400167(16)	0.01069(4)
Pb2	4(e)	0.86784(2)	0.121498(16)	0.043767(17)	0.01283(4)
Pb3	4(e)	0.10405(2)	0.120319(18)	0.378868(18)	0.01602(4)
Pb4	4(e)	0.36642(2)	0.154081(17)	0.080554(17)	0.01252(4)
Pb5	4(e)	0.83160(2)	0.870840(16)	0.244852(17)	0.01320(4)
Te1	4(e)	0.64658(4)	0.11351(3)	0.71833(3)	0.00789(5)
O1	4(e)	0.6111(4)	0.2680(3)	0.6744(3)	0.0142(7)
O2	4(e)	0.4471(4)	0.0751(3)	0.6016(3)	0.0112(6)
O3	4(e)	0.6850(5)	0.9547(3)	0.7472(3)	0.0174(7)
O4	4(e)	0.1433(4)	0.0755(3)	0.9712(3)	0.0117(6)
O5	4(e)	0.8656(4)	0.0498(3)	0.2837(3)	0.0159(7)
O6	4(e)	0.8056(4)	0.0922(3)	0.5744(3)	0.0152(7)
O7	4(e)	0.8451(4)	0.1523(4)	0.8219(3)	0.0191(8)
O8	4(e)	0.4783(5)	0.1185(3)	0.8490(3)	0.0199(8)

2.2.2 Description of the structure

The structure is basically build up by layers of interconnecting Pb-O chains and [TeO6]-octahedra, perpendicular to [010].

The Te atom is coordinated to six oxygen atoms in form of a regular octahedron with bond lengths between 1.887 Å and 1.974 Å, which are regularly distributed in the layers. All Pb atoms are coordinated to five oxygen atoms, with bond lengths varying between 2.198 Å and 2.743 Å. There are also some long range Pb - O bonds present, with bond lengths above 3 Å (Tab. 2.2).

In the layers, pictured in 2.2(a), Pb-O chains are expanded in direction [101]. Here pairs of PbO build up a zig-zag double chains, along [010]. The PbO pairs are arranged alternately, in a way that Pb or O is surrounded only by its corresponding counter-ion. These double chains can be recognised from Litharge, the red low temperature modification of PbO [42], although in Pb_5TeO_8 the PbO-coordination spheres are more distorted, where the bond lengths of Pb-O in the chains vary between 2.198 Å and 2.743 Å. These chains are connected through the [TeO$_6$]-octahedra and neighbouring lead atoms, where one oxygen of the [TeO$_6$] octahedron is part of the PbO chains.

The layers are connected by the [TeO$_6$]-octahedra and some long range Pb-O bonds. One oxygen atom of the [TeO$_6$]-octahedron is not part of the layers and is positioned in-between the layers at O1. The bond lengths of those oxygen atoms to the Pb atoms vary between 2.357 Å and 2.624 Å. Since the layers are only connected by [TeO$_6$]-octahedra and secondary

(a) Layer of interconnecting Pb-O chains with [TeO$_6$] octahedra at y = 0.5

(b) Projection on plane (100)
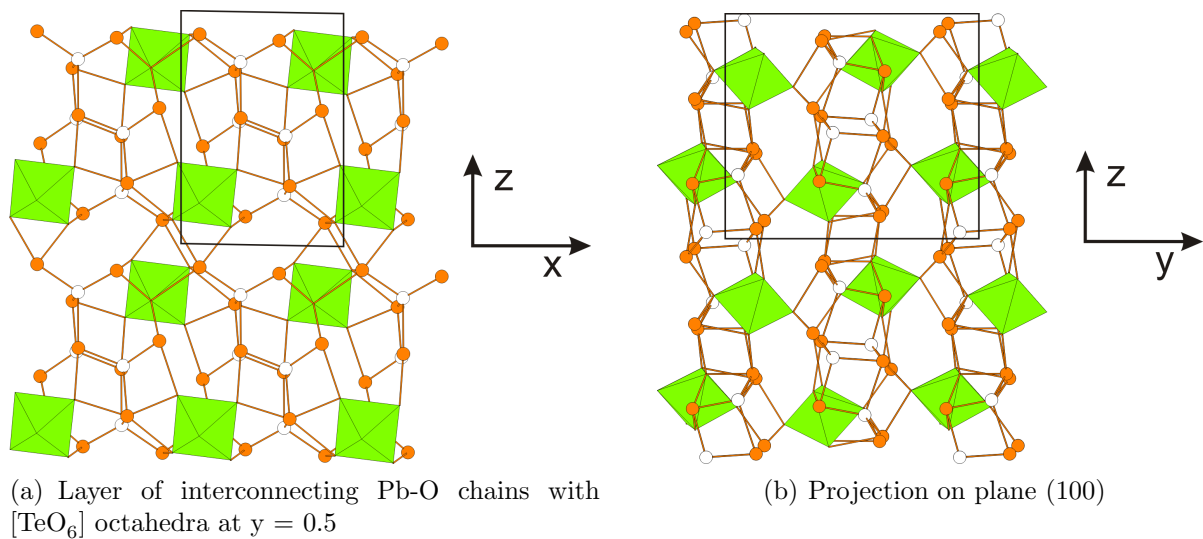
Figure 2.2: Structure of Pb$_5$TeO$_8$. Pb atoms are displayed as orange spheres, [TeO$_6$]-units as green octahedra and oxygen atoms are shown as white spheres. Only Pb-O bonds below 3 Å are displayed.

Table 2.2: Selected bond lengths [Å] and angles [°] in Pb$_5$TeO$_8$

Pb1 - O	2.253	2.326	2.370	2.534	2.809
	3.493	3.592	3.861	3.874	3.962
Pb2 - O	2.272	2.373	2.397	2.624	2.699
	3.535	3.741	3.962		
Pb3 - O	2.198	2.271	2.561	2.684	
	3.092	3.287	3.329	3.497	3.933
Pb4 - O	2.222	2.291	2.357	2.653	
	3.081	3.473	3.548		
Pb5 - O	2.202	2.401	2.501	2.536	2.740
	3.318	3.805			

Te - O1	1.930	Te - O6	1.971
Te - O2	1.974	Te - O7	1.887
Te - O3	1.953	Te - O8	1.891

	cis-oxygen		trans-oxygen
O - Te- O	84.69 - 94.80	O - Te- O	172.96 - 176.72

Pb- O bonds, the Pb atoms facing free space on one side. It is likely that the lone pair of Pb is located in this space.

Chapter 3

Pb_2TeO_5

This structure was already solved by Wedel et al [27], but during some experiments this compound was obtained and its crystal structure redetermined, with a different result.

3.1 Experimental

3.1.1 Preparation

Single crystals of Pb_2TeO_5 were synthesised by pressing a well-ground mixture of 0.893 g (4.0 mmol) PbO and 0.319 g (2 mmol) TeO_2 into a pellet and heating it according to temperature program 1 in Fig. 1.1(a). The sample had a grey-yellowish colour, containing few small crystals. A yellowish plate was selected for single crystal x-ray diffraction.

3.1.2 Data collection and refinement

Unit cell determination gave a monoclinic cell, although the data collection program was optimized for point group $\bar{1}$. Reflections were measured in 10 runs with ϕ and ω scans, from $\Theta = 3.75 - 45.04°$. Therefore a good resolution was achieved. 11937 reflections have been recorded, of which 11504 fulfilled the criterion of $I > 2\sigma(I)$.

The structure could be solved in space group $C2/c$, but the R values were still unsatisfactory. After a numerical absorption correction with the program HABITUS they became much better.

Wedel et al. have refined the structure of Pb2TeO5 in space group Cc [27], but according to their data, a refinement in space group $C2/c$ was not successful. Based on the reflections conditions (h+k = 2n for hkl; h,l = 2n for h0l and k = 2n for 0k0) a distinction between space groups $C2/c$ and Cc is not possible. A detailed analysis of the atomic coordinates in Wedels report revealed a pair-wise relation of atoms implying an inversion symmetry, leading to $C2/c$ as the right space group.

More parameters of the data collection and the refinement, as well as the crystal data are given in Tab. C.2 in the appendix.

3.2 Structure

3.2.1 Structure solution

The compound crystallises in a monoclinic cell with cell parameters $a = 13.0853(6)$ Å, $b = 5.7071(3)$ Å and $c = 7.5225(3)$ Å. The monoclinic angle is $\beta = 123.772(2)°$ and the volume

Table 3.1: List of atom positions and Wyckoff positions in Pb_2TeO_5

Atom	Wyckoff	x	y	z	U_{eq}
Pb1	8(f)	0.839174(13)	0.494955(16)	0.497828(19)	0.01182(6)
Te1	4(a)	0	0	$\frac{1}{2}$	0.00613(6)
O1	4(e)	0	0.1251(4)	$\frac{1}{4}$	0.0121(5)
O2	8(f)	0.16401(19)	0.8950(4)	0.6284(3)	0.0134(4)
O3	8(f)	0.0579(2)	0.2980(3)	0.6309(3)	0.0130(4)

$V = 4.6698(4)$ Å^3. Because of reasons mentioned before, the space group is $C2/c$, in contrast to the original paper [27].

3.2.2   Description of the structure

The Te atom is in an almost regular octahedral coordination with bond length ranging from 1.899 Å and 2.012 Å. These octahedra are connected via corner-sharing $\frac{1}{\infty}[TeO_{4/1}O_{2/2}]$-chains along [001], as pictured in Fig. 3.1(a). All O-Te-O angles of trans-oxygen atoms in the octahedra are 180°, but the Te-O1-Te angle is only 138.42°. This is because the $[TeO_6]$-octahedra are tilted from the c axis in direction [010] (Fig. 3.1(b)). Tilting occurs also along [100]. Every octahedron has the same tilt angle in direction [100] and [001], but in opposite sense to the adjacent.

Table 3.2: Selected bond lengths [Å] and angles [°] in Pb_2TeO_5

Pb - O1	2.879	3.8113	4.014	4.089	4.137
Pb - O2	2.358	2.523	3.019	3.605	3.658
Pb - O3	2.367	2.588	2.696	3.559	

Te - O1	1.914	(2x)
Te - O2	1.899	(2x)
Te - O3	2.012	(2x)

	cis-oxygen		trans-oxygen	
Ox - Te- Oy	87.7 - 92.3		Ox - Te- Ox	180.0
		Te - O1 - Te	138.4	

The $\frac{1}{\infty}[TeO_{4/1}O_{2/2}]$ chains are connected through Pb atoms and are distributed regularly in the space between chains. Every Pb atom is equispaced surrounded by three chains (Fig. 3.1(c)).

The lead atoms form seven primary bonds to oxygen and four secondary bonds. Values of the bond lengths vary between 2.358 Å and 3.019 Å for the primary bonds, and from 3.559Å to 3.904 Å for the secondary bonds (Tab. 3.2). All primary bonded oxygen atoms are arranged in a hemisphere around the Pb atoms facing the $\frac{1}{\infty}[TeO_5]$-chains. It is likely that the lone pair of the Pb atom is located in the other hemisphere.

(a) Projection on (010)

(b) Projection on (100)

(c) Projection on (001)
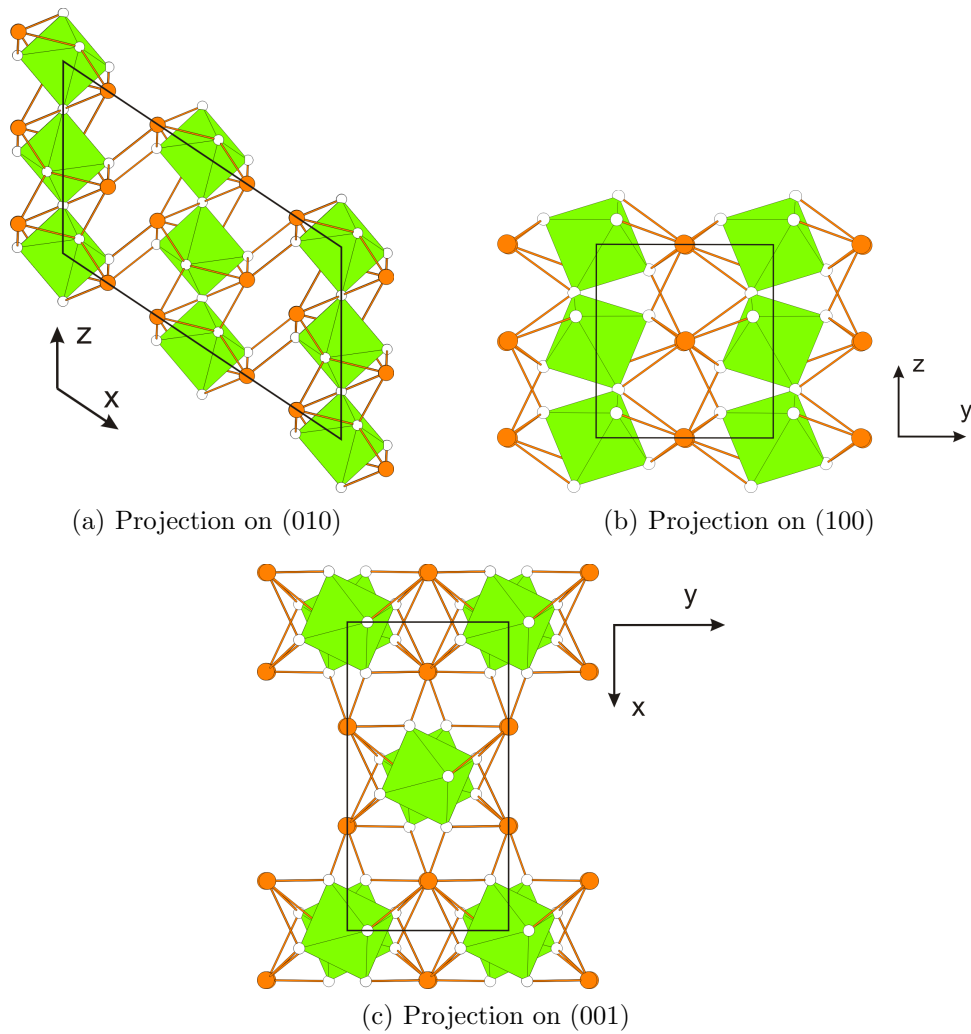
Figure 3.1: Structure of Pb_2TeO_5 projected on different planes. $[TeO_6]$-units are displayed as green octahedra, Pb as orange spheres and oxygen as white spheres. Pb-O bonds below 3 Å are drawn.

Part III

Perovskite structures

Chapter 4

General

4.1 Introduction

This chapter deals with compounds adopting the perovskite structure. A detailed description of two new double-perovskite compounds Pb_2CdTeO_6 and Pb_2CaTeO_6 is given. Pb_2CoTeO_6 and Pb_2MnTeO_6 have been reinvestigated. All these compounds were synthesised previously by Bayer [15] and Politova, who also listed cell parameters [16].

4.2 Perovskite and double-perovskite structure

Many structures can be derived from the well-known perovskite structure with general formula ABX_3, which is displayed in Fig. 4.1(a). Here cation B is coordinated to six anions X and build up a regular network of corner-sharing octahedra. The voids are occupied by cation A and are in a 12-coordination by X, resulting in a cuboctahedral coordination sphere. Compounds with ideal perovskite structure crystallise in space group $Pm\bar{3}m$.

(a) Perovskite structure   (b) Double-perovskite structure
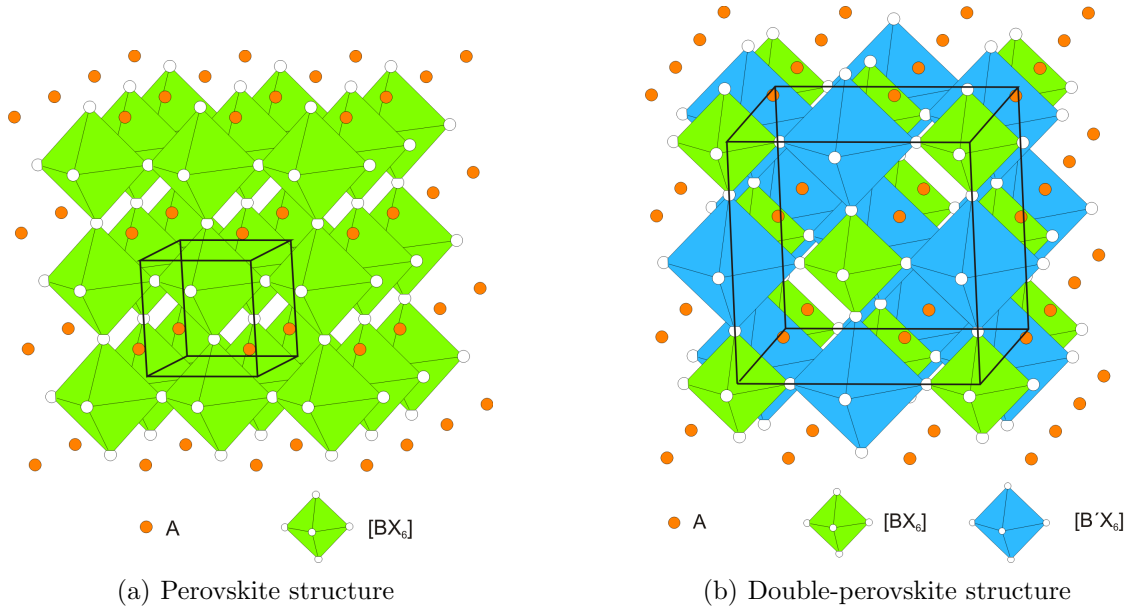
Figure 4.1: Perovskite and double-perovskite structure

Although many elements can adopt the perovskite structure, there is a limitation in combining these due to their charge. For monovalent anions like H and halides, the A-site cation is also monovalent like alkali metals or methyl ammonium, whereas divalent cations like alkaline earth metals, Ni or Cu occupy the B-site. A greater variation is given for oxide perovskites. Possible combinations of $A + B$ charge are $(3^+ + 3^+)$, $(2^+ + 4^+)$, $(1^+ + 5^+)$ and $(0 + 6^+)$.

If cations on one or both sites are substituted by combinations of cations, ordered perovskites can be obtained. One-site ordered perovskites are usually called double perovskites. Ordering can occur in different ratios on the two sites. For the B-site B:B' ratios of 1:1 and 1:2 are the most common ones, whereas a ratio of 1:3 is relatively rare. Not so on the A-site, where compounds of all cation ratios are known. In complex or quadruple perovskites both cation sites can be ordered. [43].

In the 1:1 B-site cation-ordered perovskite structure with general formula $A_2BB'X_6$ half of the cation B is substituted by another cation B'. A limitation on the combination is the charge of the ions and their coordination number. In oxide perovskites with divalent cations on the A-site there are four possible combinations of B-site cations: $B^{4+}B^{4+}$, $B^{3+}B^{5+}$, $B^{2+}B^{6+}$ and $B^{1+}B^{7+}$.

The bond length of the cation B' to the anion can be larger or smaller than those of the original cation B, and in some Jahn-Teller distortion of the $[B'X_6]$ octahedra is observed. The two octahedra types can attend a rock-salt or checkerboard ordering, depending on the arrangement of the B-site cations [44].

The structure of an ideal 1:1 B-site cation-ordered perovskite with rock-salt ordering is displayed in Fig. 4.1(b). A compound which crystallises in this structure is the elpasolite mineral with formula K_2NaAlF_6 [45]. Due to the substitution of the cations the original cubic P cell changes to a cubic F-centred cell, along with doubling of all cell parameters (Figs. 4.1(a) and 4.1(b)).

Alterative descriptions of the perovskite structure are found in literature. Here cation A and the anions X build up a cubic close packing. The other cations occupy 1/8 of the octahedral voids.

All structures described here belong to the 1:1 B-site cation-ordered perovskite family, with Pb^{2+} on the A-site and Te^{6+} on one B-site.

4.3 Parameters

There are various parameters given in literature to describe perovskites. A selection of the most important and useful ones is given below.

4.3.1 Tolerance factor

Based on the tolerance relationship developed by Goldschmidt [46] a tolerance factor t can be calculated for every perovskite related structure. A variation of this formula for double perovskites is given in 4.1. With the tolerance factor the expected symmetry may be predicted. For a factor close to unity, the ideal cubic double-perovskite symmetry is expected. Structures with lower or higher tolerance factor are likely to have a lower symmetry.

$$t = \frac{(r_A + r_X)}{\sqrt{2}(\bar{r}_{(B,B')} + r_X)} \tag{4.1}$$

r_A and r_X are the ionic radii according to the general formula $A_2BB'X_6$ and $\bar{r}_{(B,B')}$ is the average ionic radii of B and B'. The values for the ionic radii were taken from Shannon [47].

According to the formula, if the ionic radius of B is 2/3 of A, it is most likely that the ideal perovskite structure is adopted.

4.3.2 Fitness factor

When classifying the assumed structure type Goldschmidt's tolerance factor shows some weakness, therefore Teraoka et al. [48] invented the fitness factor Φ. The formula is given in 4.2, where r_A, r_B and r_O are the ionic radii of the cations A, B and the anion O, respectively. Tab. 4.1 lists the conditions for the structure type, derived from the value of the Fitness factor.

$$\Phi = \frac{\sqrt{2} \cdot r_A}{r_B + r_O} \tag{4.2}$$

Table 4.1: Conditions to estimate the symmetry from the value of the fitness factor

Φ	Symmetry
> 1	cubic
0.93 - 1	tetragonal
0.90 - 0.93	orthorhombic
< 0.90	monoclinic

4.3.3 Volume ratio

To measure the degree of distortion, it is useful to compare the coordination spheres of the A and the B-site cations. For ideal perovskites the ratio $V_A : V_B$ is 5:1.

4.4 Octahedral tilting

In structures where cations are too small or too large for their voids in the structure, they need to compensate this. Often this is achieved by distortion of the coordination spheres or tilting of the octahedra, which can be observed in a large number of non-ideal perovskite structures [49]. Some attempts have been made to describe the octahedral tilt. The most common approach was described by Glazer in 1972. It was later extended to Jahn-Teller distorted perovskites and double perovskites [50, 51].

4.4.1 Glazer Notation

Glazer [52, 53] introduced a notation for quantifying and describing octahedral tilting in perovskite structures. In general, the tilting of the $[BX_6]$ octahedra occurs about the (pseudo)-cubic axes. If the values of the angles from the axes are different, the general notation is *abc*. A positive superscript is used to declare if two octahedra in successive layers have the same sense of tilt, negative ones declare an $anti-phase$ tilt. A 0 superscript is used, if no tilting occurs in this direction. Therefore a notation $a^+a^+a^+$ would imply three equal tilts in the same sense about all axes and $a^0a^0a^0$ would be the notation for the ideal perovskite structure. Glazer found 23 independent tilt systems for undistorted octahedra. As tilting of the octahedra lead to a symmetry reduction, a space group can be assigned to every tilt system. Howard and Strokes later made some corrections of the original assignment of Glazer [44].

To calculate the tilt angles of the octahedra it is often necessary to transform the cell first into the (pseudo)cubic perovskite cell and then into a Cartesian coordinate system. This can be performed by using the equations given in Chapter 1. A derivation for calculating tilt angles in perovskite structures is given in the appendix.

For more information on the theory of perovskites see Mitchells book *Perovskites: Modern and Ancient* [2].

Chapter 5

Pb_2CdTeO_6

5.1 Experimental

5.1.1 Preparation

Single crystals of Pb_2CdTeO_6 were obtained by finely grinding a mixture of 2.01 g (9.0 mmol) PbO, 0.194 g (1.5 mmol) CdO and 0.238 g (1.5 mmol) TeO_2 and pressing into a pellet. The pellet was put in a corundum crucible and heated in a first heating step to $800°$ following temperature program 1 in Fig. 1.1(a). The dark yellow powder was regrind, pressed and heated to $900°$ according to temperature program 2 in Fig. 1.1(b). Colourless crystals of nearly isometric shape were isolated from a red powder. A small single crystal was selected for single-crystal structure analysis.

Microcrystalline phase-pure Pb_2CdTeO_6 was synthesized by heating a finely ground and pressed mixture of 2.01 g (9.0 mmol) PbO, 0.287 g (1.7 mmol) $CdCO_3$ and 0.239 g (1.5 mmol) TeO_2 according to temperature program 3 in Fig. 1.1(c). A second and a third annealing step was carried out, under the same conditions as the first one, with regrinding after every step. The strategy used for synthesising crystals was not successful, because beside the desired compound also Pb_5TeO_8 was formed. Furthermore, better results were obtained when using carbonates as starting materials, instead of oxides.

The study of the thermal behaviour is described in chapter 14.

5.1.2 Data collection and refinement

A monoclinic cell was determined for the compound, although data was collected based on a triclinic cell with ω and ϕ scans in 11 runs to obtain a good redundancy. The data was then integrated on a monoclinic cell in the standard setting.

Structure solution in space group $C2/c$ was not successful, therefore it was solved in space group $P1$. It was then converted with the program PLATON into the monoclinic space group. Details of the data collection and refinement are listed in Tab. C.3 in the appendix.

5.2 Structure

5.2.1 Structure solution

The unit cell was determined as monoclinic, with cell parameters $a = 10.0716(3)$ Å, $b = 5.7197(2)$ Å, $c = 10.1577(3)$ Å , $\beta = 107.528(2)°$ and the volume of the unit cell is $V = 557.98(3)$ Å^3. Space group $C2/c$ with Z=4 could be assigned to the structure. The

atom positions are listed in Tab. 5.1. Pb$_2$CdTeO$_6$ crystallises in a subgroup of the ideal double-perovskite K$_2$NaAlF$_6$, space group $Fm\bar{3}m$. The group-subgroup relation of the compound and its aristotype is discussed later in section 9.

A tolerance factor of 0.945 according to equation 4.1 and a fitness factor of 0.801 according to equation 4.2 is in good accordance with the monoclinic structure.
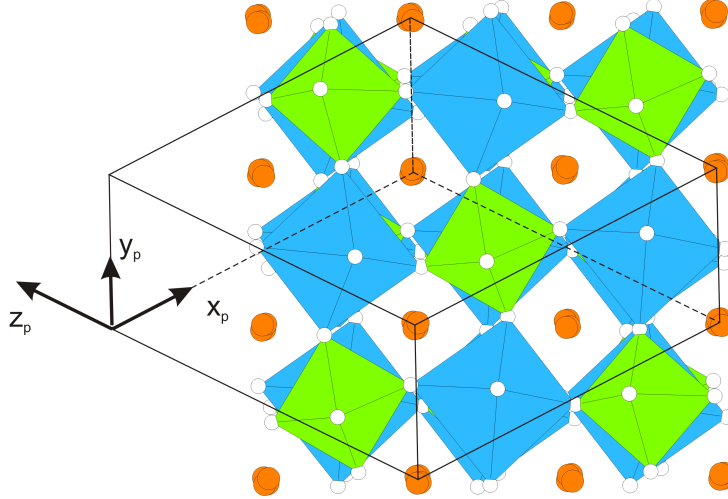
Figure 5.1: Structure of Pb$_2$CdTeO$_6$ in direction a of the pseudo-cubic perovskite cell. Blue displayed are the [CdO$_6$]-octahedra, green the [TeO$_6$]-octahedra. Oxygen atoms are drawn as white spheres and Pb atoms as orange spheres.

Table 5.1: List of atom positions and Wyckoff positions in Pb$_2$CdTeO$_6$

Atom	Wyckoff	x	y	z	U_{eq}
Pb	8(f)	0.1285(10)	0.2691(2)	0.6226(10)	0.01085(4)
Te	4(c)	$\frac{1}{4}$	$\frac{1}{4}$	0	0.00442(5)
Cd	4(e)	0	0.24320(4)	$\frac{1}{4}$	0.00775(5)
O1	8(f)	0.1004(2)	0.2973(4)	0.0798(2)	0.0124(3)
O2	8(f)	0.1631(2)	0.9759(3)	0.8989(2)	0.0134(4)
O3	8(f)	0.3469(2)	0.0494(4)	0.1493(2)	0.0144(4)

5.2.2 Description of the structure

The structure can be derived from the double perovskite structure displayed in Fig. 4.1(b). The tellurium atoms occupy one half of the B-site cation position and are positioned at an inversion centre. They are coordinated to six oxygen atoms and build up almost regular octahedra, with bond length between 1.917 Å and 1.933 Å (Tab. 5.2). The angles O1-Te-O1, O2-Te-O2 and O3-Te-O3, respectively, are 180°, although the angles between cis-oxygen and the central Te atom are not perfectly rectangular and cause a low distortion of the octahedra (Fig. 5.2(a)). The value of these angles range from 87.1° to 92.9 °.

The second B-site cation in octahedral coordination is Cd. It is shifted from the ideal position 0.0168 Å in direction [0$\bar{1}$0]. These octahedra are much more distorted than the [TeO$_6$]-octahedra (Fig. 5.2(b)). The distance between the central Cd atom and the O atoms range

from 2.249 Å to 2.354 Å (Tab. 5.2). The angles between trans-oxygen atoms and the center cadmium atom range from 163.1° to 164.4°. The angles between cis-oxygen atoms and the central cadmium atom differ from the ideal rectangular angle. This leads to a tilting of the $[TeO_6]$ and $[CdO_6]$-octahedra, which is described later in section 5.2.3.

Table 5.2: Bond lengths in [Å] and angles in [°] in Pb_2CdTeO_6

Pb - O1	2.519	2.591	3.270	3.430			
Pb - O2	2.476	2.780	3.197	3.331			
Pb - O3	2.482	2.806	3.108	3.267			
Te - O1	1.933	(2x)	Cd - O1	2.271	(2x)		
Te - O2	1.933	(2x)	Cd - O2	2.249	(2x)		
Te - O3	1.917	(2x)	Cd - O3	2.364	(2x)		

cis-oxygen		trans-oxygen	
O1 - Te- O2	87.07	O1 - Te- O1	180.00
O1 - Te- O3	88.43	O2 - Te- O2	180.00
O2 - Te- O3	88.62	O3 - Te- O3	180.00
O1 - Cd - O2	88.08	O1 - Cd- O1	164.33
O1 - Cd - O3	81.13	O2 - Cd- O3	163.10
O2 - Cd - O2	112.29		
O3 - Cd - O3	83.87		

(a) $[TeO_6]$-octahedron

(b) $[CdO_6]$-octahedron
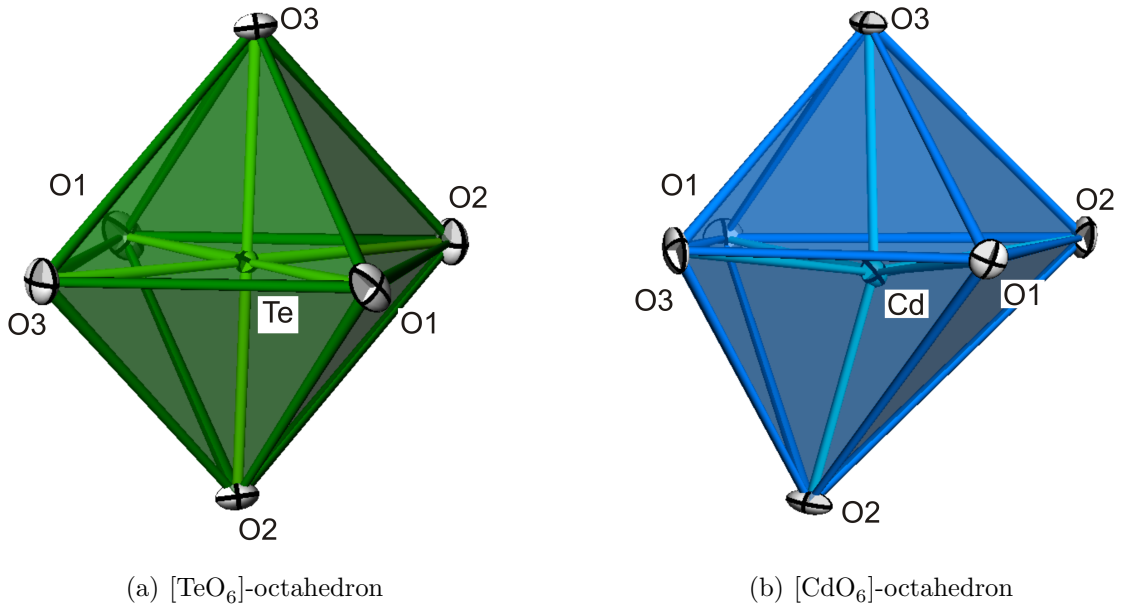
Figure 5.2: Comparison of the octahedral coordination-polyhedra of Te and Cd. The ellipsoids are drawn at 50% of the probability density function.

The lead atoms build up irregular cuboctahedra by oxygen atoms within a [6 + 6] coordination (Fig. 5.3). The primary bonds have a lengths between 2.482 Å and 2.806 Å, whereas

those of the secondary bonding oxygen atoms range between 3.108 Å to 3.430 Å (Tab. 5.2). The closer oxygen atoms are situated in a hemisphere around the central lead atom, the remaining six - but one - atoms can be found in the other hemisphere as displayed in Fig. 5.3. Due to this separation, it is likely that the lone pair of Pb^{2+} is located in this gap.
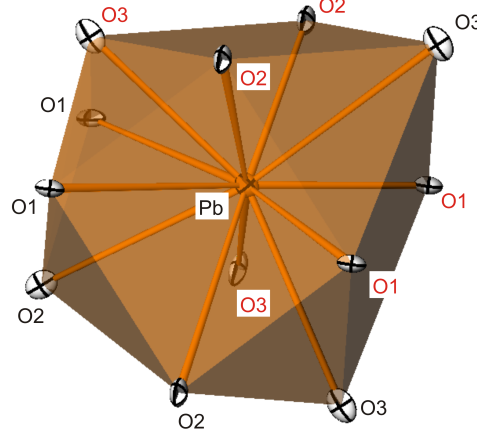
Figure 5.3: Distorted [PbO$_{12}$]-cuboctahedron. Oxygen with Pb-O bond lengths below 3 Å are labelled red. The ellipsoids are drawn at 50% of the probability density function.

The dislocation of the Pb atom from the centre of the polyhedron was reported for other lead containing perovskite structures [1,54,55]. The polarisation of the $6s^2$ lone pair of Pb^{2+} is responsible for this dislocation, beside other factors like the charge of the B-site cations [51].

Double-perovskite cell

Due to its structural relationship to the double perovskite, a pseudo- cubic cell can be assembled for easy comparison. To obtain the dimensions and orientation of the pseudo-cubic cell, a cell transformation is necessary. The cell transformation matrix (5.1) was calculated according to the Bärnighausen tree in Fig. 9.1.

$$P = \begin{pmatrix} \frac{1}{2} & \frac{1}{2} & \frac{1}{2} \\ \frac{1}{2} & \frac{1}{2} & \frac{1}{2} \\ \overline{1} & 0 & 1 \end{pmatrix}, \quad D(P) = 1 \qquad P^{-1} = \begin{pmatrix} \frac{1}{2} & \overline{\frac{1}{2}} & \overline{\frac{1}{2}} \\ 1 & 1 & 0 \\ \frac{1}{2} & \overline{\frac{1}{2}} & \frac{1}{2} \end{pmatrix}, \quad D(P^{-1}) = 1 \qquad (5.1)$$

Formula A.5 and the matrix given above were used to calculate the cell dimensions of the new cell $a = 8.2743$ Å, $b = 8.2743$ Å, $c = 8.1584$ Å and angles $\alpha = 90.37°$, $\beta = 89.63°$, $\gamma = 92.54°$. In Fig. 5.4 the geometric relation between the cubic cell of the elpasolite structure and the monoclinic cell of Pb$_2$CdTeO$_6$ is displayed.
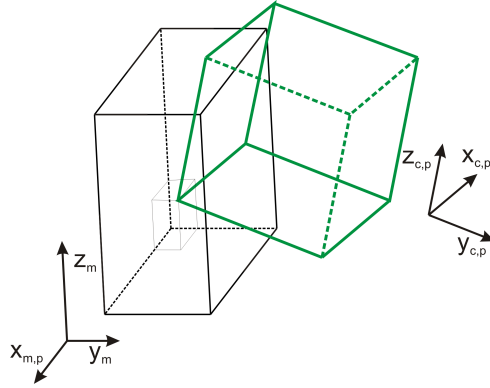
Figure 5.4: Comparison of the monoclinic cell of Pb_2CdTeO_6, space group $C2/c$ and the cubic elpasolite-cell, space group $Fm\overline{3}m$. Index m represents the monoclinic cell and index c the cubic cell. Index p stands for projection of the axis.

5.2.3   Octahedral tilting

As mentioned before the $[TeO_6]$- and $[CdO_6]$-octahedra in Pb_2CdTeO_6 are considerably tilted. They attend a rock-salt ordering according to [56]. The Te atoms alternate with Cd atoms in the layer, as well as from one layer to another (Fig. 5.5).
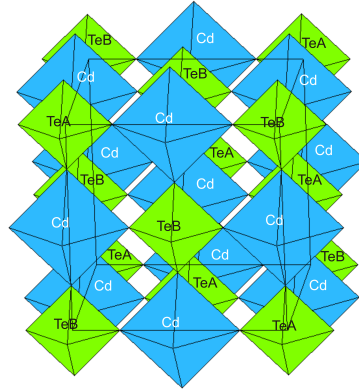
Figure 5.5: Octahedra tilt scheme of Pb_2CdTeO_6. The unit cell refers to the double-perovskite cell

Due to the distortion of the Cd atoms from the centre of the octahedra and the presence of three different octahedra, each tilted differently, too many restrictions have to be made to declare the tilt system with Glazer notation. As the octahedra are not independent, it is not reasonable to give the Glazer notation for the different octahedra exclusively.

Despite the distorted structure, it is possible to calculate the tilt angles. To achieve this, first a transformation into the double-perovskite cell was performed by using equation A.7 with matrix P (5.1). After this, equation A.8 was used to transform it to a Cartesian coordinate system.

The tilt angles are not the same for every $[TeO_6]$ octahedron. There are two different types of $[TeO_6]$-octahedra, but only one type of $[CdO_6]$-octahedra, due to their oxygen environment. The two octahedra types are alternating in every layer and from one layer to another. The scheme is given in picture 5.5.

The tilt angles of the $[TeO_6]$-octahedra were calculated as described in the Appendix. To

obtain the tilt angle in one direction, a mean value of the calculated angles between the bonds and the pseudo-cubic axis is given. Due to the distortion of the [CdO$_6$]-octahedra the values for the individual bond tilts differ greatly from each other, therefore both a mean value and additionally the tilt angles of each single Cd-O bond is given in Tab. 5.4. The shift of the Cd atom from the centre of the octahedron was not taken into account, as the value is very small and therefore negligible.

Table 5.3: Clockwise tilt angle of each different octahedron in Pb$_2$CdTeO$_6$, given in [°].

Tilt along double-perovskite axis	Te A	Te B	Cd
a	13.6	-3.0	-7.2
b	3.3	13.6	-7.4
c	-9.5	7.0	-1.3

Table 5.4: Tilting angles for Cd- O bonds in Pb$_2$CdTeO$_6$, given in [°].

Tilt along double-perovskite axis	Cd -					
	O1a	O1b	O2a	O2b	O3a	O3b
a	-2.1	-13.4	-	-3.0	-	-10.5
b	-13.5	-2.6	-3.0	-	-10.5	-
c	-	-	9.8	-12.4	-5.4	2.9

The [CdO$_6$]-octahedra are no always tilted in the opposite sense as the neighbouring [TeO$_6$]-octahedra. Rigid octahedra have to compensate the clockwise tilt of their neighbouring octahedra by a counter clockwise tilting according to [52]. All Cd-O bonds in one direction are tilted in the same sense, except those in direction c (Tab. 5.4).

5.2.4 Superstructure

The precession images in Fig. 5.6 show distinct strong supercell reflections. In planes with even indices, the strong reflections are extinct due to a centring of the cell. Precession images were derived from the measurement of another crystal than the one for the structure solution.

From this image the transformation matrix for the basic structure is calculated. The matrix is given in 5.2.

$$P = \begin{pmatrix} \frac{1}{2} & 0 & \overline{\frac{1}{8}} \\ 0 & 1 & 0 \\ 0 & 0 & \frac{1}{4} \end{pmatrix}, \quad D(P) = \frac{1}{8} \tag{5.2}$$

With this matrix the dimension of the basis cell were calculated according to formula A.5. A monoclinic cell with the following dimensions was obtained: $a = 5.0358$ Å, $b = 5.7197$ Å, $c = 3.1558$ Å and $\beta = 129.89°$. The volume of the cell with a value of $V = 69.74$ is $\frac{1}{8}$ of the original cell. The determinant of the transformation matrix P 5.2 is as well $\frac{1}{8}$. Therefore the structure Pb$_2$CdTeO$_6$ is an 8-fold superstructure.
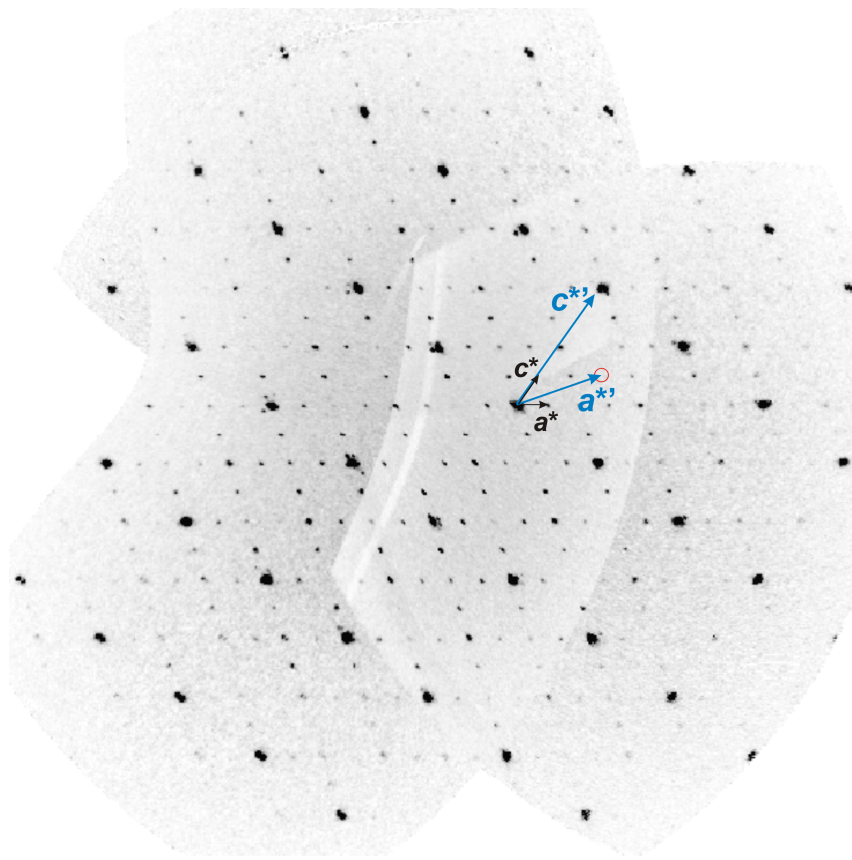
Figure 5.6: Pseudo-precession image of plane $(h\overline{3}l)$ in the monoclinic setting of the Pb_2CdTeO_6 structure. Reciprocal lattice vectors a* and c* of the reduced cell of the superstructure and the basic structure (caption ') are given

Chapter 6

Pb_2CaTeO_6

6.1 Experimental

6.1.1 Preparation

The conditions applied for Pb_2CdTeO_6 were not successful for growing single crystals of Pb_2CaTeO_6.

A well-ground mixture of 0.671 g (3.0 mmol) PbO, 0.083 g (1.5 mmol) CaO and 0.284 g (1.8 mmol) TeO_2 was heated according to temperature program 4 in 1.1(d). Small colourless single crystals of irregular habit were separated from a brick-red powder. During the experiments $PbCa_2Al_8O_{15}$ could be identified as a secondary phase and is described later.

Pure-phase Pb_2CaTeO_6 was obtained by heating a well-ground and pressed mixture of 0.387 g (0.50 mmol) $2\,PbCO_3 \cdot Pb(OH)_2$, 0.075 g (0.75 mmol) $CaCO_3$ and 0.12 g (0.76 mmol) TeO_2 in a platinum crucible, according to temperature program 3 in 1.1(c). After regrinding, a second heating step under the same conditions was carried out.

6.1.2 Data collection and refinement

The crystal was found to have a monoclinic cell with cell parameters very close to those of Pb_2CdTeO_6. The data collection strategy was based on a triclinic cell to obtain all reflections. The crystal was measured with ω and ϕ scans in 8 runs. It was then integrated in a monoclinic cell and then converted to the standard setting. Initial structure solution was not possible in space group $P2_1/c$, hence it was again integrated in the triclinic system. After a successful structure solution in space group $P\bar{1}$, the structure data were checked with PLATON, which suggested a higher symmetry and space group $P2_1/c$. It was then transformed and finally refined in this space group.

Parameters of the data collection and refinement are listed in Tab. C.4 in the appendix.

6.2 Structure

6.2.1 Structure solution

Pb_2CaTeO_6 crystallises in the monoclinic space group $P2_1/c$ Z=4, with cell parameters $a = 10.2293(3)$ Å, $b = 5.7926(2)$ Å and $c = 10.1698(3)$ Å. The monoclinic angle is $\beta = 108.6400(10)°$ and the volume $V = 571.00(3)$ Å^3. The atom positions are given in Tab. 6.1. The relation to its aristotype, the double perovskite is described later in chapter 9.
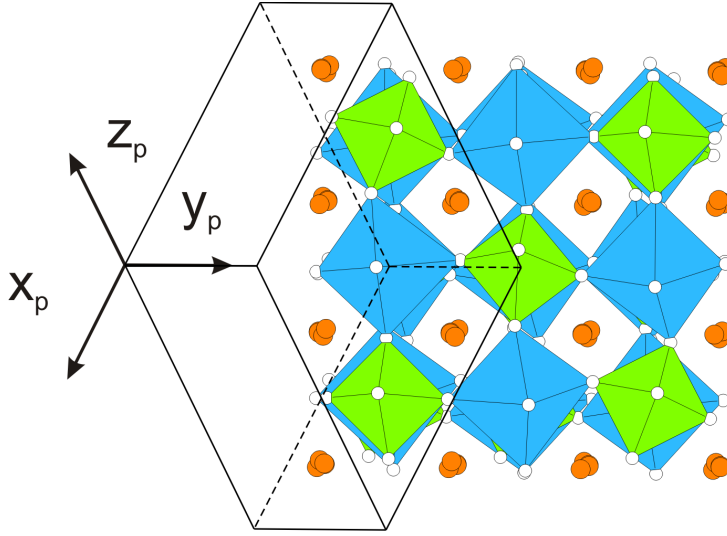
Figure 6.1: Structure of Pb$_2$CaTeO$_6$ in direction a of the pseudo-cubic double-perovskite cell. The [CaO$_6$]-octahedra are displayed in blue, the [TeO$_6$]-octahedra in green. Oxygen atoms are drawn as white spheres and Pb atoms as orange spheres.

Table 6.1: List of atom positions and Wyckoff positions in Pb$_2$CaTeO$_6$

Atom	Wyckoff	x	y	z	U_{eq}
Pb1	4(e)	0.37441(3)	0.52862(5)	0.62617(3)	0.01423(8)
Pb2	4(e)	0.88729(3)	0.01862(5)	0.62379(3)	0.01681(9)
Ca1	4(e)	0.25380(13)	0.0026(2)	0.74854(13)	0.0075(2)
Te1	2(a)	0	0	0	0.00578(12)
Te2	2(d)	$\frac{1}{2}$	0	$\frac{1}{2}$	0.00567(12)
O1	4(e)	0.1238(6)	0.5326(10)	0.3945(6)	0.0190(12)
O2	4(e)	0.9099(5)	0.7767(10)	0.4090(5)	0.0164(11)
O3	4(e)	0.5816(5)	0.2140(9)	0.6504(5)	0.0146(11)
O4	4(e)	0.6551(5)	0.0495(9	0.4347(5)	0.0124(10)
O5	4(e)	0.5895(5)	0.7475(10)	0.6173(6)	0.0152(11)
O6	4(e)	0.1202(6)	0.6892(10)	0.6404(5)	0.0198(12)

6.2.2 Description of the structure

The structure is very similar to Pb$_2$CdTeO$_6$, which was described in the previous chapter. The lattice parameters are slightly larger than those of the Cd compound and due to a loss of centring, Pb$_2$CaTeO$_6$ exhibit a symmetry reduction. Te and Ca occupy the B-sites, whereas Pb is found on the A-site. Te is located a two different special positions, both on an inversion centre. The [TeO$_6$] and [CaO$_6$]-octahedra attend a rock-salt ordering (Fig. 6.3). Pb is located between these octahedra in 12-fold coordination by oxygen atoms.

In comparison with Pb$_2$CdTeO$_6$, the 4(c) position of Te in $C2/c$ splits into 2(a) and 2(d) in space group $P2_1/c$ for Pb$_2$CaTeO$_6$. Therefore there are two different [TeO$_6$] octahedra. The bond length of the Te atom to its octahedral coordinated oxygen atoms varies from 1.905 to 1.931 Å for Te1 and 1.924 and 1.938 Å for Te2 (Tab. 6.2). The angles of the [TeO$_6$]-octahedra are comparable to those in Pb$_2$CdTeO$_6$ (Tab. 5.2). The octahedra are only slightly distorted,

Table 6.2: Selected bond lengths [Å] and angles [°] in Pb_2CaTeO_6

Pb1 - O1	2.874		
Pb1 - O2	2.515	3.324	3.402
Pb1 - O3	2.809		
Pb1 - O4	3.402		
Pb1 - O5	2.565	2.996	3.068
Pb1 - O6	2.422	2.746	3.338
Pb2 - O1	2.606	3.044	3.198
Pb2 - O2	2.503	2.666	3.312
Pb2 - O3	2.618	3.015	3.155
Pb2 - O4	2.540		
Pb2 - O5	3.410		
Pb2 - O6	3.416		

Te1 - O1	1.913 (2x)	Te2 - O4	1.927 (2x)
Te1 - O2	1.931 (2x)	Te2 - O5	1.924 (2x)
Te1 - O3	1.905 (2x)	Te2 - O6	1.938 (2x)
Ca - O1	2.297	Ca - O4	2.355
Ca - O2	2.300	Ca - O5	2.246
Ca - O3	2.326	Ca - O6	2.362

cis-oxygen		trans-oxygen	
Ox - Te1 - Oy	87.1 - 92.9	Ox - Te1 - Ox	180.0
O - Cd - O	81.2 - 107.0	O - Cd - O	162.8

the picture differs not much from the one for the Cd compound, and hence they are not displayed explicitly. The Ca-O bond lengths are in the same range as the Cd-O bonds, only the individual bond length differs slightly. The same applies for the angles.

The bond lengths of the Pb atoms to the oxygen atoms vary from 2.422 Å to 3.541 Å (Tab. 6.2). A separation of oxygen in two hemispheres around the Pb atom, which was observed for the Cd compound, was not noticed for this compound. In contrast to the $[CaO_6]$-octahedra, which differ not much in their form to the $[CdO_6]$-octahedra in Pb_2CdTeO_6, the $[PbO_{12}]$-polyhedra are much more distorted than those in the Cd compound (Fig. 6.2).

The expansion of the unit cell is due to a slightly larger Ca^{2+}-cation, which has an ion radius of 1 Å compared to a radius of 0.95 Å for Cd^{2+} [47]. The tolerance factor calculated with formula 4.1 on page 22 is 0.937 and the fitness factor is 0.792. This expresses the observations done before very well.

Double-perovskite cell

As the symmetry reduction from Pb_2CdTeO_6 is *klassengleich* without cell transformation, the same transformation matrix can be used to obtain the pseudo-cubic double-perovskite cell. The dimensions calculated with this matrix are $a = 8.3034$ Å, $b = 8.3034$ Å and $c = 8.2849$ Å. The angles are $\alpha = 89.75°$, $\beta = 90.25°$ and $\gamma = 91.53°$. The geometric relation to the cubic double-perovskite is the same as for the Cd compound, with respect to a different origin shift (Fig. 5.4).
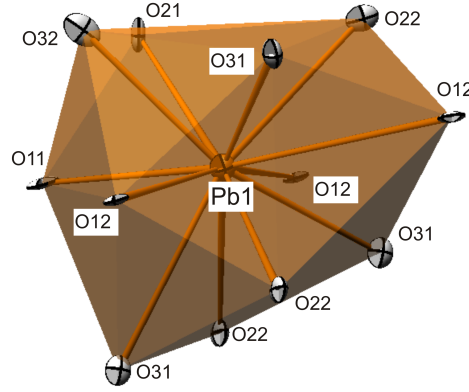
Figure 6.2: Distorted [PbO$_{12}$]-cuboctahedral coordination sphere with Pb1 in the centre

6.2.3   Octahedral tilting

Despite the greater Ca atom and its dislocation, it has not much effect on the tilting of the octahedra. The effect of the dislocation of the Ca atom and the Ca-O bond length variation, compared to the Cd compound, is too small to influence the structure significantly. Due to the splitting of the Wyckoff positions there are now four different octahedra for Te and two for Ca. The scheme is given in Fig. 6.3.
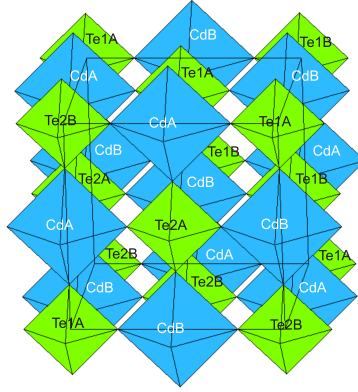
Figure 6.3: Octahedra tilt scheme of Pb$_2$CaTeO$_6$. The unit cell refers to the pseudo cubic double-perovskite cell

Table 6.3: Counter-clockwise tilt angles of each different octahedron in Pb$_2$CaTeO$_6$, given in [°].

Tilt along double-perovskite axis	Te1 A	Te1 B	T2 A	Te2 B	Ca A	Ca B
a	5.9	-0.7	6.2	17.5	-5.9	-6.1
b	-0.6	5.8	17.5	6.4	-6.2	-6.0
c	-11.2	9.6	3.2	-4.7	1.3	-3.9

Table 6.4: Tilting angles for Ca-O bonds in Pb_2CaTeO_6 in [°]

| Tilt along double-perovskite axis | Ca A - | | | | | |
	O1	O2	O3	O4	O5	O6
a	1.7	-	-5.2	-15.3	-4.7	-
b	-5.6	-1.3	-	-5.3	-	-12.8
c	-	10.4	4.9	-	-7.4	-2.5

| Tilt along double-perovskite axis | Cd B - | | | | | |
	O1	O2	O3	O4	O5	O6
a	-5.7	-1.3	-	-4.6	-	-12.8
b	1.4	-	-5.2	-15.4	-4.7	-
c	-	-13.0	-7.4	-	4.9	-0.1

6.2.4 Superstructure

The precession images in 5.6 show distinct strong supercell reflections. The picture shows the $(hk\bar{3})$ plane. In planes with even indices, the strong reflexes are extinct due to F-centering of the basic cell (Fig. 6.4).

The transformation matrix P was calculated from the image and is given in 6.1.

$$P = \begin{pmatrix} \frac{3}{8} & 0 & \overline{\frac{1}{4}} \\ 0 & 1 & 0 \\ \frac{1}{8} & 0 & \frac{1}{4} \end{pmatrix}, \quad D(P) = \frac{1}{8} \tag{6.1}$$

Cell transformation gave a monoclinic cell with the following dimensions: $a = 3.635$ Å, $b = 5.7726$ Å, $c = 4.142$ Å and $\beta = 125.09°$. The volume is $V = 71.38$ Å^3 and the determinant of the transformation matrix P 6.1 is $\frac{1}{8}$, therefore it is an 8-fold superstructure.
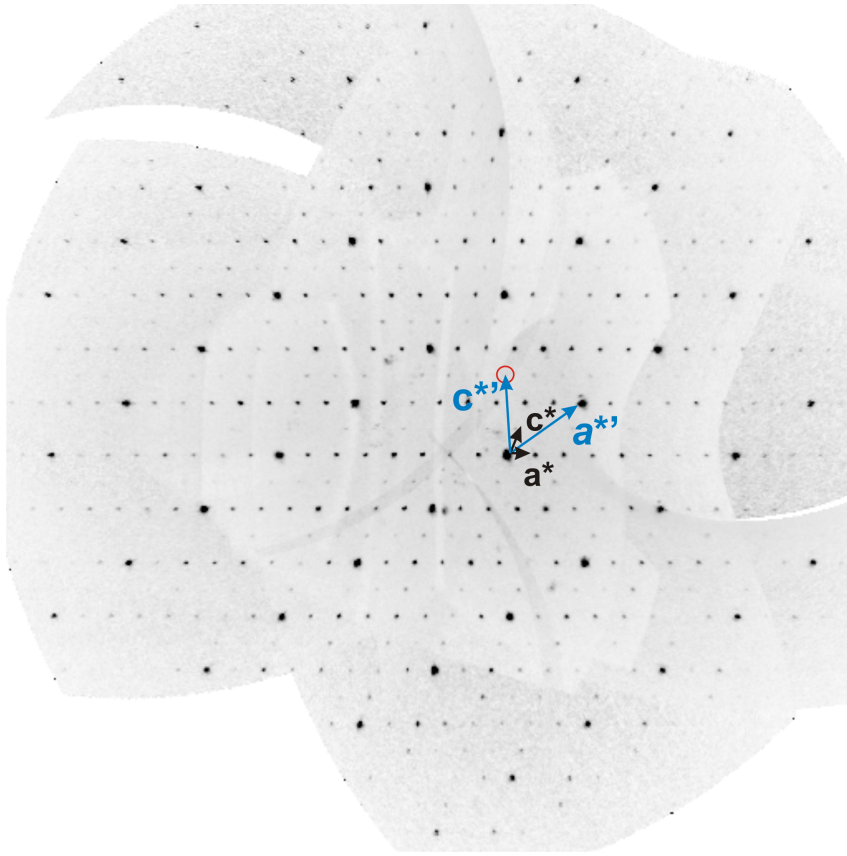
Figure 6.4: Precession image of plane ($h\overline{3}l$) of Pb_2CaTeO_6. Reciprocal lattice vectors a* and c* of the reduced cell of the superstructure and the basic structure (caption ') are given

Chapter 7

Pb$_2$CoTeO$_6$

The structure of Pb$_2$CoTeO$_6$ was reported by Wedel et al [28]. The reported lattice parameters of the tetragonal unit cell are $a = 5.661(5)$ Å and $c = 8.004(7)$ Å, where a multiplied by $\sqrt{2}$ amounts to the value of c and fulfils the metrical condition of a cubic cell within the standard deviation. Moreover, a close inspection of the atomic coordinates of respective atom pairs in the tetragonal model shows that these pairs match also for a cubic model within their standard uncertainty. It seems most likely that the true symmetry of Pb$_2$CoTeO$_6$ is cubic. This assumption was supported by calculation of the tolerance factor, which is 0.996 and 1.020 for a high spin and a low spin Co respectively, and the fitness factor with values of 1.05 and 1.03, both would support a cubic cell according to Tab. 4.1. Based on these findings, it seemed appropriate to redetermine the crystal structure of Pb$_2$CoTeO$_6$.

7.1 Experimental

7.1.1 Preparation

Crystals of Pb$_2$CoTeO$_6$ were prepared from 1.2814 g (5.7 mmol) PbO, 0.2158 g (2.9 mmol) CoO and 0.9143 g (5.7 mmol) TeO$_2$. The well-ground mixture was heated according to temperature program 5 in Figure 1.1(e). Four different kinds of crystals were identified in the sample. Beside the cobalt blue block-shaped crystals of the title compound, black blocks, dark-red cubic crystals and numerous colourless nearly isometric crystals were isolated. The black crystals could be determined as Pb$_5$TeO$_8$ and the colourless ones as alumina. The dark red crystals could be identified as the new compound Pb$_6$Co$_9$TeO$_{30}$, which is described later in chapter 11.

7.1.2 Data collection and refinement

According to the original publication [28] data collection was based on a tetragonal cell. Data were collected in 9 runs with ϕ and ω scans. 5818 reflections were measured, of which 5750 fulfilled the criterion of $I > 2\sigma(I)$.

The data was later integrated for a tetragonal and a cubic cell. Structure solution and refinement have been performed in the tetragonal and the cubic system with space groups, $Fm\bar{3}m$ and $I4/mmm$ respectively. The values given in Tab. 7.1 list the parameters of both refinement before numerical absorption correction was applied, as this is also dependent on the cell metric and would therefore make a comparison more difficult.

As seen in Tab. 7.1 the structure could be refined to much better R values in the cubic system than in the tetragonal. The highest difference peak is only 1.789 eÅ^{-3} in the cubic

Table 7.1: Comparison of the cubic and tetragonal solution of Pb$_2$CoTeO$_6$

	cubic	tetragonal
Crystal data		
Space group	$Fm\bar{3}m$	$I/4mmm$
a (Å)	8.01380(10)	5.6676(4)
c (Å)		8.0065(9)
V (Å^3)	514.65(11)	257.18(4)
Z	4	2
R_{int}	0.0441	0.411
Refinement		
Refinement on	F^2	F^2
$R[F^2 > 2\sigma(F)]$	0.0150	0.0310
$\omega R(F^2)$	0.0340	0.0803
S	1.582	1.033
No. of reflections	137	325
No. of parameters	8	16
$\delta\rho_{max}$ (e Å^{-3}),	1.789	5.712
$\delta\rho_{min}$ (e Å^{-3})	-1.655	-2.098
Extinction method	SHELX	SHELX
Extinction coefficient	0.00028(6)	0.0014(5)

system, in contrast to 5.712 eÅ^{-3} for the tetragonal solution. The lowest density peak is as well lower for the cubic solution, than for the tetragonal.

The measured reflections fulfilled all the reflection conditions for space group $Fm\bar{3}m$ ($h + k = 2n, h + l = 2n$ and $k + l = 2n$ for hkl; $k, l = 2n$ for $0kl$; $h + l = 2n$ for hhl and $l = 2n$ for $00l$) according to the International Tables of Crystallography A [57]. The cubic cell parameter is as well exactly $a_{cub} = a_{tetr} \cdot \sqrt{2}$, within the standard uncertainty.

Not much information is given on the structure refinement in the original publication [28], therefore it is not clear, why the tetragonal system was eventually chosen instead of the cubic.

Details of the final refinement in the cubic system, as well as parameters of the data collection are given in C.5 in the appendix. The atom positions are listed in Tab. 7.2.

Table 7.2: List of atom positions and Wyckoff positions in Pb$_2$CoTeO$_6$

Atom	Wyckoff	x	y	z	U_{eq}
Pb	8(c)	$\frac{1}{4}$	$\frac{1}{4}$	$\frac{1}{4}$	0.01563(10)
Te	4(a)	$\frac{1}{2}$	$\frac{1}{2}$	0	0.00440(11)
Co	4(b)	$\frac{1}{2}$	0	0	0.084(2)
O	24(e)	0.2392(5)	0	0	0.0288(10)

7.2 Structure

7.2.1 Structure solution

Due to the reasons described before the crystal system of Pb_2CoTeO_6 is cubic, space group $Fm\bar{3}m$, with cell parameter $a = 8.01380(10)$ Å and volume $V = 514.65(11)$ Å^3.

7.2.2 Description of the Structure

The compounds crystallises in the undistorted 1:1 B-site ordered perovskite structure, which is described in detail in the introduction. Here the Te atoms and the Co atoms occupy the B-sites and the Pb atoms the A-sites. The bond lengths are given in Tab. 7.3.

Table 7.3: Bond lengths [Å] in Pb_2CoTeO_6

Pb - O	2.835	(12x)
Te - O	1.917	(6x)
Co - O	2.090	(6x)

7.2.3 Superstructure

The precession images show superstructure reflections (Figure 7.1). The transformation matrix 7.1 relates the double perovskite structure to the simple perovskite structure according to the Bärnighausen tree in Tab. 9.1. The cell parameter of the basic structure is $a = 4.002$ Å and the structure Pb_2CoTeO_6 is a 8-fold superstructure with respect to the perovskite aristotype.

$$P = \begin{pmatrix} 2 & 0 & 0 \\ 0 & 2 & 0 \\ 0 & 0 & 2 \end{pmatrix}, \quad D(P) = 8 \qquad P^{-1} = \begin{pmatrix} \frac{1}{2} & 0 & 0 \\ 0 & \frac{1}{2} & 0 \\ 0 & 0 & \frac{1}{2} \end{pmatrix}, \quad D(P^{-1}) = \frac{1}{8} \qquad (7.1)$$
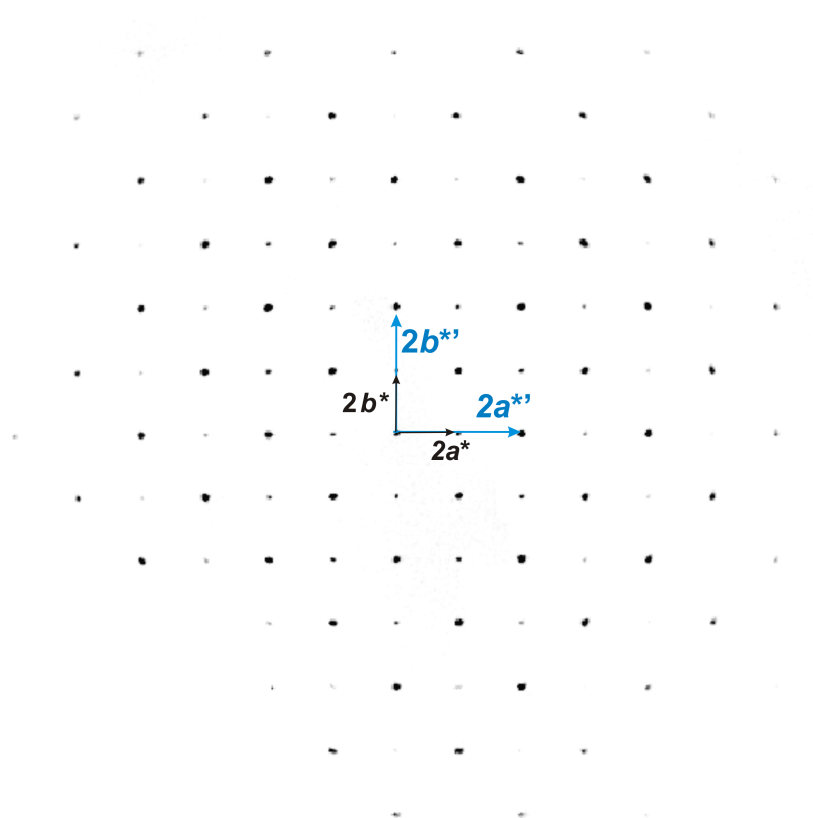
Figure 7.1: Precession image of plane $(hk4)$ in Pb_2CoTeO_6

Chapter 8

Pb_2MnTeO_6

This structure was likewise described before by Wulff et. al. [29]. It was stated that this compound is of the simple perovskite structure, where Mn and Te occupy the same sites in the unit cell and are statistically distributed. Due to the different sizes of the Mn and Te atoms and a typical Mn^{2+}-O bond length of 2.1 Å, which is 0.2 Å greater than those of the average Te^{6+}-O bond, the reported structure solution is questionable. It is much more likely that this compound adopts the double-perovskite structure, with one cation on the octahedral site distinctive larger than the other one. As the compound was originally measured on a CAD 4 diffractometer with a point detector, it is likely that only the strong basic structure reflections where measured. To be sure of this assumption the structure was redetermined.

8.1 Experimental

8.1.1 Preparation

Crystals of Pb_2MnTeO_6 were obtained by heating a well ground mixture of 1.286 g (5.8 mmol) PbO, 0.333 g (2.9 mmol) $MnCO_3$ and 0.463 g (2.9 mmol) TeO_2 according to temperature program 1. After another regrinding step the sample was again heated according to temperature program 2. Few crystals were found, one little dark blue round one was selected for single crystal X-ray diffraction.

8.1.2 Data collection and refinement

Data was collected based on a cubic cell with ω and ϕ scans in 8 runs. The data was then integrated on a cubic cell. The structure could be solved in space group $Fm\overline{3}m$ without any problems.

The precession images showed clear superstructure reflections (Fig. 8.1). Calculations gave the same matrix as for Pb_2CoTeO_6, given in matrix (7.1). As expected, this is the transformation matrix to the basic perovskite structure. The cell parameter of the basic structure is $a = 4.0527$ Å and therefore only slightly longer than in the original literature with $a = 4.045(3)$ Å.

As there is not much information given on the structure solution and refinement in the original publication, space group $Pm\overline{3}m$ [29] was chosen. More details on the current data collection and refinement are summarized in Tab. C.6 in the appendix.
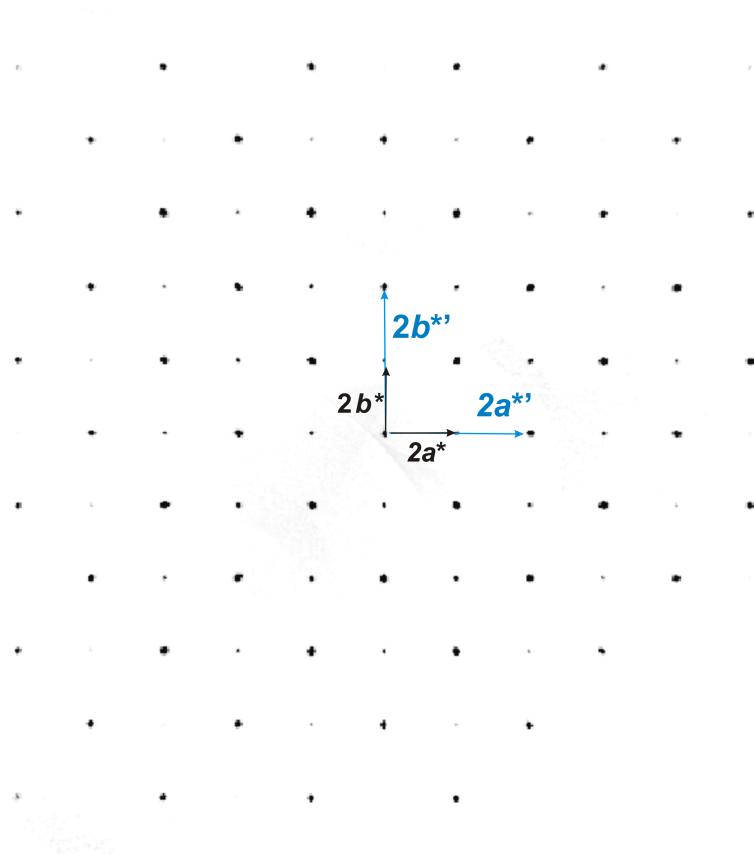
Figure 8.1: Precession image of plane $(hk\overline{4})$ in Pb_2MnTeO_6

Table 8.1: List of atom positions and Wyckoff positions in Pb_2MnTeO_6

Atom	Wyckoff	x	y	z	U_{eq}
Pb	8(c)	$\frac{1}{4}$	$\frac{1}{4}$	$\frac{1}{4}$	0.01977(14)
Te	4(a)	0	0	0	0.00483(12)
Mn	4(b)	$\frac{1}{2}$	0	0	0.0100(3)
O	24(e)	0	0	0.2366(6)	0.0397(15)

8.2　Structure

8.2.1　Structure solution

Due to the reasons described before, the compound crystallises in the cubic structure of the undistorted double perovskite with space group $Fm\overline{3}m$ and cell parameter $a = 8.10540(10)$ Å. The volume of the unit cell is $V = 532.505(11)$ Å^3. The atom positions are given in Tab. 8.1.

8.2.2　Description of the structure

The structure is of the elpasolite structure, which was already described in the introduction. An alternative illustration of the double-perovskite structure is given in Fig. 8.2. Here the face-sharing $[PbO_{12}]$-cuboctahedra are displayed, with Te and Mn atoms in the octahedral voids.

　　The Mn atoms and Te atoms occupy the B-sites and Pb the A-site. The Mn-O bond lengths
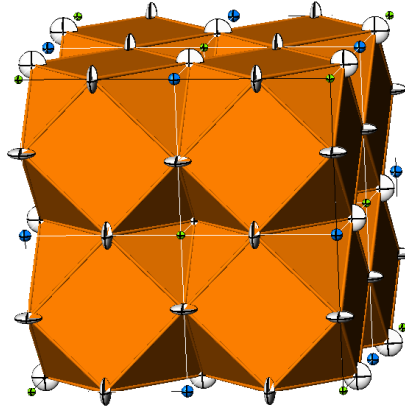
Figure 8.2: Clinographic projection of the unit cell of Pb_2MnTeO_6. The $[PbO_{12}]$-coordination spheres are displayed as face-linked cuboctahedra. The Te atoms (green) and the Mn atoms (blue) are located in the octahedral voids. Oxygen atoms are displayed as white ellipsoids, drawn at 50% of the probability density function.

Table 8.2: Selected bond lengths [Å] in Pb_2MnTeO_6

Pb - O	2.868	(12x)
Te - O	1.918	(6x)
Mn - O	2.135	(6x)

is 2.135 Å and therefore even longer than the Co-O bonds in Pb_2CoTeO_6. The Pb-O length is with a value of 2.868 Å also slightly longer than in the Co compound. The Te-O distance is ideal with a value of 1.918 Å (Tab. 8.2). The $[TeO_6]$-octahedra and $[MnO_6]$-octahedra attend a rock-salt ordering.

Chapter 9

The Bärnighausen family tree

In a Bärnighausen family tree, group- subgroup-relations are displayed [58]. Starting from the aristotype every arrow points to a maximal subgroup. The letters t, k and i are used to declare, if the subgroup is *translationsgleich*, *klassengleich* or *isomorph*. The index declares the magnitude of symmetry operations lost with the transformation. The following integer gives the index of the symmetry-reduction. Sometimes a cell transformation or an origin shift is necessary. These are specified by vector sums and modified coordinates, respectively.

Translationsgleiche subgroups have the same translation lattice as the supergroup. The loss of symmetry leads to a lower crystal system. A *klassengleiche* symmetry reduction does not change the crystal system, but a loss of centering or change in cell dimensions. *Isomorphe* subgroups are a special case of *klassengleiche* subgroups. Here the space group type does not change; due to an enlargement of the unit cell, symmetry operations are lost.

A part of the Bärnighausen family tree for double-perovskites is given in Fig. 9.1. It shows group-subgroup relations of the structures described before according to [59].

In the aristotype, that is the structure of the mineral elpasolith K_2NaAlF_6, aluminium and sodium are coordinated to six fluorine anions. These octahedra build up a lattice of corner-sharing octahedra. Potassium cations occupy the voids between the octahedra and are coordinated to twelve anions. Starting from the aristotype K_2NaAlF_6 the symmetry reduction $t3$ leads to the Ba_2CuWO_6. The cell changes from a cubic F-centered to a tetragonal I-centered cell. The reason for this reduction is a Jahn-Teller distortion of the $[CuO_6]$-octahedra along the [001] direction. To obtain the tetragonal I-centered cell, a cell transformation is needed. This transformation does not change the dimensions of the unit cell, but the coordinates of the atoms. As a consequence, the anion position in the cubic double-perovskite structure splits into two different Wyckoff positions in Ba_2CuWO_6. Copper and tungsten now occupy the octahedral sites and barium the cuboctahedral sites.

A structural distortion occurs also in Na_3AlF_6 at 900K. An additional octahedral tilting along [0 0 1] causes the actual symmetry reduction to the orthorhombic system. This implies the small anomaly of the sodium ions in the z coordinate.

In Sr_2NiTeO_6, octahedral tilting occurs in two directions [1 0 0] and [0 1 0], which leads to a symmetry reduction with index $t2$ in the monoclinic system [60]. A $k2$ reduction gives the structure of Pb_2CdTeO_6. Here a cell transformation, as well as an origin shift is needed. Finally, another symmetry reduction with an index $k2$ and an origin shift of $\left(\frac{1}{4}, \frac{1}{4}, 0\right)$ leads to Pb_2CaTeO_6, the other compound described in a previous chapter. Reasons for the symmetry reduction of both structures were described in this chapter.

$F4/m\overline{3}2/m$

$\boxed{K_2NaAlF_6}$

K:8c	Al:4a	Na:4b	F:24e
$\overline{4}3m$	$m\overline{3}m$	$m\overline{3}m$	$4m.m$
$\frac{1}{4}$	0	$\frac{1}{2}$	0.219
$\frac{1}{4}$	0	$\frac{1}{2}$	0
$\frac{1}{4}$	0	$\frac{1}{2}$	0

t3

$\frac{1}{2}(\mathbf{a\text{-}b}),\frac{1}{2}(\mathbf{a\text{+}b}), \mathbf{c}$

$x - y, x + y, z$

$I4/m2/m2/m$

$\boxed{Ba_2CuWO_6}$

Ba:4d	Cu:2a	W:2b	O:4e	O:8h
$\overline{4}m2$	$4/mmm$	$4/mmm$	$4mm$	$m.2m$
0	0	0	0	0.251
$\frac{1}{2}$	0	0	0	0.251
$\frac{1}{4}$	0	$\frac{1}{2}$	0.287	0

t2

$I2/m2/m2/m$

$\boxed{Na_3AlF_6 \ 900K}$

Na:4j	Al:2a	Na:2c	F:4i	F:8n
$mm2$	mmm	mmm	$mm2$	$..m$
0	0	0	0	0.234
$\frac{1}{2}$	0	0	0	0.217
0.251	0	$\frac{1}{2}$	0.219	0

t2

$I12/m1$

$\boxed{Sr_2NiTeO_6}$

Sr:4i	Te:2a	Ni:2d	O:4i	O:8j
m	$2/m$	$2/m$	m	1
0.5	0	0	0.048	0.239
0	0	0	0	0.242
0.75	0	$\frac{1}{2}$	0.760	0.976

k2

$\mathbf{a\text{-}c}, \mathbf{b}, \mathbf{a\text{+}c}$

$-\frac{1}{4}, -\frac{1}{4}, -\frac{1}{4}$

$\frac{x-z}{2}, y, \frac{x+z}{2}$

$C12/c1$

$\boxed{Pb_2CdTeO_6}$

Pb:8f	Te:4c	Cd:4e	O:8f	O:8f	O:8f
1	$\overline{1}$	2	1	1	1
0.128	$\frac{1}{4}$	0	0.100	0.163	0.347
0.269	$\frac{1}{4}$	0.243	0.297	-0.024	0.049
0.623	0	$\frac{1}{4}$	0.080	-0.101	0.149

k2

$\frac{1}{4}, \frac{1}{4}, 0$

$P12_1/c1$

$\boxed{Pb_2CaTeO_6}$

Pb:4e	Pb:4e	Te:2a	Te:2d	Ca:4e	6x O:4e
1	1	$\overline{1}$	$\overline{1}$	1	1
0.374	0.887	0	$\frac{1}{2}$	0.254	x
0.529	0.019	0	0	0.003	y
0.626	0.623	0	$\frac{1}{2}$	0.749	z

Figure 9.1: Part of the Bärnighausen family tree for 1:1 B-site ordered double-perovskites.

Part IV

# Structures of quarternary compounds

Chapter 10

Pb_6CdTeO_{10}

This compound was obtained when trying to synthesise Pb_3TeO_6, according to the experimental details given by Kosse et al [19].

10.1 Experimental

10.1.1 Preparation

The sample was prepared from 2.26 g (8.5 mmol) $PbCO_3$, 0.25 g (1.4 mmol) $CdCO_3$ and 0.25 g (1.4 mmol) TeO_3, which was heated according to the temperature program pictured in Fig. 10.1. A yellowish fragment was isolated from the sample and selected for single crystal X- ray diffraction.
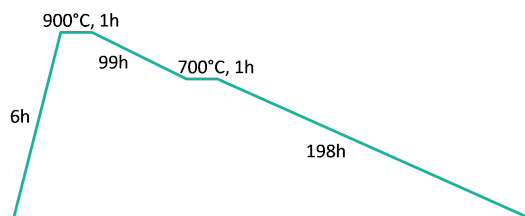
Figure 10.1: Temperature Program for Pb_6CdTeO_{10}

A microcrystalline pure-phase sample of Pb_6CdTeO_{10} was obtained by heating a well-ground and pressed mixture of 2.008 g (9.0 mmol) PbO, 0.287 g (1.7 mmol) $CdCO_3$ and 0.239 g (1.5 mmol) TeO_2 according to temperature program 3 in Fig. 1.1(c). A second and a third annealing step was carried out, under the same conditions as the first one, with regrinding after every step. The thermal behaviour of this compound is described in chapter 14.

10.1.2 Data collection and refinement

Data collection strategy was optimised based on a triclinic cell. The crystal was measured in 11 runs with ω and ϕ scans. Data was then integrated for an orthorhombic cell. Structure solution was not successful with SHELX, therefore it was solved with SIR-92 in space group $P1$. Platon suggested a higher symmetry, why it was then transformed to space group $C222_1$.

Details of the data collection and refinement are given in Tab. C.7 in the appendix.
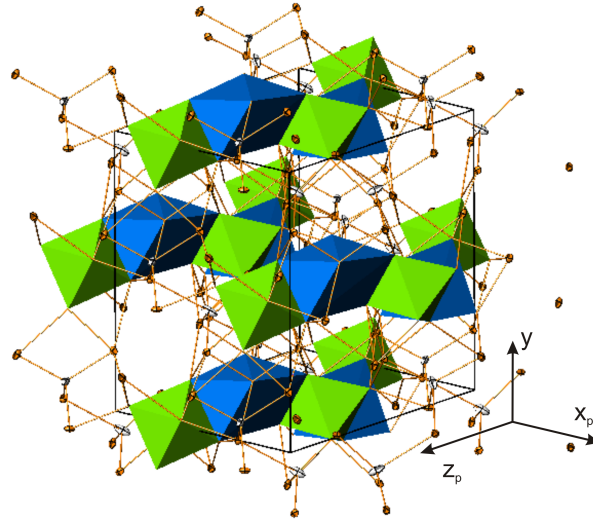
10.2   Structure

10.2.1   Structure solution

Pb_6CdTeO_{10} crystallises in the non centrosymmetric orthorhombic space group $C222_1$ with cell parameters $a = 9.1206(2)$ Å, $b = 11.5674(3)$ Å and $c = 11.3113(3)$ Å and a volume of the unit cell of $V = 1193.36(5)$ Å^3. A list of atom positions is given in Tab. 10.1.

**Table 10.1:** List of atom positions and Wyckoff positions in Pb_6CdTeO_{10}

Atom	Wyckoff	x	y	z	U_{eq}
Pb1	4(a)	0.70120(4)	0	0	0.01203(7)
Pb2	4(b)	0	0.99227(2)	$\frac{1}{4}$	0.01391(6)
Pb3	8(c)	0.29123(3)	0.215832(19)	0.24144(2)	0.01375(5)
Pb4	8(c)	0.49465(3)	0.281308(16)	0.515104(16)	0.01165(5)
Cd	4(b)	0	0.42231(4)	$\frac{1}{4}$	0.01022(10)
Te	4(a)	0.32554(6)	0	0	0.00554(9)
O1	8(c)	0.4823(5)	0.0608(3)	0.1018(3)	0.0097(8)
O2	8(c)	0.1495(5)	0.3265(4)	0.1283(3)	0.0112(8)
O3	8(c)	0.1833(5)	0.9318(4)	0.8958(3)	0.0103(8)
O4	8(c)	0.3295(5)	0.8595(4)	0.0934(3)	0.0104(8)
O5	8(c)	0.1249(7)	0.1219(4)	0.3465(4)	0.0253(12)

10.2.2   Description of the structure

Figure 10.2: Clinographic projection of the structure of Pb_6CdTeO_{10}. The $[TeO_6]$-octahedra are displayed in green and the $[CdO_6]$-prism in blue. The Pb atoms are displayed as orange ellipsoids and oxygen atoms as white ellipsoids, which represent 50% probability level.

The structure is build up by chains of corner-sharing $[TeO_6]$-octahedra and $[CdO_6]$-prism, which are connected through Pb atoms. A clinographic projection of the unit cell is given in Fig. 10.2.

(a) Projection on (010)

(b) Projection on (100)
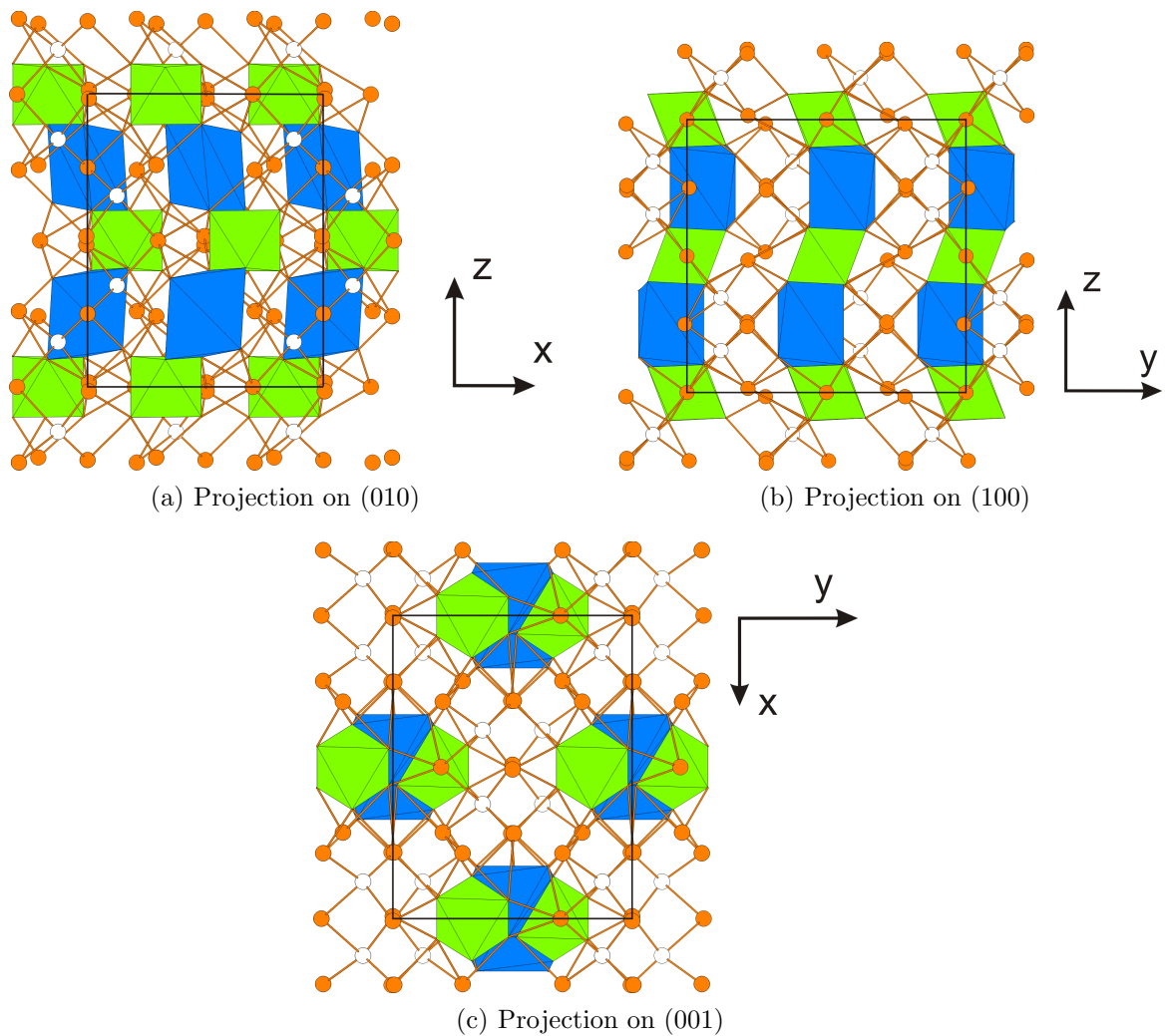
(c) Projection on (001)

Figure 10.3: Projection of the structure of Pb_6CdTeO_{10} on different planes. The $[TeO_6]$-octahedra are displayed in green and the CdO_6]-prism in blue. Oxygen atoms are drawn as white spheres and Pb atoms as orange spheres.

The Cd atoms are located at a 2-fold rotation axis along [010] and are coordinated to six oxygen atoms, which build up a trigonal prism (Fig. 10.4). The Cd-O bond lengths vary slightly between 2.232 Å and 2.467 Å (Tab. 10.2).

The coordination sphere of the Te atom has the shape of an almost regular octahedron. The bond lengths vary between 1.922 Å and 1.966 Å. The angles between trans-oxygen and the centre Te atom are slightly below the ideal of 180°. Those of cis-oxygen are also not ideal and differ between 86.7° and 95.1°.

The $[TeO_6]$-octahedra and $[CdO_6]$-prism share corners and are connected to chains along [001] (Figs. 10.3(a) to 10.3(c)), where Cd and Te are alternating in the chains. The chains are slightly bent, therefore the Te-Cd-Te angles are 123.59° and 149.04°, respectively. Due to the special positions of the Cd and Te atoms, four of these chains are distributed in the unit cell.

The lead atoms are distributed between the Cd-Te chains and connect adjacent chains into a three-dimensional network.
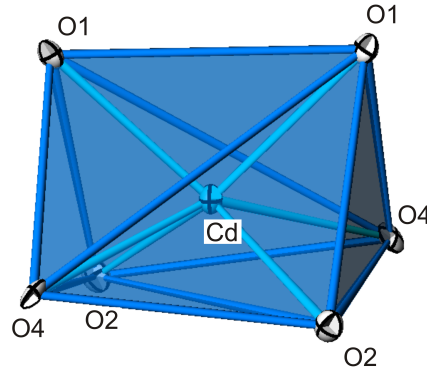
Figure 10.4: Coordination sphere of cadmium. The ellipsoids represent 50% probability level.

**Table 10.2:** Selected bond lengths [Å] and angles [°] in Pb$_6$CdTeO$_{10}$

Pb1 - O	2.410	(2x)	2.521	(2x)	2.742	(2x)	3.906	(2x)
Pb2 - O	2.177	(2x)	2.507	(2x)	3.811	(2x)	3.974	(2x)
Pb3 - O	2.213		2.225		2.509		2.731	
	2.958		3.260					
Pb4 - O	2.219		2.261		2.452		2.585	
	2.881		3.326		3.666			
Cd - O	2.232	(2x)	2.324	(2x)	2.467	(2x)		
Te - O	1.922	(2x)	1.939	(2x)	1.966	(2x)		

cis-oxygen			trans-oxygen		
O - Te - O	86.70 - 95.10	(12x)	O - Te - O	175.46 - 177.90	(3x)
O - Cd - O	68.99 - 92.88	(6x)	O - Cd - O	138.11 - 145.70	(3x)
Te - O1 - Cd	103.11		Te - Cd - Te	123.59	
Te - O4 - Cd	98.86			149.04	

There are four distinct positions of Pb in the unit cell. Two are on special positions Pb1 and Pb2 on 2-fold rotation axes. The two lead atoms Pb3 and Pb4 at general positions are coordinated to five oxygen atoms with bond lengths below 3 Å and another bond at about 3.3 Å. They are all arranged in a hemisphere around the Pb atoms and create a kind of a pyramid with two apices in case of Pb3 and a distorted prismatic pyramid in case of Pb4 (Fig. 10.5(c) and 10.5(d)).

Pb1 and oxygen atoms build up distorted octahedra with bond lengths between 2.410 Å and 2.742 Å (Fig. 10.5(a)). The Pb2 atoms are coordinated to only four oxygen, with bond lengths between 2.177 Å and 2.507 Å. The other bonds are considerably longer (> 3.8 Å). Here the oxygen atoms are also arranged in a hemisphere which leaves space for the lone pair electrons of the Pb atoms (10.5(b)).

This structure has some similarities with Pb$_2$TeO$_5$, where also chains along [001] are present, but build only by [TeO$_6$]-octahedra, which are connected through corners. An interesting feature of the Pb$_6$CdTeO$_{10}$ structure is the unusual shape of the Cd-coordination sphere and the low coordination number of some Pb atoms, compared to the other structure described here. Despite the higher amount of Pb atoms in Pb$_5$TeO$_8$ no deeper similarities to this structure are found.
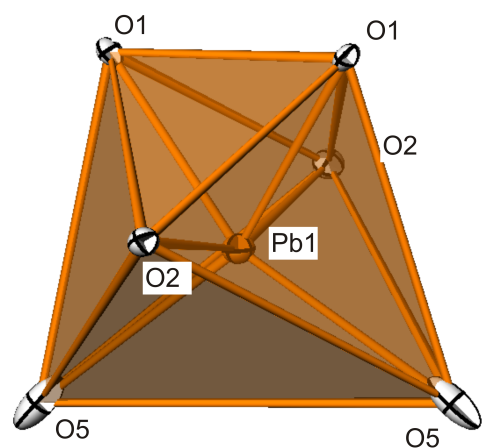
(a) Octahedral coordination sphere of Pb1
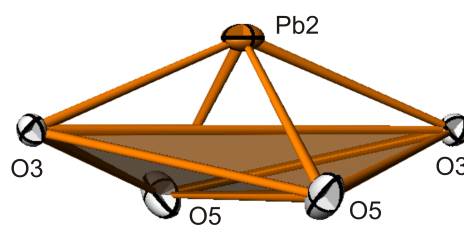
(b) 4-fold coordination sphere of Pb2

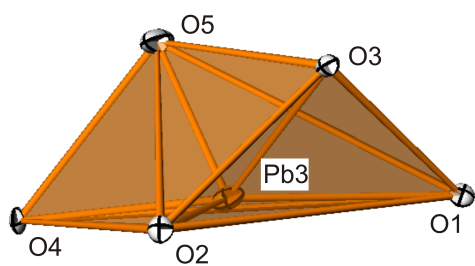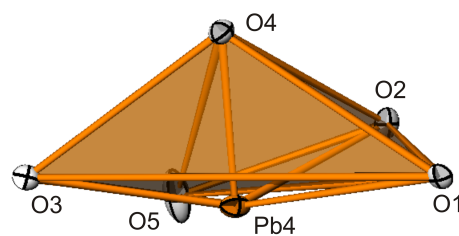(c) Pyramidal coordination sphere of Pb3

(d) Pyramidal coordination sphere of Pb4

Figure 10.5: Pb-O coordination spheres in Pb_6CdTeO_{10}. The ellipsoids represent 50% probability level.

Chapter 11

$Pb_6Co_9Te_5O_{30}$

The isotypic structure of $Pb_6Ni_9Te_5O_{30}$ was described by Wedel and Müller- Buschbaum [30].

11.1 Experimental

11.1.1 Preparation

Crystals of the title compound were obtained from the same sample as Pb_2CoTeO_6 described in chapter 7. A well defined cobalt-blue crystal was selected for single-crystal X-ray diffraction.

11.1.2 Data collection and refinement

The data collection strategy was optimized based on point group $\overline{3}$. The crystal was measured with ω and ϕ scan in 8 runs and therefore a good redundancy was obtained. The structure was first solved in space group $P6_3$, but Platon suggested a higher symmetry. Hence it was transformed into space group $P6_322$. Parameters of the data collection, structure solution and refinement are given in Tab. C.8 in the appendix.

11.2 Structure

11.2.1 Structure solution

The compound crystallises in a hexagonal cell, with lattice parameters $a = 10.39150(10)$ Å and $c = 13.6273(2)$ Å. The compound attends space group $P6_322$, with a unit cell volume of $V = 1274.37$ Å^3. A list of the atom positions is given in Tab. 11.1.

11.2.2 Description of the structure

The structure is basically built up by layers of corner-sharing $[TeO_6]$ and $[CdO_6]$-octahedra, connected through face-sharing $[TeO_6]$ and $[CdO_6]$ octahedra and lead atoms. A clinographic projection of the unit cell is given in Fig. 11.1.

Each Te and Co atoms is coordinated to six oxygen atoms and form slightly distorted octahedra. The Te-O bond lengths vary between 1.91 Å to 1.99 Å, the angles between cis-oxygen atoms are not ideal 90° and vary between 84.1° and 99.1°. The angles between trans-oxygen atoms and the Te- atom are slightly smaller than the ideal 180°, with values between 168.5° and 178.9°. The coordination sphere of Co is even more distorted, with bond lengths from 2.07 Å to 2.26 Å and angles from 72.3° to 108.1° and 153.7° to 174.8°, respectively.

Table 11.1: List of atom positions and Wyckoff positions in $Pb_6Co_9Te_5O_{30}$

Atom	Wyckoff	x	y	z	U_{eq}
Pb1	6(g)	0.38844(4)	0	0	0.01895(9)
Pb2	6(g)	0.26739(3)	0.26739(3)	0	0.01224(8)
Te1	4(f)	$\frac{1}{3}$	$\frac{2}{3}$	0.90388(5)	0.00417(12)
Te2	6(h)	0.16725(5)	0.33450(11)	$\frac{1}{4}$	0.00445(10)
Co1	4(f)	$\frac{1}{3}$	$\frac{2}{3}$	0.11816(11)	0.0065(3)
Co2	2(b)	0	0	$\frac{1}{4}$	0.0089(3)
Co3	6(h)	0.16897(12)	0.3379(2)	$\frac{3}{4}$	0.0066(2)
Co4	6(h)	0.0097(2)	0.50485(12)	$\frac{3}{4}$	0.0059(2)
O1	12(i)	0.3484(5)	0.5264(5)	0.9967(5)	0.0071(7)
O2	12(i)	0.1724(8)	0.5045(7)	0.8370(4)	0.0086(11)
O3	12(i)	0.3240(9)	0.4816(7)	0.3295(4)	0.0080(11)
O4	12(i)	0.1703(8)	0.1805(7)	0.3276(3)	0.0106(10)
O5	12(i)	0.3365(6)	0.3242(6)	0.8288(3)	0.0075(9)
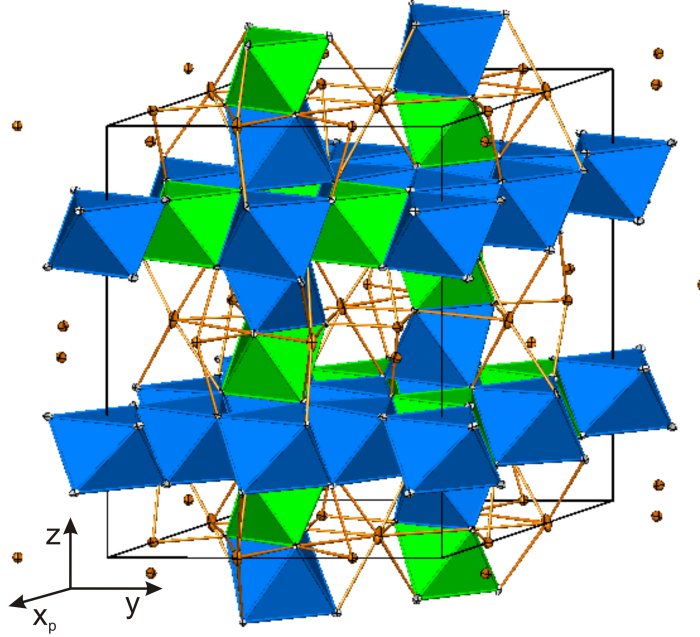
Figure 11.1: Clinographic projection of the structure of $Pb_6Co_9Te_5O_{30}$. The $[TeO_6]$-octahedra are displayed in green and the $[CoO_6]$-octahedra in blue. Lead atoms are drawn as orange spheres. The layers of edge-sharing $[TeO_6]$- and $[CoO_6]$-octahedra are perpendicular to the *c*-axis and are generated by face-sharing $[TeO_6]$- and $[CoO_6]$-octahedra.

These octahedra build up layers, perpendicular to [001] (Fig. 11.1). As shown in Fig. 11.2(a) the octahedra are edge-sharing in these layers. All octahedra are equally orientated, the oxygen atoms build up two layers perpendicular to [001]. The cations Te and Co are located in-between the oxygen layers at $z=\frac{1}{4}$ and $\frac{3}{4}$ respectively. The average thickness of the layer is 2.1 Å.

The layers can be described as an assembly of rings of six octahedra, some with a hole in the middle. There are two types of such rings, one only with $[CoO_6]$-octahedra (caption *A*) and one

where [TeO$_6$] and [CoO$_6$]-octahedra are alternating (caption B). Six rings - three of each kind - are then linked together, forming a honeycomb sheet, where the centre of this arrangement is a [CoO$_6$]-octahedron. Cobalt at the Co2 position occupies these central positions and is located at a 3-fold rotation axis parallel [001] and a 2-fold rotation axis in the same direction. The Te and Co atoms which form the adjacent rings, are located at 2-fold rotation axes along [001], positions Te2 and Co4. The [CoO$_6$]-octahedra rings are formed by Co atoms at Co3.

The B holes in the layer are larger than the A holes. The distances of the oxygen atoms in hole A are 2.9 Å, where those of the oxygen atoms at O3 in hole B are 3.3 Å. This is quite surprising, because the [TeO$_6$]-octahedra require less space than the [CoO$_6$]-octahedra. The effect of the greater hole B is not caused by greater Co-O bond length of the Co4 octahedra but is explained by the smaller Te-O bond length, which cause a greater tilt of the [CoO$_6$]-octahedra in the layer. Another reason is, that [CoO$_6$]-octahedra are connected to these holes, which require more space themselves.

Every second layer is rotated by 180°, due to a 2$_1$ screw axis. The distance of the layers from one to the other is about 4.7 Å.

(a) Layer of edge- sharing Te and Co octahedra at z= 0.25

(b) Space between two layers at z = 0.5. Only Pb-O bonds below 3 Å are drawn. Pb atoms at Pb1 are drawn as orange spheres and those at Pb2 as purple spheres. Black spheres represent oxygen atoms.
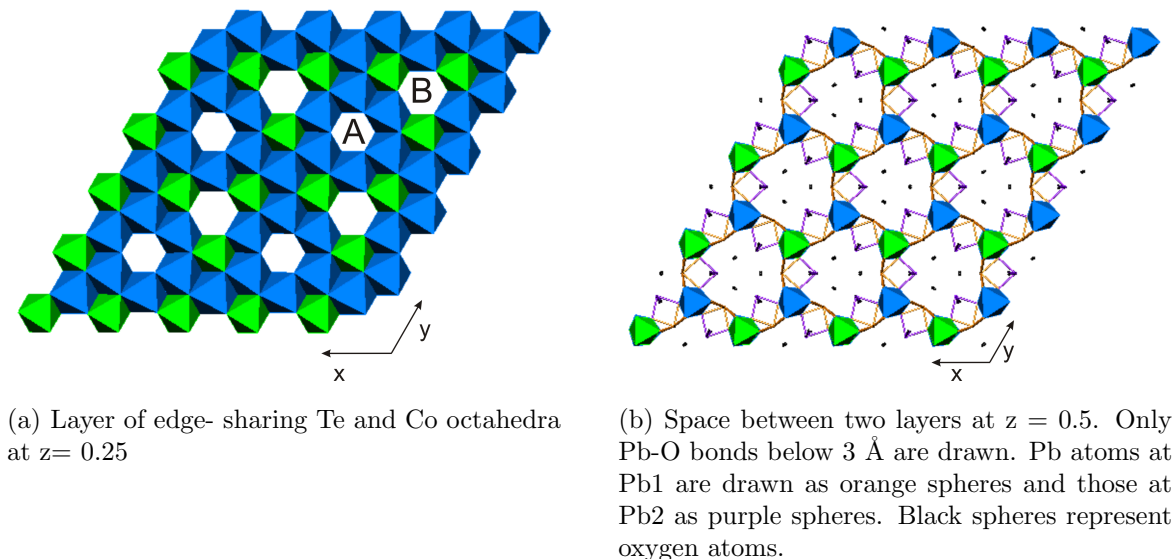
Figure 11.2: Layer and space between layers. The [TeO$_6$]-octahedra are displayed in green and [CoO$_6$]-octahedra in blue.

The layers are linked by pairs of face-sharing [TeO$_6$]- and [CoO$_6$]-octahedra, build up by atoms at position Te1, Co1 and O1. The cations are located at a 3-fold rotation axis along [001]. They link to the layers by capping the holes, where the A holes are connected to [TeO$_6$]-octahedra, and the B holes by [CdO$_6$]-octahedra. Since there are equal numbers of rings exclusively built up by [CoO$_6$]-octahedra and rings built up by alternation [TeO$_6$] and [CoO$_6$]-octahedra, the number of the capping octahedra-pairs are the same.

The bond distance of the Te1-O1 bond is significantly larger than those of the other Te-O bonds (Tab. 11.2). Its value is 1.99 Å compared to a range of 1.91 Å to 1.94 Å for the other bonds. An even greater effect can be observed for the Co1-O1 bond, with a bond distance of 2.26 Å in contrast to 2.01 - 2.11 Å.

The reason for this effect is probably the coordination of the lead atoms. Due to the space requirement of the Pb lone pair, the space between the layers is expanded, which goes along with a lengthening of the Te-O and Co-O bonds.

Table 11.2: Selected bond lengths [Å] and angles [°] in $Pb_6Co_9Te_5O_{30}$

Pb1 - O1	2.417 (2x), 3.159 (2x)	Pb2 - O1	2.385 (2x)
Pb1 - O2	2.727 (2x)	Pb2 - O2	3.796 (2x)
Pb1 - O3	2.726 (2x)	Pb2 - O3	3.768 (2x)
Pb1 - O4	3.229 (2x)	Pb2 - O4	3.326 (2x), 3.457 (2x)
Pb1 - O5	3.741 (2x)	Pb2 - O5	2.425 (2x)
Te1 - O1	1.994 (3x)	Te2 - O3	1.917 (2x)
Te1 - O2	1.910 (3x)	Te2 - O4	1.931 (2x)
		Te2 - O5	1.944 (2x)
Co1 - O1	2.262 (3x)	Co2 - O4	2.109 (6x)
Co1 - O3	2.008 (3x)		
Co3 - O2	2.083 (2x)	Co4 - O2	2.066 (2x)
Co3 - O4	2.092 (2x)	Co4 - O3	2.112 (2x)
Co3 - O5	2.110 (2x)	Co4 - O5	2.074 (2x)
cis-oxygen		trans-oxygen	
O - Te1 - O	84.1 - 99.1	O - Te1 - O	168.5
O - Te2 - O	86.0 - 93.6	O - Te2 - O	177.8 - 178.9
O - Co1 - O	72.3 - 108.1	O - Co1 - O	153.7
O - Co2 - O	79.2 - 97.1	O - Co2 - O	175.0
O - Co3 - O	78.9 - 96.2	O - Co3 - O	173.3 - 174.3
O - Co4 - O	77.9 - 96.9	O - Co4 - O	169.0 - 174.8
Te1 - O1 - Co1	86.4		

The lead atoms are located in the space between the layers, at about equal distances to the layers at 2- fold rotation axes along [010]. The coordination sphere of the lead atoms is distinguished in two parts. Accounting only bonds below 3 Å, Pb atoms at positions Pb1 have six coordination partners and those at Pb2 four. The difference to the next oxygen atoms is 0.4 Å in case of Pb1 and 0.9 Å for Pb2. It is likely that the $6s^2$ lone pair of Pb^{2+} is located in this space. All primary bonding oxygen are located between the two Pb atoms, leaving space on the other side of the Pb atoms for their lone pairs.

The structure has some similarities with hexagonal perovskites, where also edge- and face-sharing octahedra are very common. One compound which also shows layers of edge-sharing octahedra, connected among others through face sharing octahedra, is the magnetoplumbite $BaFe_{12}O_{19}$ [61].

Chapter 12

$PbAl_8Ca_2O_{15}$

This compound does not contain Te, but was found as a side product during experiments trying to synthesise Pb_2CaTeO_6.

12.1 Experimental

12.1.1 Preparation

A mixture of 1.16g (1.50 mmol) $2\,PbCO_3 \cdot Pb(OH)_2$, 0.075 g (0.75 mmol) $CaCO_3$ and 0.117 g (0.73 mmol) TeO_2 was well ground and put in a corundum crucible. It was then heated for 18 hours to 950°C, kept at this temperature for 6 hours and then cooled for 18 hours to room temperature. Few colourless crystals were isolated from a brick red powder. A colourless block-shaped crystal was selected for single crystal X-ray diffraction.

The educt mixture did not contain aluminium. The origin of the Al atoms in the crystals is the corundum crucibles, which were seriously attacked during the high-temperature synthesis. Directed attempts to synthesise the compound were successfully from PbO, $CaCO_3$ and $Al(OH)_3$ in stoichiometric ratio at temperatures above 1000°C, but not pure-phase.

12.1.2 Data collection and refinement

The crystal was found to have an orthorhombic cell, but was measured based on a triclinic cell to record all possible reflections. Data was collected on ω and ϕ scans in 7 runs. It was then integrated in the orthorhombic system. Structure solution was successful in space group *Pnma*. The parameters of the data collection, structure solution and refinement are given in Tab. C.9 in the appendix.

12.2 Structure

12.2.1 Structure solution

The compound crystallises in the orthorhombic system, with a unit cell of $V = 1334.95(3)$ Å^3. The other cell parameters are $a = 5.37020(10)$ Å, $b = 27.9903(4)$ Å and $c = 8.88110(10)$ Å. The space group is *Pnma*. A list of the atom positions and their Wyckoff positions are displayed in Tab. 12.1, selected bond lengths and angles are given in Tab. 12.2.

Table 12.1: List of atom positions and Wyckoff positions in PbCa$_2$Al$_8$O$_{15}$

Atom	Wyckoff	x	y	z	U_{eq}
Pb1	4(c)	0.928092(16)	$\frac{1}{4}$	0.455720(10)	0.00952(2)
Ca1	8(d)	0.06047(5)	0.110812(11)	0.56641(3)	0.00581(4)
Al1	8(d)	0.12604(10)	0.038858(18)	0.83700(6)	0.00558(7)
Al2	8(d)	0.01851(10)	0.189427(18)	0.84718(6)	0.00553(7)
Al3	8(d)	0.97314(10)	0.161643(18)	0.18773(6)	0.00615(7)
Al4	8(d)	0.19006(10)	0.058661(19)	0.19385(6)	0.00720(8)
O1	4(c)	0.5422(4)	$\frac{1}{4}$	0.6021(2)	0.0100(3)
O2	8(d)	0.2543(2)	0.05825(5)	0.00377(13)	0.00904(17)
O3	8(d)	0.8352(2)	0.06360(4)	0.79567(14)	0.00794(16)
O4	8(d)	0.1025(2)	0.97666(4)	0.80357(14)	0.00847(17)
O5	8(d)	0.8882(2)	0.15915(5)	0.00045(14)	0.00939(18)
O6	8(d)	0.3323(2)	0.17341(5)	0.80944(14)	0.00910(17)
O7	8(d)	0.7575(2)	0.19359(5)	0.29947(15)	0.00959(18)
O8	8(d)	0.5308(3)	0.10693(5)	0.21771(14)	0.01045(19)
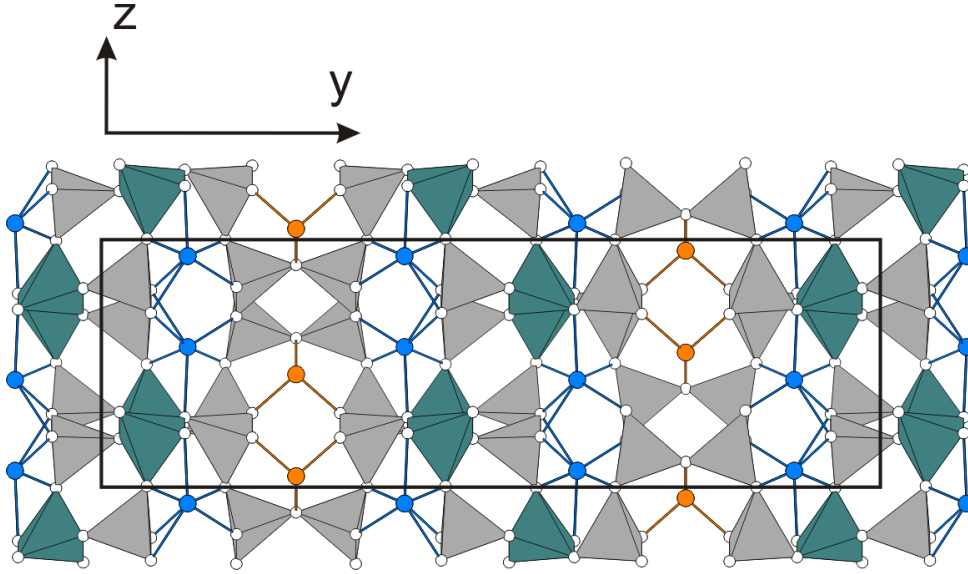
Figure 12.1: Structure of PbAl$_8$Ca$_2$O$_{15}$ projected on (100). [AlO$_4$]-tetrahedra are displayed in grey, [AlO$_5$]-units as green trigonal bipyramides. The Pb atoms are drawn as orange spheres and the Ca atoms as blue spheres.

12.2.2   Description of the structure

The structure is build up by a regular network of interconnecting [AlO$_4$]-tetrahedra and [AlO$_5$]-bipyramides. The Ca atoms and the Pb atoms are distributed in this network. A projection of the unit cell is given in Fig. 12.1.

Al atoms at positions Al1, Al2 and Al3 are coordinated to four oxygen atoms and form slightly distorted tetrahedra. The bond lengths vary from 1.72 Å to 1.77 Å (Tab. 12.2). The tetrahedral angles vary from about 100° to 119°.

(a) Coordination sphere of Ca

(b) Trigonal bipyramidal coordination sphere of Al4
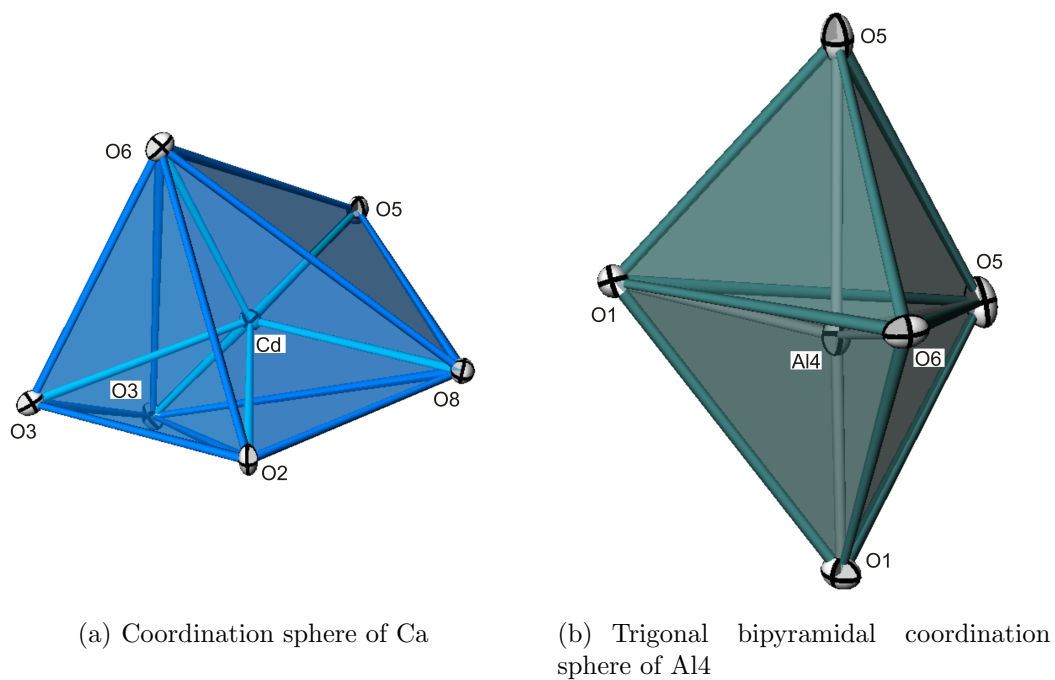
Figure 12.2: Coordination spheres of Ca and Al4.

(a) Double rings formed by corner-sharing $[AlO_4]$-tetrahedra, of Al atoms at position Al2

(b) Assembly of $[Al_{04}]$-tetrahedra and $[Al_{05}]$-trigonal bipyramides, of Al atoms at positions Al1, Al3 and Al4
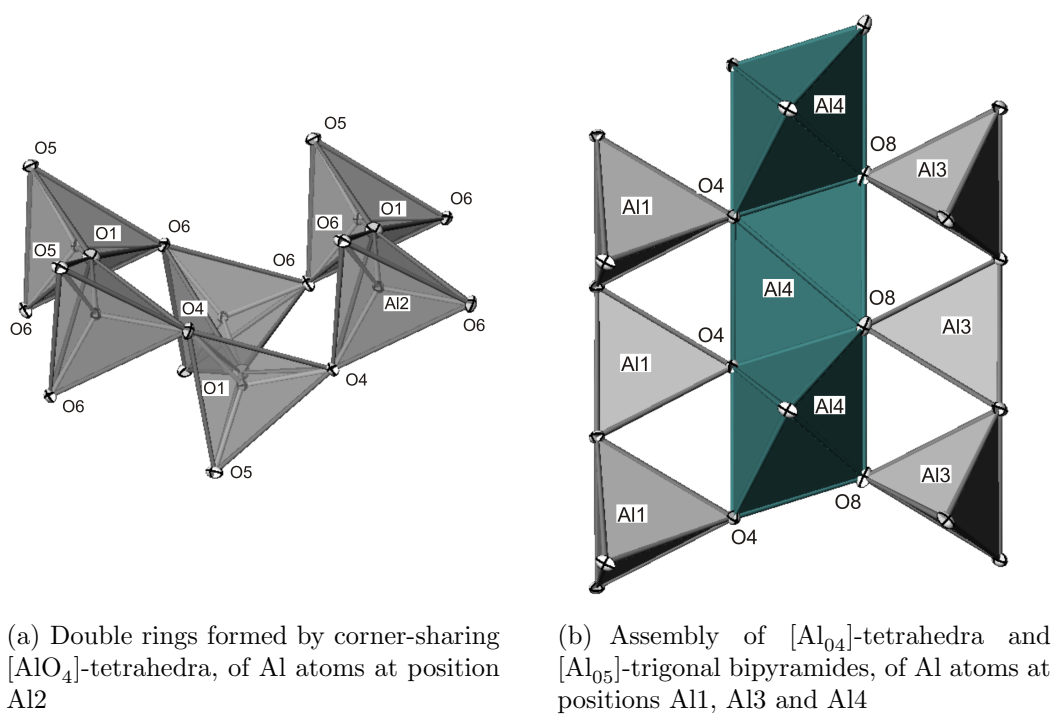
Figure 12.3: Different assemblies of the Al-O coordination polyhedra
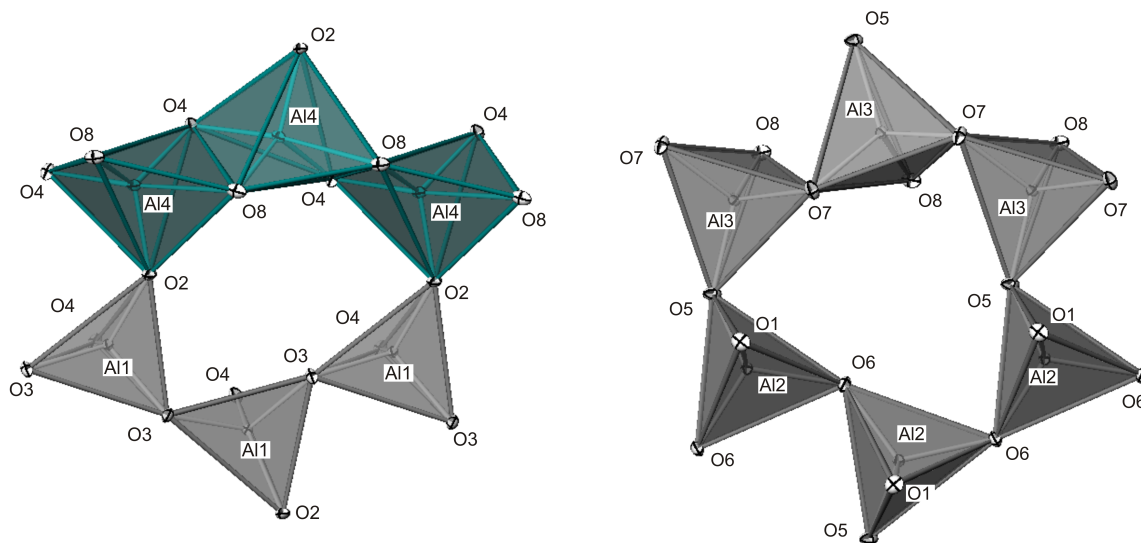
(a) Rings formed by [Al1O$_4$]-tetrahedra and [Al4O$_5$]-trigonal bipyramides

(b) Rings formed by [Al2O$_4$] and [Al3O$_4$] tetrahedra

Figure 12.4: Rings formed by corner sharing Al tetrahedra and edge sharing Al bipyramides

In contrast Al4 atoms are surrounded by oxygen atoms in the form of a trigonal bipyramid, with one bond significantly larger than the others. A clinographic projection of the [AlO$_5$] trigonal bipyramid is given in Fig. 12.2(b). The bond length for the Al4-O bonds varies from 1.723 Å to 1.857 Å and 2.285 Å for the long bond. although the long bond is about 0.4 Å larger than the others, it is still much smaller for this atom than for the other Al atoms. According to bond valence calculations this longer bond contributes 0.18 vu to the valence sum of Al and therefore is included to the primary coordination sphere.

Due to the long bond, the Al4 atom is shifted from the centre plane of the bipyramid towards one apex of the bipyramid. The O-Al4-O angles of oxygen in the plane are between 114.04° and 122.2°. The angle between the apex oxygen and those of the plane varies from 77.1 - 103.1°. The main axis of the bipyramid is also tilted and has an angle of 172.2°.

The [AlO$_4$]-tetrahedra are corner linked to other tetrahedra and bipyramides. The [AlO$_5$] bipyramides also share edges with other bipyramids. The tetrahedra formed by Al2 are connected to two condensed four membered rings (Fig. 12.3(a)). This double ring is not planar, but shaped in form of a half-ring. Three [Al2O$_4$]-tetrahedra are linked together with three [Al3O$_4$]-tetrahedra to a six-membered ring as pictured in Fig. 12.4(b).

These three [Al3O$_4$]-tetrahedra link to three edge-sharing [Al4O$_5$] bipyramids, which are then linked to three Al1 tetrahedra. This assembly has also the shape of a half ring. A picture of this assembly is given in Fig. 12.3(b). The [Al1O$_4$]-tetrahedra form as well six-membered ring with three [Al4O$_5$] bipyramids of the next assembly (Fig. 12.4(a)). The distribution of these structure units is displayed in Fig. 12.5.

The position of the Pb atoms is located at a mirror plane. They bond only to three oxygen atoms with bond lengths below 3 Å. The coordination sphere has the shape of a trigonal pyramid with Pb at the top. The oxygen atoms with bond length of 3.035 Å are also located at the side

Table 12.2: Selected bond lengths [Å] and angles [°] in $PbCa_4Te_4O_{14}$

Al1 - O	1.721	1.747	1.769	1.771
Al2 - O	1.750	1.759	1.771	1.776
Al3 - O	1.726	1.768	1.773	1.774
Al4 - O	1.723	1.780	1.781	1.857
	2.285			
Pb - O	2.293	2.446	3.035	3.280
	3.545	3.567	3.876	3.974
Ca - O	2.293	2.298	2.329	
	2.406	2.531	2.712	
O - Al1 - O	101.27 - 118.88			
O - Al2 - O	102.89 - 119.08			
O - Al3 - O	104.75 - 117.86			
O - Al4 - O	77.08 - 103.11		114.04 - 122.22	
	172.62			
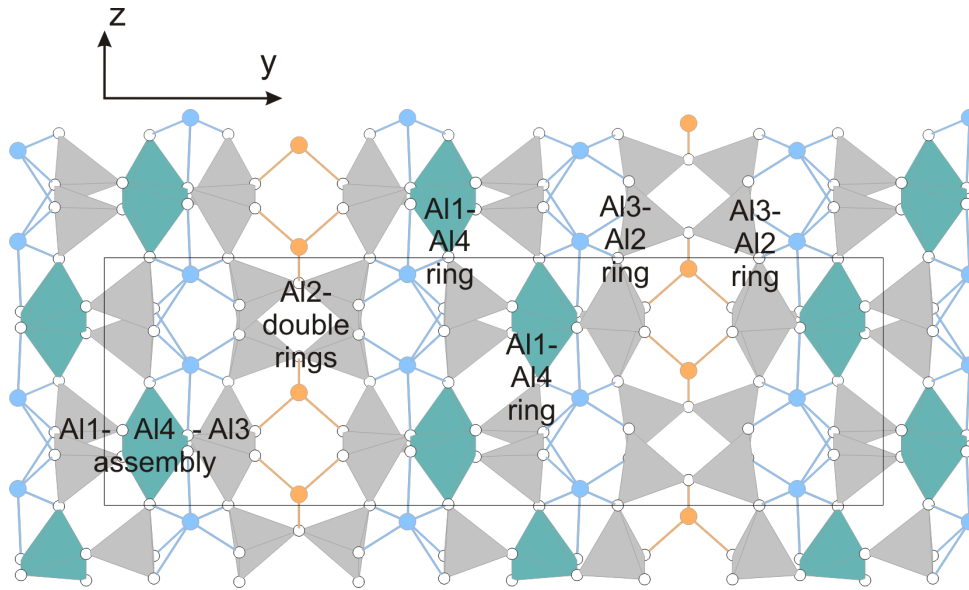
Figure 12.5: Distribution of the Al-structure units in $PbAl_8Ca_2O_{15}$

of the shortly bonded oxygen atom. The remote oxygen atoms are located on the other side of the hemisphere, leaving space for the lone pair electrons of Pb. The Pb atoms connect the Al2 double rings and the Al1,3,4 assembly over the oxygen of the $[Al3O_4]$- tetrahedra (Fig. 12.5).

The coordination sphere of Ca in a 6-fold coordination is irregular shaped (Fig. 12.2(a)). The Ca-O bond lengths vary from 2.293 to 2.712 Å. The Ca atoms fill the space between the Al-O network, which is not occupied by Pb (Fig. 12.1). The Ca atoms are located between three Al1,3,4 assemblies and one Al2 double ring. The $[CaO_6]$-spheres themselves are corner-sharing and form zig-zag chains along [100].

Chapter 13

Preliminary structure models

The structure models presented here are preliminary, due to poor quality of the crystals and possible twinning they could not be refined to satisfying R values.

13.1 $PbCa_4Te_3O_{14}$

13.1.1 Experimental

Preparation

A mixture of 1.032 g (1.33 mmol) $2\,PbCO_3 \cdot Pb(OH)_2$, 0.600 g (10.3 mmol) $CaCO_3$ and 0.959 g (6.5 mmol) TeO_2 was well-ground and pressed into a pellet. It was then heated in a corundum crucible according to temperature program 6 in Fig. 1.1(f). A small colourless crystal was selected for single crystal X-ray diffraction.

Data collection and refinement

The crystal was measured on basis of a triclinic cell in 8 runs. Data was then integrated using a monoclinic cell in the standard setting. Structure solution was not possible, therefore CELLNOW and TWINABS were applied. With their help two twin domains were determined, where 5366 unique reflections were assigned to the first domain and 5368 to the second one. The structure could now be solved, but to unsatisfying R values. A second crystal with the same unit cell dimensions was measured, again on basis of a triclinic cell in 11 runs. This time a direct structure solution was possible and to better R values than for the first measurement. Several twin laws have been applied, best result was achieved with the matrix displayed below (13.1).

$$\begin{pmatrix} 0 & 1 & 0 \\ 1 & 0 & 0 \\ 0 & 0 & \bar{1} \end{pmatrix} \tag{13.1}$$

One problem in the current model pertains to the anisotropic displacement parameters of Te, which are negative. Site occupancies were refined to the ideal values and therefore fixed again. Still the R values could not be refined to satisfying values and additionally the oxygen atoms could not be refined anisotropically. Attempts to grow crystals of higher quality were not successful. Parameters of data collection and structure refinement are listed in Tab. C.10 in the appendix.

13.1.2   Structure
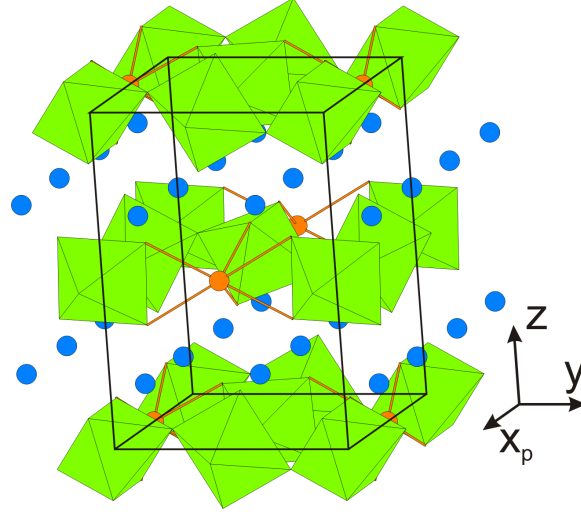
Figure 13.1: Unit cell of $PbCa_4Te_3O_{14}$. The $[TeO_6]$-octahedra are displayed in green. The Pb atoms are painted as orange spheres and Ca atoms as blue spheres. Pb-O bonds below 3 Å are drawn.

The structure was finally solved in space group $P2_1/n$, with cell parameters $a = 7.4514(7)$ Å, $b = 7.4457(7)$ Å and $c = 10.4067(9)$ Å. The monoclinic angle is $\beta = 90.095(5)°$ and the volume of the unit cell $V = 577.37(9)$ Å^3. The compound crystallises in a distorted chiolite structure [62]. A list of atom positions is given in Tab. 13.1.
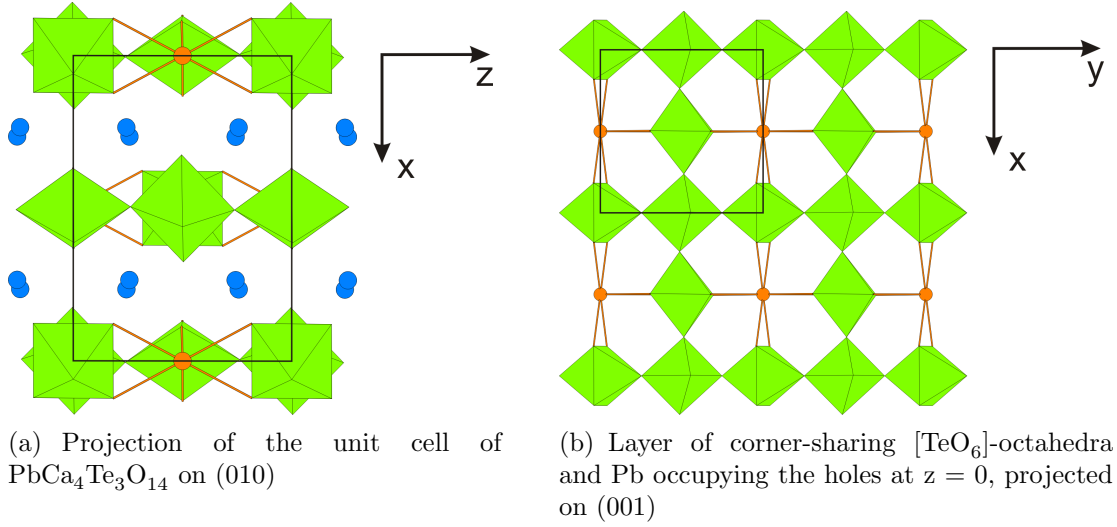
Table 13.1: List of atom positions and Wyckoff positions in $PbCa_4Te_3O_{14}$

Atom	Wyckoff	x	y	z	U_{eq}
Pb1	2(d)	$\frac{1}{2}$	0	0	0.0227(2)
Te1	2(a)	0	0	0	0.00415(17)
Te2	2(b)	0	0	$\frac{1}{2}$	0.00388(17)
Te3	2(c)	$\frac{1}{2}$	0	$\frac{1}{2}$	0.00513(16)
Ca1	4(e)	0.2432(3)	0.2366(3)	0.2348(2)	0.0128(4)
Ca2	4(e)	0.7571(3)	0.2372(3)	0.2350(2)	0.0122(4)
O1	4(e)	0.0000(7)	0.2528(7)	0.0602(4)	-0.0016(7)
O2	4(e)	0.1821(10)	0.9603(8)	0.1212(6)	0.0043(9)
O3	4(e)	0.9959(18)	0.5542(14)	0.1755(10)	0.029(2)
O4	4(e)	0.4993(18)	0.6781(15)	0.1309(11)	0.030(2)
O5	4(e)	0.4963(17)	0.3047(14)	0.1125(11)	0.026(2)
O6	4(e)	0.8170(9)	0.9586(8)	0.1228(6)	0.0031(9)
O7	4(e)	0.238(4)	0.487(5)	0.995(3)	0.133(13)

Structure Description

As in the ideal chiolith structure with general formula $A_5B_3X_{14}$ [62, 63], a network of corner-sharing $[TeO_6]$-octahedra builds up layers perpendicular to [001], where one fourth of the octa-

hedra is replaced by a Pb atom (Fig. 13.1).

(a) Projection of the unit cell of $PbCa_4Te_3O_{14}$ on (010)

(b) Layer of corner-sharing $[TeO_6]$-octahedra and Pb occupying the holes at z = 0, projected on (001)

Figure 13.2: Different projection of the structure of $PbCa_4Te_3O_{14}$. The $[TeO_6]$-octahedra are displayed in green. The Pb atoms are painted as orange spheres and Ca atoms as blue spheres. Pb-O bonds below 3 Å are drawn.

Table 13.2: Selected bond lengths [Å] and angles [°] in $PbCa_4Te_4O_{14}$

Ca1 - O	2.308	2.327	2.332
	2.416	2.547	2.567
Ca2 - O	2.284	2.330	2.376
	2.422	2.507	2.571
Pb - O	2.553 (2x)	2.701 (2x)	
	2.702 (2x)	2.757 (2x)	
Te1 - O	1.874 (2x)	1.895 (2x)	1.984 (2x)
Te2 - O	1.867 (2x)	1.901 (2x)	1.950 (2x)
Te3 - O	1.780 (2x)	1.871 (2x)	1.944 (2x)

cis-oxygen		trans-oxygen	
O - Te - O	83.7 - 96.3	O - Te - O	180
O - Ca1 - O	83.5 - 94.0	O - Ca1 - O	167.8 - 176.0
O - Ca2 - O	72.5 - 105.1	O - Ca2 - O	167.3 - 175.6

The holes are arranged in a way, that the Pb atoms connect four octahedra, as displayed in Fig. 13.2(b). Therefore two-thirds of the Te octahedra are only connected to two other octahedra, the others, with Te occupying the Te1 position, are linked to four other octahedra. The $[TeO_6]$-octahedra are almost perfect, but in contrast to the ideal chiolith structure tilted. Tilting occurs along [100] and [010], with tilt angles about 45°. Every second layer is shifted half of the *ab* base diagonal in direction [110]. All the atoms in the layer occupy special positions at inversion centres.

The Pb-O coordination sphere has the shape of a compressed cube, caused by the tilting of the $[TeO_6]$-octahedra (Fig.13.3).
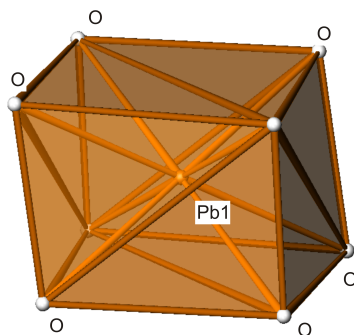
Figure 13.3: [PbO$_8$] cubic coordination sphere.

The Ca atoms are located between the layers, shifted from the ideal position of the chiolith structure (Fig.13.2(a)). They are coordinated to six oxygen atoms and build up a layer of corner- and edge-sharing distorted octahedra. They also share corners with those [TeO$_6$]-octahedra, which are connected to [PbO$_8$]-cubes.

13.1.3   Discussion

The cell parameters were found to be almost the same as for Ca$_5$Te$_3$O$_{14}$ [64]. In this structure one Ca atom occupies the 2(d) position, but its anisotropic temperature factor is 5 times higher than those for the other Ca atoms. There is no doubt about the Pb atom occupancy in the here presented structure, as the refined site occupancies are very stable. Furthermore orthorhombic space group *Cmca* is reported in [64], therefore the volume of the cell was twice that of the monoclinic cell. Although the monoclinic angle in the here presented structure is very close to 90° and *a* compared to *b* are almost equal, they deviate too much from the orthorhombic metric. It is very likely that the cell for Ca$_5$Te$_3$O$_{14}$ was wrongly assigned, due to twinning. Ca-O bond lengths vary from about 2.3 Å to 2.6 Å and hence are 0.2 Å shorter than the average Pb- O bond lengths. This was also reported for compound Ca$_5$Te$_3$O$_{14}$. Due to the reasons described above the sum formula reported for Ca$_5$Te$_3$O$_{14}$ is doubtful. Attempts to grow single crystals of Ca$_5$Te$_3$O$_{14}$ were not successful.

The systematic polysynthetic twinning of chiolite structures is well known and reported for other compounds [65]. That is one reason why many of the structure determinations have been performed on powders. The question whether the true symmetry is monoclinic or orthorhombic arise also for the distorted structure of α-Na$_5$Cr$_3$F$_{14}$, but latest results suggest monoclinic space group $P2_1/n$ [65].

In contrast to most other compounds described here, no separation of Pb-O bonds in primary and secondary ones could be observed.

13.2   PbCuTeO$_5$

13.2.1   Experimental

Preparation

This compound was isolated from a sample containing 0.671 g (3.0 mmol) PbO, 0.119 g (1.5 mmol) CuO and 0.322 g (2.0 mmol) TeO$_2$, which was heated in four hours to 750°C and after 48 h cooled slowly to room temperature. Different crystals were isolated with black, dark green and turquoise colour. The black ones were identified as PbCu$_3$TeO$_7$ [31] , the dark green as a

derivative of $Pb_{22}Te_7MO_{44.5}$ (see Chapter 13.3), but there was no equivalent in literature for the turquoise crystal, therefore a very thin one was selected for single crystal X- ray diffraction.

Data collection and Refinement

Data were collected in 7 runs on a triclinic cell. Integration showed some hint of twinning, therefore CELLNOW was applied. Two twin domains of same size were recognized, but numerous reflections were assigned to both domains.

The composition of the compound stayed ambiguous until EDX measurements were performed, which gave a Pb:Cu:Te ratio of 1:1:1. The structure could then be solved in space group $P\bar{1}$, but converged at to high R values. An image of the crystal from EDX measurements is given in Fig. 13.4.
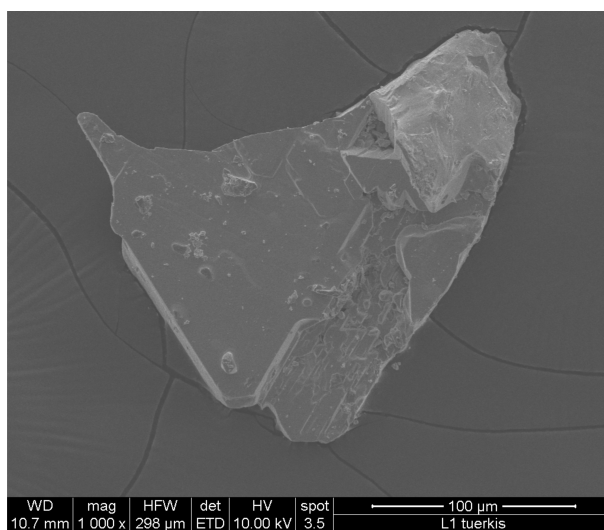
Figure 13.4: Image of a crystal of $PbCuTeO_5$ measured with EDX.

The major problems in the structure model are the high R values and the remaining electron densities, caused probably by a more complex twinning than the modelled one. Attempts to grow crystals of better quality were not successful, therefore the current solution was the best achieved. Parameters of the data collection and current refinement are given in Tab. C.11 in the appendix.

13.2.2 Structure

Preliminary structure model

The cell parameters for the current solution are a = 6.4119(4) Å, b = 11.2601(8) Å and c = 12.2686(8) Å and angles of α = 107.708(5)°, β = 90.939(5)° and γ = 90.452(5)°. The volume of the unit cell is V = 843.62 Å^3 with space group $P\bar{1}$.

Description

The structure is built up by a network of corner-sharing [TeO_6]-octahedra, linked by Pb and Cu atoms, where the [TeO_6]-octahedra are not connected only through trans-oxygen atoms in the octahedron, but also cis-oxygen atoms (Fig. 13.5). These chains are generally orientated along
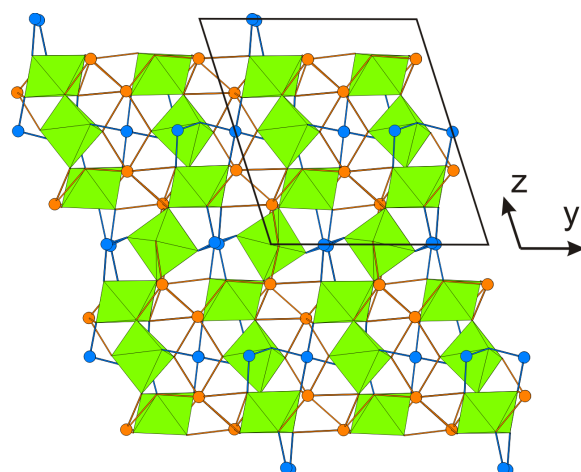
**Figure 13.5:** Projection of the structure of $PbCuTeO_5$ on (100). $[TeO_6]$-octahedra are displayed in green, Cu atoms as blue spheres and Pb atoms as orange spheres. Pb-O bond below 3 Å and Cu-O bonds below 2 Å are plotted.

$[\bar{2}21]$, but deflected. Te and O atoms build up almost regular octahedra with angles close to $90°$ and $180°$ respectively (Tab. 13.4).

The oxygen-coordination spheres of the Cu atoms are not easy definable due to their Jahn-Teller distortions. They are either coordinated to [4+2] oxygen, [4+1] or 4 oxygen atoms, if long range Cu-O bonds up to 2.7 Å are respected. Those which build up distorted octahedra, occupy a special position at an inversion centre, Cu atoms at position Cu3 to Cu5 are in a square-pyramidal coordination sphere and Cu2 build square-planar coordination spheres. If only the short range oxygen bonds are considered, then the coordination sphere for all Cu atoms is square-planar. Images of all coordination spheres are given in Figs. 13.6(a) to 13.6(c). The primary coordination spheres of Cu build chains of corner-sharing planes in no particular direction and are connected to the $[TeO_6]$-octahedra through one oxygen atom.

(a) Octahedral coordination sphere

(b) Square-pyramidal coordination sphere

(c) Square-planar coordination sphere
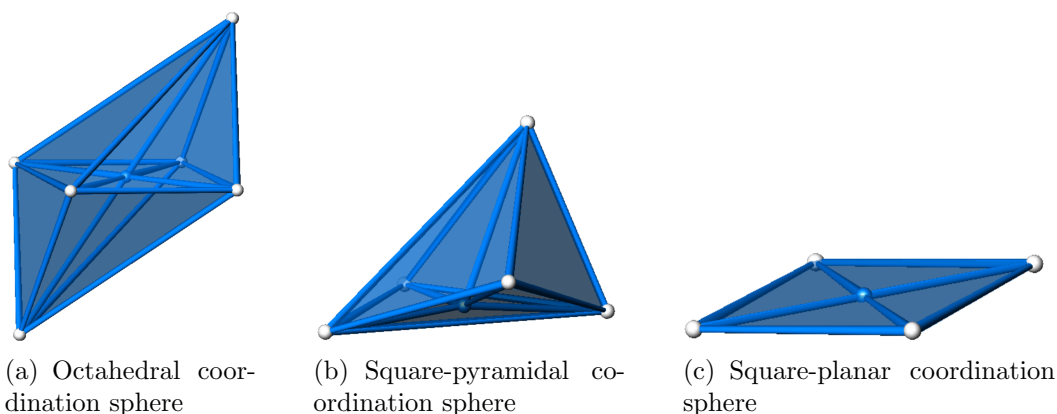
Figure 13.6: Coordination spheres of Cu. Cu atoms are displayed as blue spheres and oxygen atoms as white spheres.

The Pb-O coordination sphere is as well difficult to describe. The bond lengths distribute from 2.390 Å to 3.618 Å. A differentiation between primary and secondary bonds can only be observed for Pb1, where oxygen atoms with bond lengths up to 2.9 Å are arranged in a hemisphere around the Pb atoms.

Table 13.3: List of atom positions and Wyckoff positions in PbCuTeO$_5$

Atom	Wyckoff	x	y	z	U_{eq}
Pb1	2(i)	0.98752(14)	0.94823(9)	0.32880(7)	0.0137(2)
Pb2	2(i)	0.01349(15)	0.55990(9)	0.17878(8)	0.0178(2)
Pb3	2(i)	0.51596(15)	0.44400(9)	0.32203(7)	0.0171(2)
Pb4	2(i)	0.48627(16)	0.06170(10)	0.17627(8)	0.0216(2)
Te1	1(a)	0	0	0	0.0043(3)
Te2	1(e)	$\frac{1}{2}$	$\frac{1}{2}$	0	0.0041(3)
Te3	2(i)	0.55003(18)	0.75370(10)	0.25305(10)	0.0048(2)
Te4	2(i)	0.97115(18)	0.26486(11)	0.24741(9)	0.0049(2)
Te5	2(i)	0.26384(19)	0.75617(11)	0.50000(9)	0.0051(3)
Cu1	1(f)	$\frac{1}{2}$	0	$\frac{1}{2}$	0.0063(6)
Cu2	1(g)	0	$\frac{1}{2}$	$\frac{1}{2}$	0.0066(6)
Cu3	2(i)	0.3034(4)	0.7577(2)	0.00104(19)	0.0066(4)
Cu4	2(i)	0.7555(4)	0.7363(2)	0.50523(18)	0.0071(5)
Cu5	2(i)	0.8072(4)	0.7428(2)	0.00790(19)	0.0077(4)
O1	2(i)	0.017(2)	0.6559(14)	0.4684(13)	0.009(3)
O2	2(i)	0.546(2)	0.6543(12)	0.9709(10)	0.003(2)
O3	2(i)	0.374(2)	0.8246(14)	0.1647(11)	0.010(3)
O4	2(i)	0.208(2)	0.8154(13)	0.6649(11)	0.008(3)
O5	2(i)	0.478(2)	0.1492(12)	0.4599(11)	0.004(2)
O6	2(i)	0.791(2)	0.4737(14)	0.0139(11)	0.007(3)
O7	2(i)	0.049(2)	0.8511(13)	0.0374(11)	0.008(3)
O8	2(i)	0.131(2)	0.3326(13)	0.1528(12)	0.013(3)
O9	2(i)	0.711(2)	0.2597(14)	0.1613(11)	0.012(3)
O10	2(i)	0.707(2)	0.6740(14)	0.3421(12)	0.011(3)
O11	2(i)	0.298(2)	0.7311(14)	0.3361(11)	0.011(3)
O12	2(i)	0.798(2)	0.7605(14)	0.1692(11)	0.012(3)
O13	2(i)	0.708(2)	0.9685(14)	0.0099(12)	0.012(3)
O14	2(i)	0.221(2)	0.2549(15)	0.3338(12)	0.012(3)
O15	2(i)	0.900(3)	0.4278(12)	0.3406(12)	0.012(3)
O16	2(i)	0.103(2)	0.8976(13)	0.4959(12)	0.012(3)
O17	2(i)	0.419(2)	0.6121(13)	0.5006(11)	0.008(3)
O18	2(i)	0.622(3)	0.9210(13)	0.3500(11)	0.015(3)
O19	2(i)	0.477(3)	0.5800(14)	0.1623(13)	0.012(3)
O20	2(i)	0.030(2)	0.0885(13)	0.1626(13)	0.011(3)

13.2.3   Discussion

Some analogies to the known Pb-Cu-Te oxide PbCu$_3$TeO$_7$ structure can be noticed [31]. The short range Cu-O bond lengths are comparable with the title compound, and the Jahn-Teller distortion is observed as well, but not that pronounced as in PbCuTeO$_5$. The Cu-O coordination spheres in PbCu$_3$TeO$_7$ are connected to chains along [100].

Table 13.4: Selected bond lengths [Å] and angles [°] in $PbCuTeO_5$. Multiple bonds are declared in the brackets beside.

Pb1 - O	2.390 - 2.671	(4x)	2.93 - 3.437	(5x)
Pb2 - O	2.399 - 2.688	(4x)	2.851 - 3.453	(6x)
Pb3 - O	2.475 - 2.719	(4x)	2.797 - 3.489	(7x)
Pb4 - O	2.470 - 2.721	(4x)	2.785 -3.618	(7x)
Te1 - O	1.895 - 1.945	(6x)		
Te2 - O	1.899 - 1.928	(6x)		
Te3 - O	1.894 - 1.981	(6x)		
Te4 - O	1.883 - 1.975	(6x)		
Te5 - O	1.904 - 1.969	(6x)		
Cu1 - O	1.895 - 1.963	(4x)	2.782	(2x)
Cu2 - O	1.912 - 1.970	(4x)	2.956	(2x)
Cu3 - O	1.925 - 1.962	(4x)	2.621	3.128
Cu4 - O	1.904 - 1.950	(4x)	2.554	2.887
Cu5 - O	1.915 - 1.944	(4x)	2.618	3.054

cis-oxygen		trans-oxygen	
O -Te - O	87.4 - 93.3	O -Te - O	180.0
		O - Te5 - O	175.5 - 178.2

in plane angles		angles of top to plane oxygen	
O - Cu1 - O	88.5 - 91.5	O - Cu1 - O	71.4 - 72.7
O - Cu2 - O	86.6 - 93.4		
O - Cu3 - O	86.0 - 95.1	O - Cu3 - O	68.8
O - Cu4 - O	83.1 - 97.2	O - Cu4 - O	70.9
O - Cu5 - O	85.3 - 95.0	O - Cu5 - O	69.0

13.3 $Pb_{22}Te_7AlO_{44.5}$

13.3.1 Experimental

Preparation

This compound was first isolated from a sample containing 0.895 g (4.0 mmol) PbO, 0.319 g (2.0 mmol) TeO_2 and 2.462 g (10 mmol) PbF_2. This mixture was well ground, pressed into a pellet and heated to 750°C during 12 h, and after 36 h it was removed from the hot furnace. A small clearing reddish crystal was selected for single-crystal X-ray diffraction.

Data collection and refinement

Data were measured based on a triclinic cell in 8 runs. Data was then integrated on a cubic cell, therefore a good redundancy was achieved. Structure solution and subsequent refinement turned out to be difficult. In a first structure model formula sum $Pb_{22}Te_7SiO_{44}F_2$ was considered; the presence of F^- was taken into account on the basis of the preparation conditions, using an excess of PbF_2 as educt. However, EDX analysis revealed no evidence of Si, but Al. Replacing Si with Al in the structure would lead to a charged compound. As O and F cannot be distinguished by X-ray methods and the compound was also obtained from a PbF_2-free sample, a sum formula

of $Pb_{22}Te_7AlO_{44.5}$ is suggested. There is still some doubt about this composition as two anion sites are not fully occupied in the final model. A list of the atom positions is given in Tab. 13.5, where the oxygen position O1 is half-occupied, those at O4 are occupied to 31.25%.

Parameters of data collection and preliminary refinement are displayed in Tab. C.12.

Table 13.5: List of atom and Wyckoff positions in $Pb_{22}Te_7AlO_{44.5}$

Atom	Wyckoff	x	y	z	U_{eq}
Pb1	32(f)	0.15510(5)	0.15510(5)	0.15510(5)	0.0227(4)
Pb2	32(f)	0.38167(6)	0.38167(6)	0.38167(6)	0.0613(7)
Pb3	24(e)	0.21531(13)	0	0	0.0309(5)
Te1	24(d)	0	$\frac{1}{4}$	$\frac{1}{4}$	0.0157(5)
Te2	4(b)	$\frac{1}{2}$	$\frac{1}{2}$	$\frac{1}{2}$	0.0125(10)
Al1	4(a)	0	0	0	0.023(6)
O1	96(k)	0.2348(12)	0.2348(12)	0.3856(19)	0.033(7)
O2	96(j)	0	0.1391(16)	0.2511(17)	0.071(7)
O3	24(e)	0.385(2)	0	0	0.041(8)
O4	32(f)	0.057(4)	0.057(4)	0.057(4)	0.05(3)

13.3.2 Structure

Preliminary structure solution

The compounds attends the cubic system with parameter $a = 16.81540(10)$ Å and a unit cell volume of $V = 4754.68$ Å^3.

Description of the Structure

The compound crystallises in a distinct perovskite super structure with z = 32 relative to an idealized compositions $ABB'X_6$. The unit cell is displayed in Fig. 13.7. The Te atoms are connected to six oxygen atoms, where $\frac{1}{8}$ of the Te position in the superstructure is replaced by Al atoms, and the coordinated oxygen atoms are occupied only by approximately $\frac{1}{3}$. The Pb atoms are distributed in the voids of this network, where $\frac{1}{12}$ of the possible Pb position in the superstructure remains unoccupied.

There is still some doubt about the composition because other cubic crystals with very similar unit cell parameters were also found in samples which were prepared in platinum crucibles. There is also the possibility that this compound is actually the same as described in the next section, as their cell parameters are almost the same. Derivatives with suggested sum formula $Pb_{22}Te_7MO_{44}$, M = Cu, Ni. Mn and Co were obtained during other experiments. All had a cell parameter of approximately $a = 16.9$ Å, but different colours. When refining the structure one or two anion sites could not be assigned unambiguously, and therefore charged compounds were obtained.

13.4 Lead orthotellurate

Kosse et al. claimed having determined the symmetry of Pb_3TeO_6 to be monoclinic [19]. When trying to prepare crystals according to their description, the compound Pb_6CdTeO_{10} was ob-
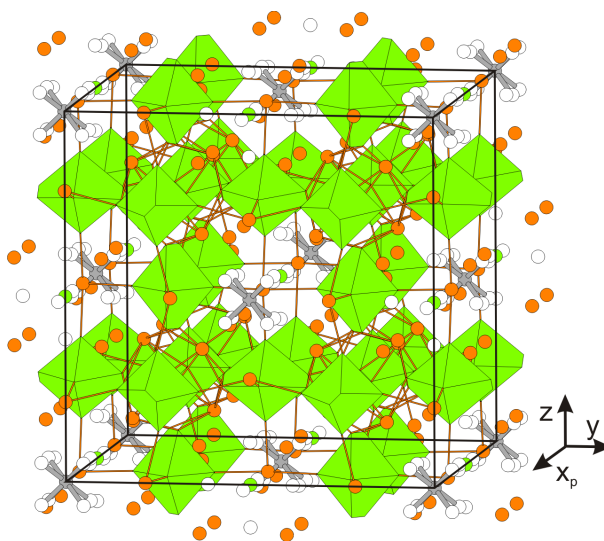
Figure 13.7: Clinographic projection of the structure of $Pb_{22}Te_7AlO_{44.5}$. The $[TeO_6]$-octahedra are displayed in green. The lead atoms are drawn as orange spheres and Al atoms as grey spheres, surrounded by non-fully occupied oxygen atoms, displayed as white spheres.

tained, with the same cell parameters they have determined for 'Pb_3TeO_6'.

13.4.1   Experimental

Preparation

The sample was prepared from 1.011 g (4.5 mmol) PbO and 0.242 g (1.5 mmol) TeO_2, which was well-ground and pressed. It was then heated according to temperature program 1 in Fig. 1.1(a) and after regrinding again heated according to temperature program 6 displayed in Fig. 1.1(f). Very small orange-red crystals could be isolated.

Data collection and structure solution

A cubic cell with cell dimensions $a \approx 33.6$ Å with very weak superstructure reflections was determined. Structure solution based on a measurement with Mo radiation remained unsuccessful. The internal R value was very high (≈ 0.3), when considering the cubic cell. Even applications of a numerical absorption correction let to no improvement in data quality. Therefore the crystal was measured again with Ag radiation, which confirmed the large cell with a refined parameter $a=33.5715(14)$ Å. However, structure solution still was not successful, even when lowering the symmetry to triclinic. The presence of very weak superstructure reflections apparently hampered a reasonable localization of the oxygen atoms. Nevertheless, the doubled parameter a with respect to the structure of $Pb_{22}Te_7O_{44.5}$ points to another double-perovskite structure, now with a 64-fold superstructure relative to the simple perovskite aristotype. To solve and refine such a large structure, high-quality data are required, that could not be achieved in the present case.

Part V

Thermal behaviour

Chapter 14

Thermal behaviour

14.1 Experimental

It was possible to synthesise four compounds in pure phase form, these are Pb_5TeO_8, Pb_6CdTeO_{10} and the two double-perovskites Pb_2CdTeO_6 and Pb_2CaTeO_6. TG and DSC measurements have been performed on all compounds. The two double-perovskite phases Pb_2CdTeO_6 and Pb_2CaTeO_6 were also analysed by temperature-dependent powder X-ray diffraction.

The synthesis of the pure phase powders is described in the corresponding chapters.

14.2 DSC and TG

14.2.1 Analysis of compound Pb_5TeO_8
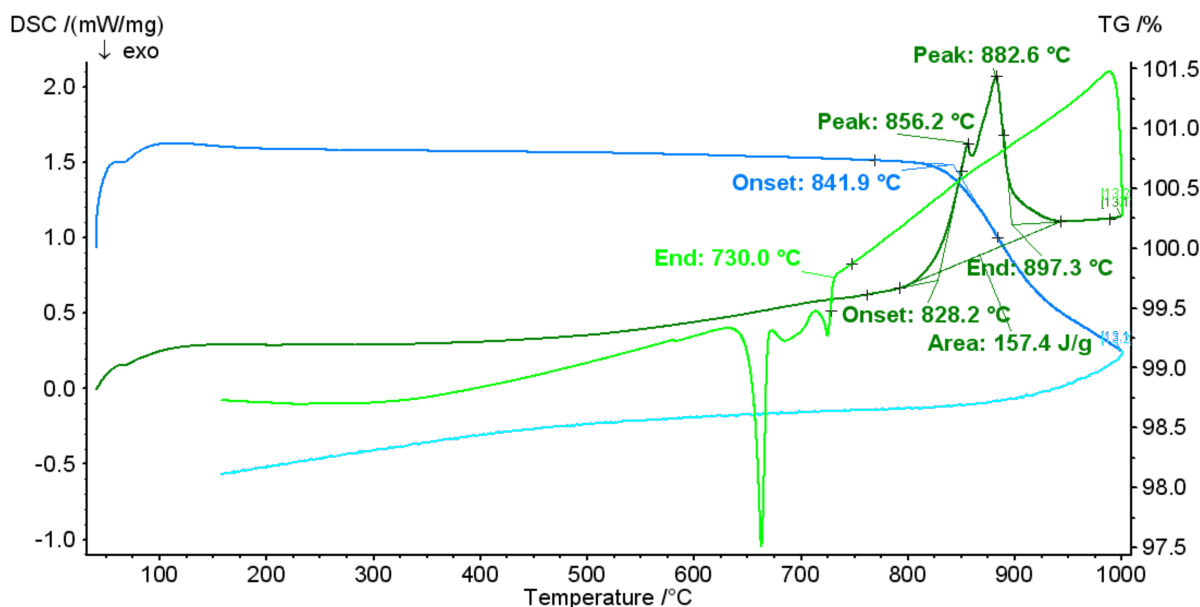
Figure 14.1: TG (blue) and DSC (green) heating curves of Pb_5TeO_8. The cooling curves are displayed in the corresponding bright colours. TG shows decomposition of the sample starting at about 840°C. The DSC curves show an endothermic effect at the same temperature.

The DSC analysis of Pb_5TeO_8 up to 1000°C shows an endothermic effect starting at 828°C according to Fig. 14.1. This goes along with a small loss in mass according to the TG curve. A single melting point can be excluded, because this would not imply a mass loss. Experimental observations showed a melting point below 900°C. Due to two effects at 856°C and 883°C it is likely that one is the melting point and the other one a phase transition point. The specific heat capacity needed for the two transformations is about 157 J/g and the molar heat capacity 203 kJ/mol. The transformation is reversible (see the cooling curve). The back transformation and recrystallisation respectively start at 730°C, indicating a large hysteresis.

The TG analysis showed decomposition above about 840°C according to Fig. 14.1 and is probably caused by volatilisation of PbO, TeO_2 or O_2, from the decomposition of TeO_3. Pure PbO transforms from the red tetragonal litharge to the yellow rhombic massicot at 488°C and finally melts at 897°C [66]. TeO_3 on the other hand starts to decompose at 400°C to TeO_2, which melts at 732°C.

When synthesising the samples, Te^{4+} in form of TeO_2 was the source for the Te. Here decomposition of TeO_3 to TeO_2 was no problem, as the Te^{4+} was oxidised to Te^{6+} by oxygen in the air. DSC and TG analysis were performed with protective gas and hence no presence of oxygen to compensate the decomposition of TeO_3. It is likely that the oxygen volatilised, due to the changed equilibrium. This would change the oxygen state of Te from VI to IV, due to the thermal behaviour of pure TeO_3 and would result in a different compound. Another compound at high temperature would explain the increase in heat capacity as well as an endothermic effect in the cooling curve at 730°, which was not present in the heating curve.

As the compound could not be analysed after TG and DSC measurements were performed, the actual high-temperature structure remains unclear, as well as the phase after the annealing step and the above explanation is only guesswork.

14.2.2 Analysis of compound Pb_6CdTeO_{10}
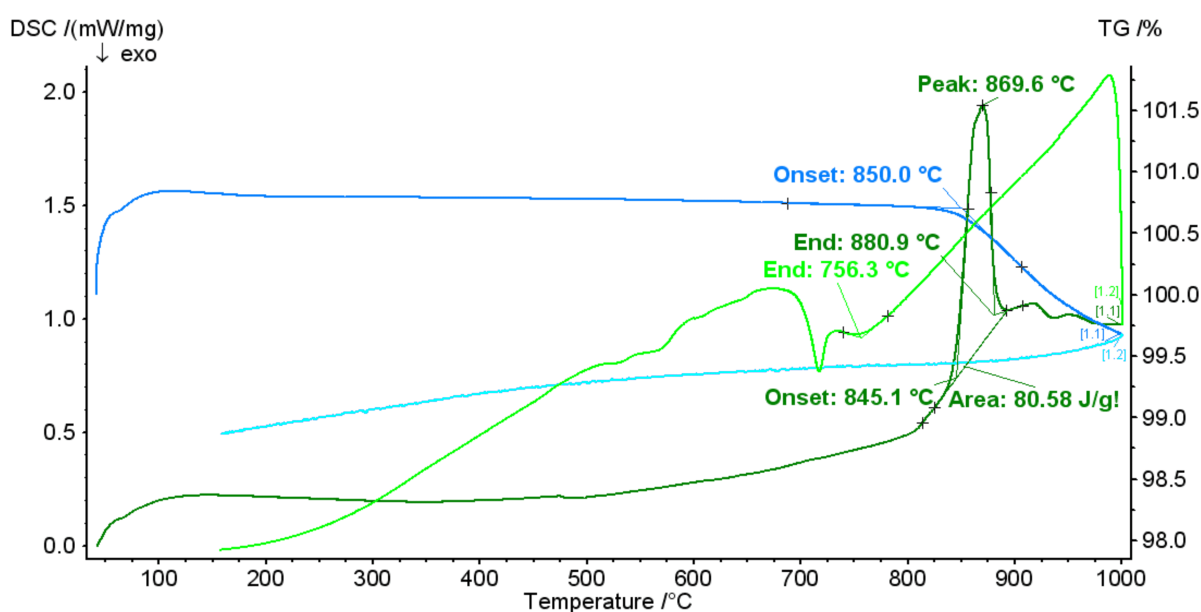
Figure 14.2: TG (blue) and DSC (green) heating and cooling (bright colours) curves of Pb_6CdTeO_{10}. The TG shows decomposition of the sample starting at 850°C. The DSC curves show an endothermic effect at about 850°C.

Similar results as for Pb_5TeO_8 were observed for this sample. The title compound shows an endothermic effect starting at 845°C according to the DSC curve in Fig. 14.2. Here only one peak in the heating curve is observed, where an increase in heat capacity is as well observed. The specific heat capacity of this transformation is 81 J/g and the molar heat capacity 132 kJ/mol. Decomposition starts at 850°C according to the TG curve. The reason the change in heat capacity and an exothermic effect in the cooling curve are probably the same as described for Pb_5TeO_8. Although the structure of this compound is non-centrosymmetric, it showed no phase transition.

14.2.3 Analysis of double-perovskites structures
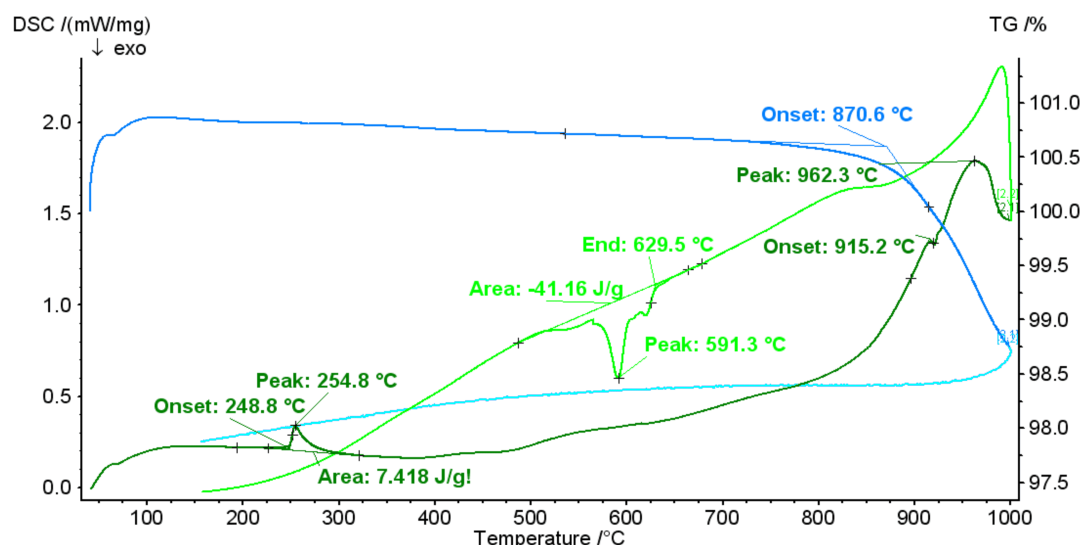
Figure 14.3: DSC (green) and TG (blue) curve of Pb_2CaTeO_6 up to 1000°C. Cooling curves displayed in the corresponding bright curves.

Analysis with DSC up to 1000°C showed phase transitions at 208°C for Pb_2CaTeO_6 and at 249°C for Pb_2CaTeO_6 (Figs. 14.3 and 14.4). The Cd-compound showed another endothermic effect at 915°C, ongoing with an increase in heat capacity. At a lower temperature of 870°C it starts to decompose according to the TG curve. Pb_2CaTeO_6 starts to loose mass at slightly higher temperatures than the Cd- compound. Besides, the effect was much lower than for the Cd- compound. In contrast it showed no second endothermic effect, but as well an increase in heat capacity.

In case of the Cd-compound the cooling curve showed an exothermic effect starting at about 630°C. A second effect was not observed, but cooling was only measured down to 170°C. Hence it is likely that the back transformation of the first phase-transformation was not monitored.

In contrast two phase transitions could be observed in the cooling curve of Pb_2CaTeO_6, although only one was monitored during heating. The first phase transition point was at 645°C, the second at 235°C. It is likely that these effects observed for both compounds at around 640°C are also caused by the volatilisation of oxygen, as described previously for Pb_5TeO_8.

To better study the observed phase transitions at low temperatures, both compounds were then measured again on the NETSCH DSC200F, which has a higher accuracy than the first one. The results are displayed in Fig. 14.5.

Here the phase transition for Pb_2CaTeO_6 was observed at 225°C and at 271°C for Pb_2CdTeO_6.
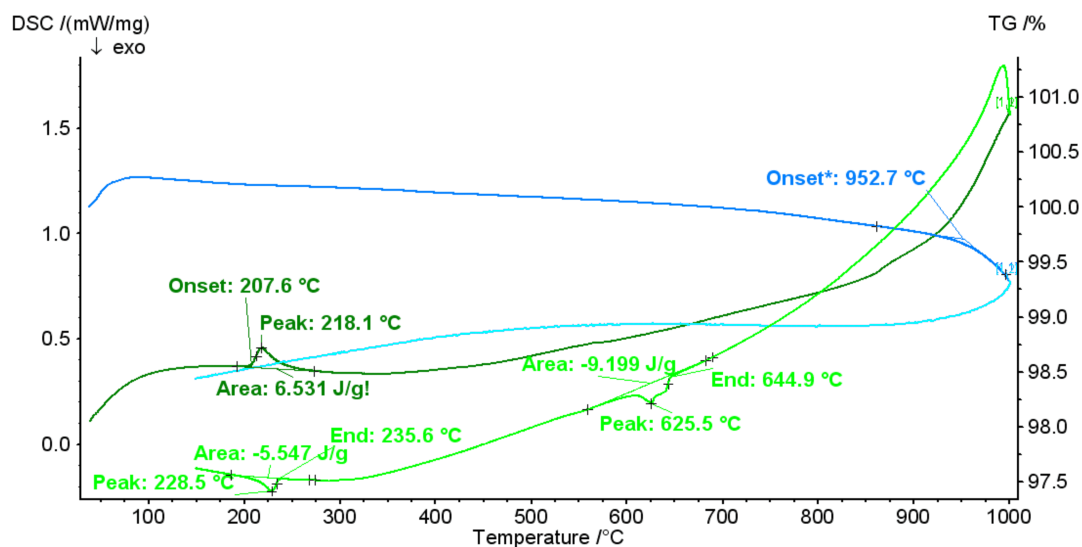
Figure 14.4: DSC (green) and TG (blue) curve of Pb_2CdTeO_6 up to 1000°C. Cooling curves displayed in the corresponding bright curves.
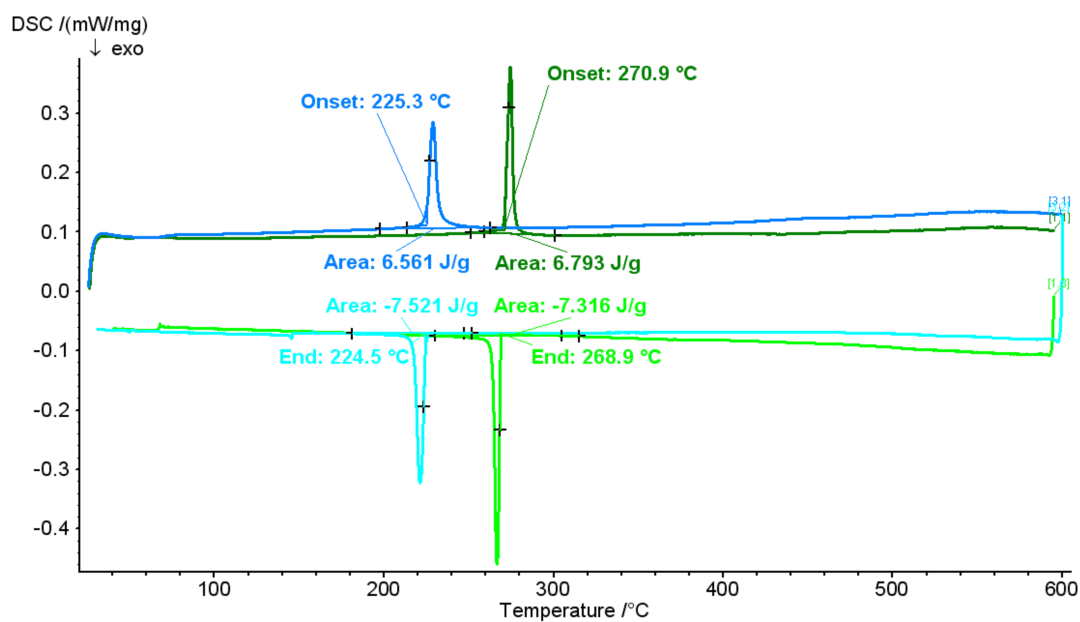
Figure 14.5: DSC curve of Pb_2CaTeO_6 (blue) and PB_2CdTeO_6 (green), the cooling curves are displayed in the corresponding bright colours. Both compounds show phase transition, the Ca- compound at 225°C and the Cd- compound at 271°C. In both cases the phase transition is reversible.

In both cases the phase transition was reversible and was monitored at about the same temperature as for the heating. The heat capacities of the transformation are very low. The specific heat capacity is 6.6 J/g and 6.8 J/g for the Ca and the Cd compound, respectively, whereas the molar heat capacity is 4.4 kJ/mol for Pb_2CateO_6 and 5.1 kJ/mol for Pb_2CdTeO_6. The transition corresponds to the structural change from the low-temperature monoclinic structure to the high-temperature cubic structure.

14.3 Temperature-dependent XRPD

To study the structural phase transitions of the two perovskite compounds Pb_2CaTeO_6 and Pb_2CdTeO_6 observed in the DSC in more detail, both compounds were measured with temperature-dependent XRPD.

14.3.1 Analysis of Pb_2CaTeO_6

XRPD data of Pb_2CaTeO_6 were measured between 30°C and 260°C in a first scan and between 30°C and 280°C in a more accurate second scan, with 1°C temperature steps close to the expected phase transition.
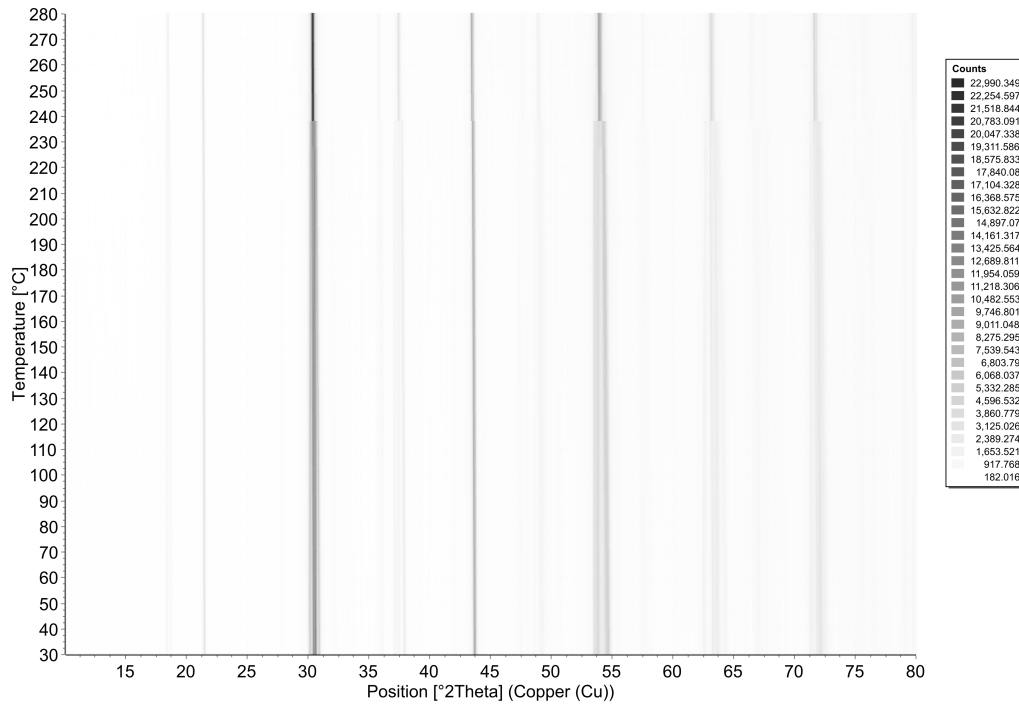
Figure 14.6: Isolines in XRPD patterns of compound Pb_2CaTeO_6 from 30 to 280 °C

A first measurement gave a phase transition between 230°C and 235°C. The second more accurate analysis revealed a phase transition temperature of 235°C according to Figs. 14.7 and 14.6 and therefore about 10°C higher than in the DSC measurement. The reason is probably the heat transfer, which is not as good as in the DSC.

The quality of the XRPD pattern was insufficient to perform an ab-initio structure solution, but with the help of the Bärnighausen family tree in Fig. 9.1 on page 48 possible structures for the high-temperature phase can be derived. Due to fever reflections in the XRPD pattern at 280°C than those at room temperature, the high-temperature phase is of higher symmetry. With the help of the Program TOPAS 2.1 a CIF- file of a cubic F-centered cell of Pb_2CaTeO_6 was simulated on the basis of the cubic perovskite structure Ba_2CaTeO_6 [67], as well as a tetragonal pattern on the basis of Ba_2CuWO_6 [68]. The pattern could be fitted with both cells, where the cell parameters of the tetragonal cell were refined to $a = 5.89$ Å and $c = 8.33$ Å, those of the cubic cell to $a = 8.33$ Å. These are in good accordance with the theoretical calculated cell parameter for the pseudo-cubic perovskite cell of $a = 8.30$ Å as demonstrated in chapter 6. The
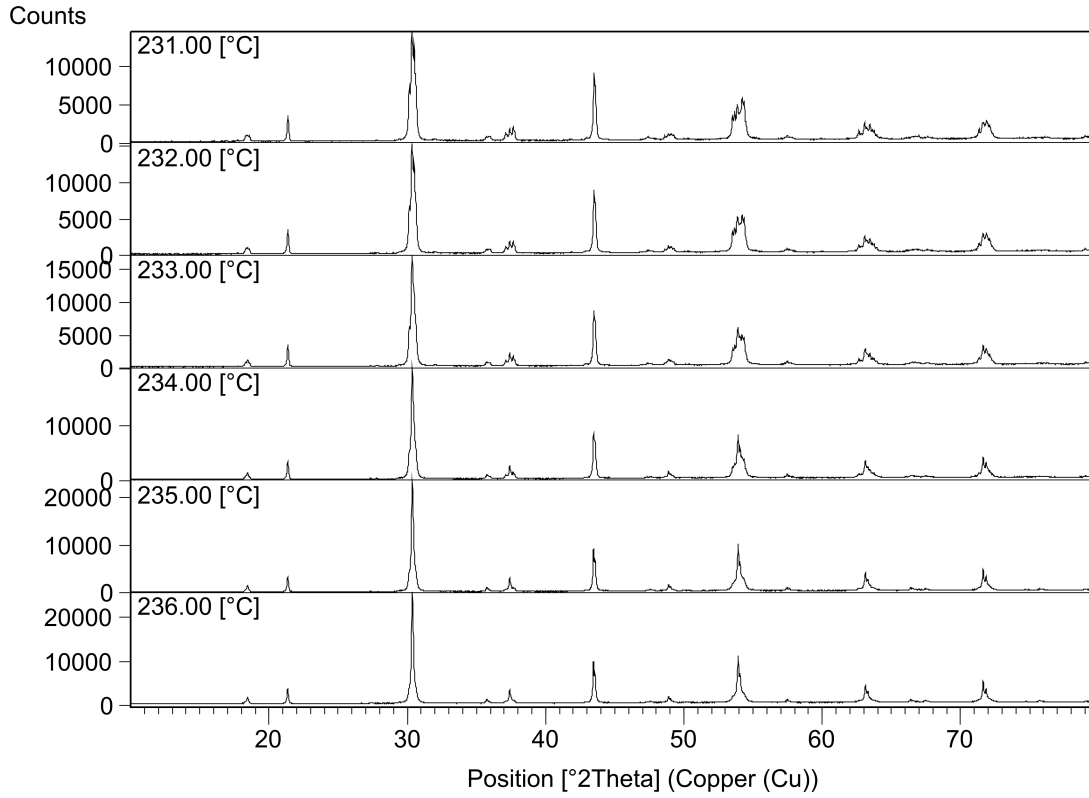
Figure 14.7: Comparison of the XRPD patterns at different temperatures
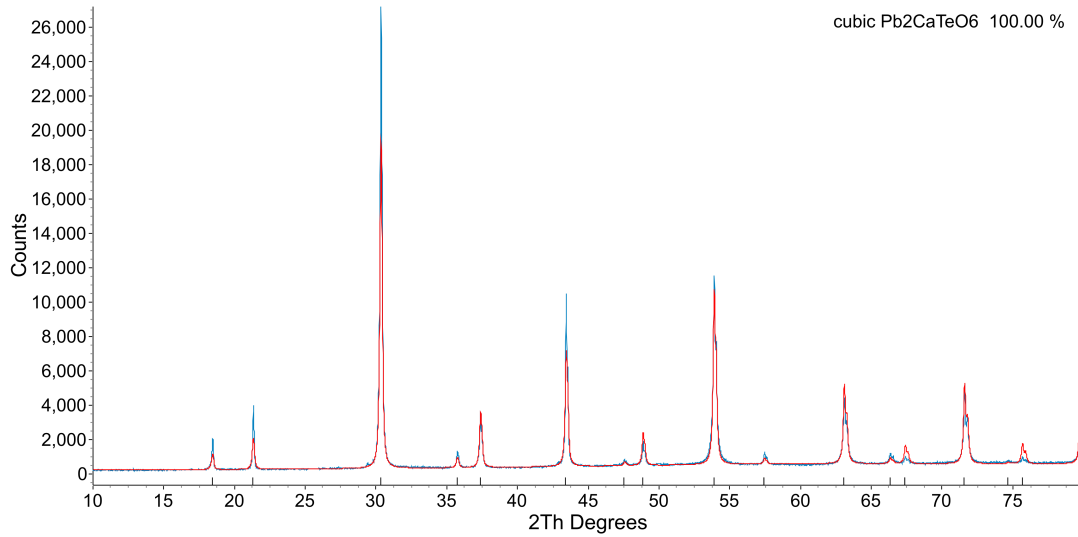
Figure 14.8: Fitted XRPD pattern of Pb_2CaTeO_6 at 280°. The measured phase is displayed in blue and the red line represents the simulation.

tetragonal cell parameters fulfil exactly the condition $c = a \cdot \sqrt{2}$, hence the metric points to the cubic system. It is likely that the structure is as well cubic, but for a final conclusion more accurate measurements on the high temperature phase are required.

Shortly before the transition temperature the cell volume increases distinctly, which is shown in Fig. 14.9. The cell parameters change as well, the development is displayed in Figs. 14.10(a)
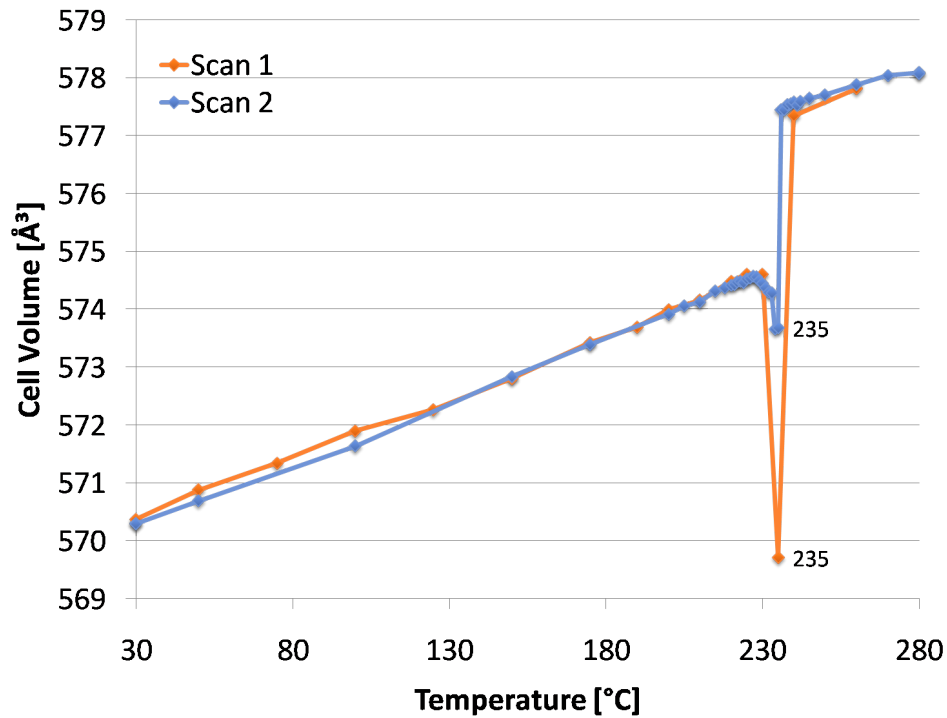
Figure 14.9: Temperature profile of the volume of the unit cell of Pb_2CaTeO_6

to 14.10(d).

A cubic cell can also be described with the monoclinic metric. There are various choices for the cell, one is given by the Bärnighausen family tree and was calculated for Pb_2CaTeO_6 in Section 5.2.2. For this choice the monoclinic angle would have the value of the ideal tetrahedral angle of 109.45°, cell parameters a and c would be equal and $b = a \cdot \sqrt{3}$.

According to Figs. 14.10(a) to 14.10(d) the cell parameters of the monoclinic cell change with the temperature to fulfil these conditions. At all temperatures the XRPD patterns could be fitted satisfactorily with the monoclinic cell, except at the actual phase transition point at 235°, where it was not possible to simulate the pattern satisfactorily. Right after the phase transitions point the above described conditions are fulfilled and therefore the metric is cubic. There was no evidence that both, the cubic and the monoclinic phase were present at the same time.
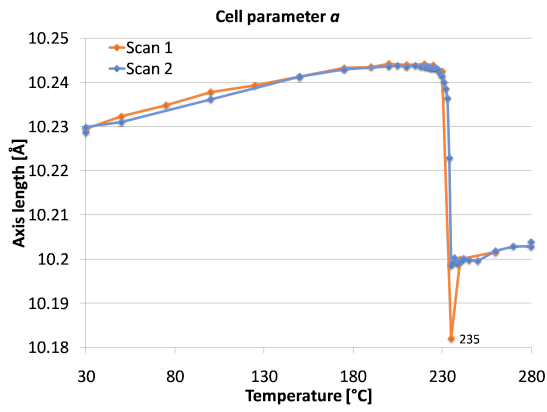
(a) Cell parameter a
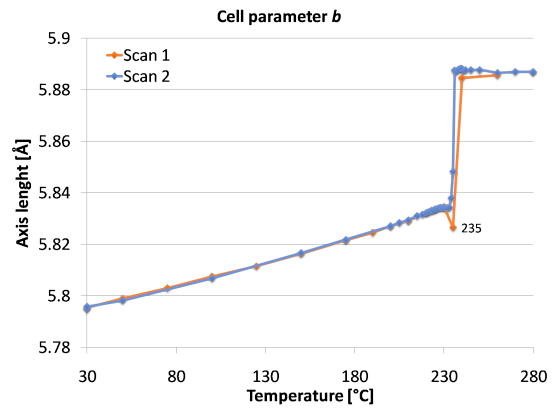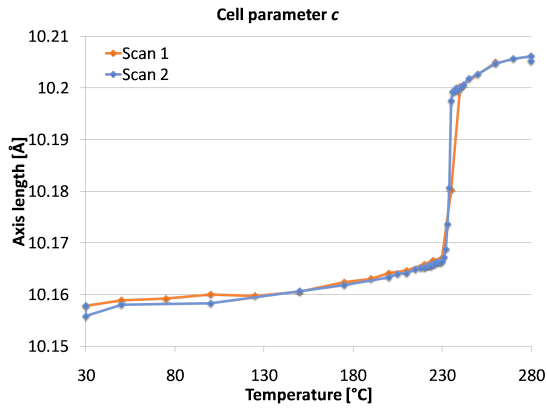
(b) cell parameter b
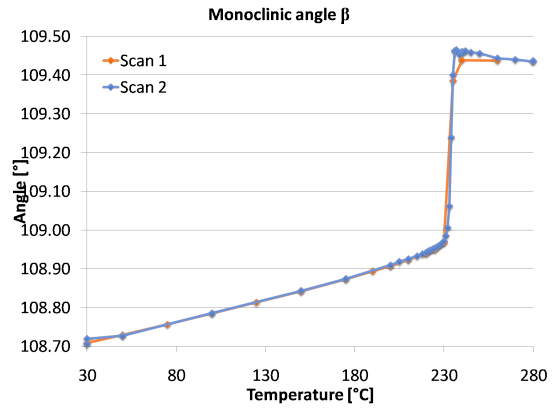
(c) Cell parameter c

(d) cell parameter β

Figure 14.10: Temperature profiles of the cell parameters of Pb_2CaTeO_6

14.3.2 Analysis of Pb$_2$CdTeO$_6$

XRPD data of Pb$_2$CdTeO$_6$ were measured between 30°C and 300°C in two scans, with 1°C steps close to the expected phase transition in the second scan. The scans in Figs. 14.11 and 14.12 show a phase transition starting at 281°C. The transition was not as sharp as observed in Pb$_2$CaTeO$_6$ and spanned over a temperature range of about 10°.
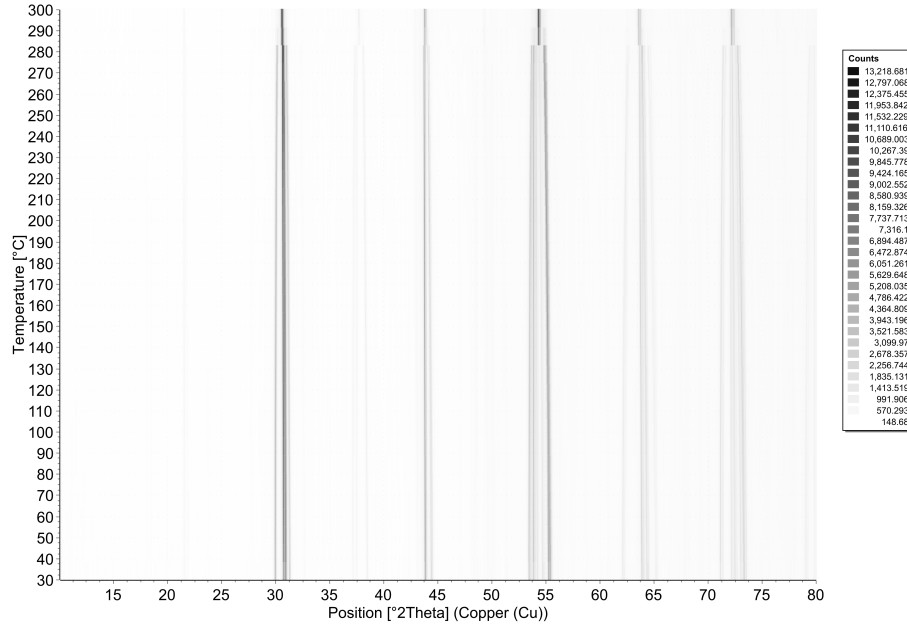
Figure 14.11: Isolines of XRPD patterns of the second scan of compound Pb$_2$CdTeO$_6$ from 30 to 300 °C

The high temperature phase could be assigned to a cubic phase with the same strategy as used for Pb$_2$CaTeO$_6$ (Fig. 14.13). The fitted cell parameter is $a = 8.28$ Å, which is slightly larger than the theoretical calculated pseudo-cubic perovskite cell parameter of $a = 8.22$ Å.

The XRPD patterns up to 280° were fitted with the monoclinic cell and cell parameters were refined. The temperature profile of the cell parameters and the volume of the unit cell are pictured in Figs. 14.14 to 14.15(d). Cell parameters a, b and β as well as the volume increase continuously with increasing temperature, but c increases first, and later decreases to the expected lengths.

Above 280°C two phases were present, therefore it was necessary to determine the fraction of the cubic and monoclinic phases. The patterns were fitted with both, the refined cubic cell and a monoclinic cell, where the cell parameters were fixed to the values at 280°C. The fractions of the phases are displayed in Fig. 14.16(b), the cubic cell parameter is given in Fig. 14.16(a). The fraction of the cubic phase increases continuously and reaches more than 90% above 288°C.

Reasons for this indistinct phase transition are either a feature of the sample or sample preparation. This effect can be observed if the amount of heat transferred to the sample is not sufficient for the phase transition, either by improper preparation or a large heat capacity of the phase transition. The second reason seems unlikely, as the heat capacity for the transformation is not much larger than for the Ca compound according to the DSC analysis shown in Fig. 14.5. It is also possible, that the sample needs more time to transform, but this could be avoided with a larger annealing time before measurement.
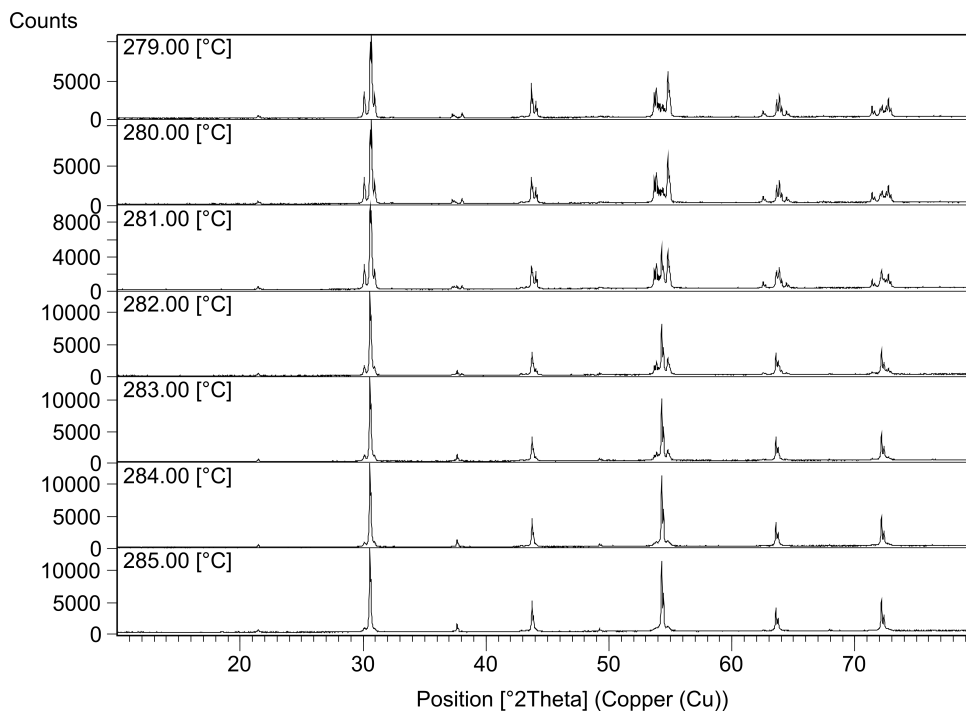
Figure 14.12: Comparison of the XRPD patterns of Pb_2CdTeO_6 at different temperatures for the second scan
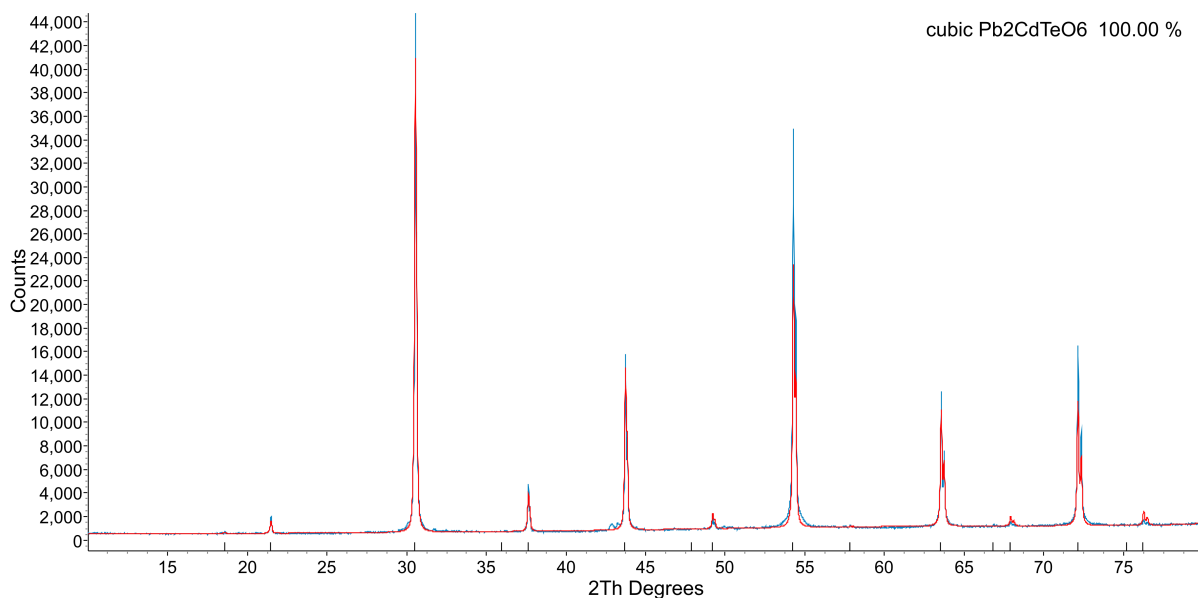
Figure 14.13: Fitted XRPD pattern of Pb_2CdTeO_6 at 300°. The measured phase is displayed in blue and the red line represents the simulation.
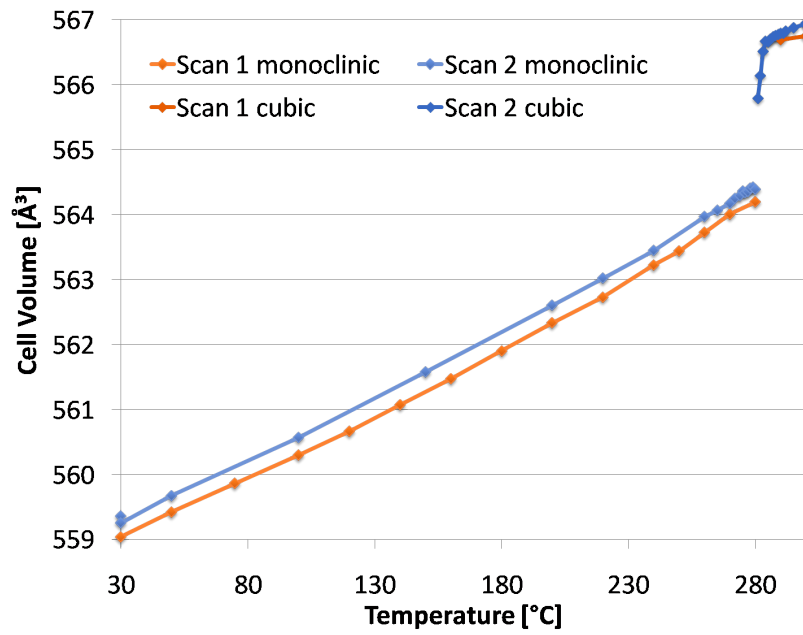
Figure 14.14: Temperature profile of the unit cell volume of Pb_2CdTeO_6
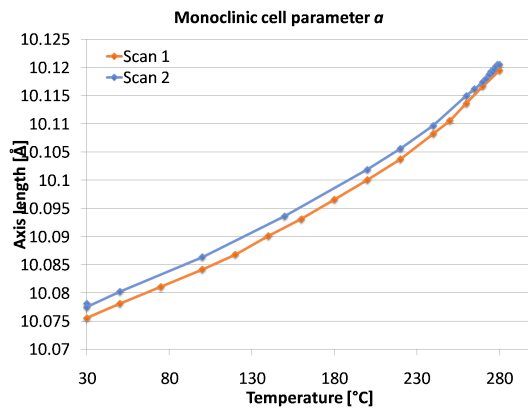
(a) Cell parameter a
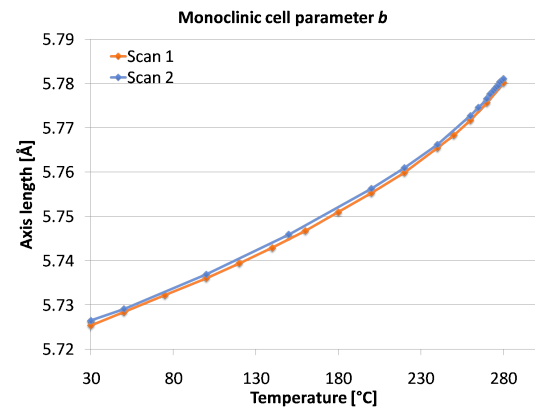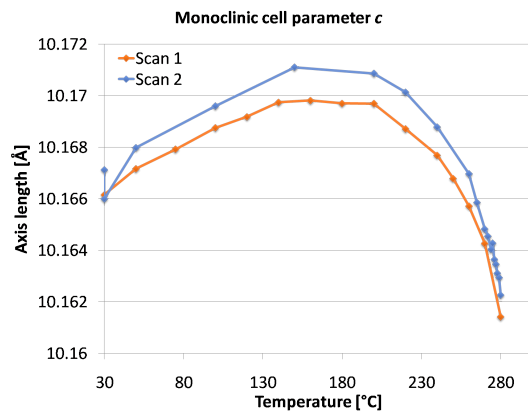
(b) cell parameter b
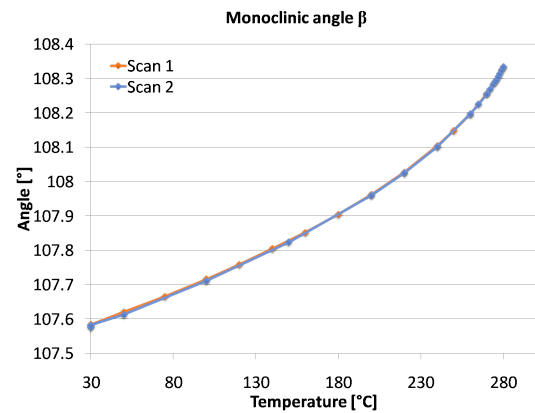
(c) Cell parameter c

(d) cell parameter β

Figure 14.15: Temperature profiles of the monoclinic cell parameters of Pb_2CdTeO_6

(a) Cubic cell parameter a

(b) Phase fraction of Pb_2CdTeO_6
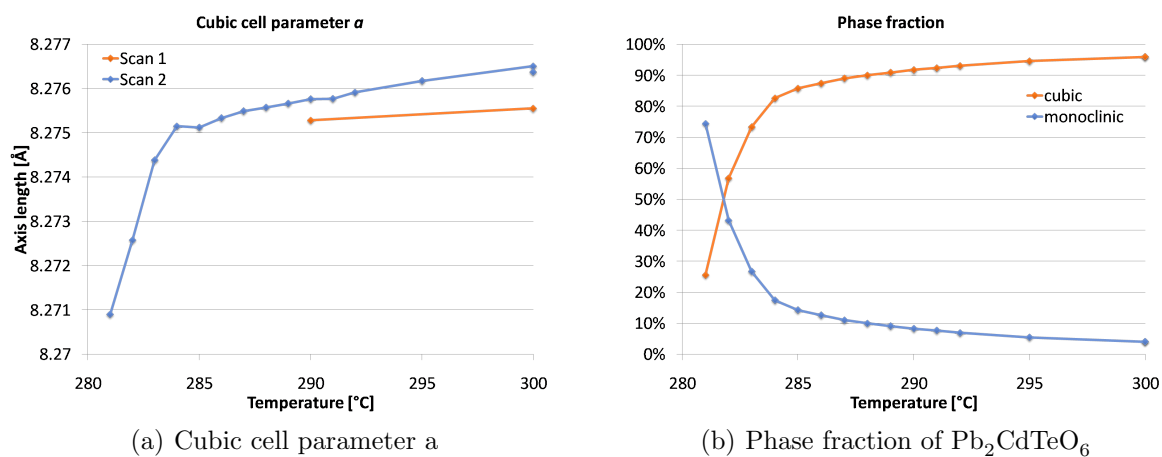
Figure 14.16: Temperature profile of the cubic cell parameter and phase fraction above $281°C$

Conclusion

The Pb^{2+} $6s^2$ lone pair is stereochemical active in almost all determined structures. The bonding oxygen atoms can be divided in primary and secondary coordinating ones, depending on their Pb-O bond lengths. The primary bonding oxygen atoms are irregularly arranged on one side of the Pb-O coordination sphere and the secondary bonding oxygen atoms are located on the other side of the Pb-O coordination sphere. Due to the gap in the Pb-O coordination sphere, it is likely that the Pb^{2+} $6s^2$ lone pair is located there.

Exceptions are the double-perovskite structures of Pb_2CoTeO_6 and Pb_2MnTeO_6. The reason for this is probably the rigid network of the $[BO_6]$-octahedra, where the effect of the Pb^{2+} electron lone pair is too weak to cause distortion. In the two other investigated double-perovskite structures Pb_2CdTeO_6 and Pb_2CaTeO_6 the voids for the Pb^{2+} cations are even larger, due to the larger B-site cations. This leads to a greater distortion of the Pb-O coordination spheres. Here the effect of the Pb^{2+} electron lone pair is also noticed, especially in Pb_2CdTeO_6, where the primary and secondary bonding oxygen atoms are distributed in two non-interconnecting coordination spheres to the Pb atom. In Pb_2CaTeO_6, the observed effect is more complex, as primary and secondary bonds are present, but evenly distributed around the Pb atom.

A summary of the bond valence calculations for Pb^{2+} is given in Tab. 14.1. Coordination numbers between 4 and 12 were observed for the Pb^{2+} cation in the various structures. The lowest were found in Pb_6CdTeO_{10} and $Pb_6Co_9Te_3O_{30}$ with a coordination number of 4 for the primary coordination sphere. These structures were also noticed to have the greatest difference in bond lengths of primary and secondary Pb-O bonds. In Pb_6CdTeO_{10} the primary Pb2-O bonds are up to 2.507 Å, where the secondary are greater than 3.811 Å. In $Pb_6Co_9Te_3O_{30}$, the greatest gap was observed for the Pb2-O bonds between 2.435 Å and 3.326 Å. In the other compounds, the difference between primary and secondary coordinating oxygen atoms varies from 0.25 Å to 0.68 Å.

A clear trend of the value of the coordination number of the Pb atoms with respect to the other cations in the structures cannot be made. The highest coordination number was observed in the ideal double-perovskite structures with 12, but also the longest minimum bond-lengths were noticed there, with 2.835 Å in Pb_2CoTeO_6 and 2.868 Å in Pb_2MnTeO_6. The shortest Pb-O bond lengths in general were observed in the Pb-rich compounds Pb_5TeO_8 and Pb_6CdTeO_{10} with 2.198 Å and 2.177 Å, respectively.

Although the bond valence theory was proofed to be a useful tool in inorganic structural chemistry, it shows some weakness when applying to atoms containing non bonding valence shell electrons [69]. The B parameters for the calculation of the experimental bond valence S_{ij} (Equation 1.1) were first assigned with a value of 0.37 for all cations, but have been corrected lately for atoms with lone pairs to higher values [70, 71]. The parameter B for Pb^{2+}-O bonds is therefore 0.49 [72].

Brows definition of a bond would include Pb-O bonds up to a length of 3.2 Å. Even though for some structures the next closest cation distances are already at 3.4 Å, which can be considered

as a limit for the primary coordination sphere, Pb-O interactions longer than this value are not negligible. If the long-range Pb-O bonds would not be counted to the valence sum of the Pb^{2+} cation, its value would be much lower than the expected value of 2 vu. For example, in Pb_2CaTeO_6 and Pb_2CdTeO_6 the bond-valence sum for the Pb^{2+}-cation would be around 1.6 vu, if only bond lengths up to 3.2 Å are considered. The bond valence sum for Pb^{2+} in the other structures were always below 2 vu, if Brown's bond model was applied. Therefore the long-range oxygen bonding interactions should also be taken into account, despite their low contribution to the bond-valence sum [33].

The Te atoms in all investigated compounds attend an octahedral coordination sphere with oxygen. The Te-O bond lengths was found the lowest in Pb_5TeO_8 with 1.887 Å and the highest in Pb_2TeO_5 with 2.012 Å. In summary the variation is minimal and in most structures it is close to the expected value of 1.977 Å. Most of the corresponding $[TeO_6]$-octahedra are almost perfect, and sometimes only slightly distorted.

In contrast to the very rigid an almost ideal $[TeO_6]$-octahedra, the coordination spheres of all other divalent cations in the determined structures (Cd^{2+}, Ca^{2+}, Co^{2+}, Cu^{2+}), as well as for Al^{3+}, are more distorted, which indicates a more structural flexibility of these building blocks. Exceptions here are as well the two compounds Pb_2CoTeO_6 and Pb_2MnTeO_6, adopting the ideal double-perovskite structures.

Table 14.1: Summary of bond valence calculations for Pb^{2+} in the investigated compounds.

Compound	atom	Bond valence sum [vu]	primary c.n.	shortest Pb-O bond [Å]	greatest gap [Å]	maximum prim. bond [Å]	minimum sec. bond [Å]
Ternary compounds							
Pb_5TeO_8	Pb1	1.956	5	2.253	0.684	2.809	3.493
	Pb2	1.860	5	2.272	0.836	2.699	3.535
	Pb3	1.777	5	**2.198**	0.408	2.684	3.092
	Pb4	1.896	5	2.222	0.428	2.653	3.081
	Pb5	1.871	5	2.202	0.575	2.743	3.318
Pb_2TeO_5	Pb1	1.978	7	2.358	0.540	3.019	3.559
Double-perovskites							
Pb_2CdTeO_6	Pb1	1.665	6	2.476	0.302	2.806	3.108
Pb_2CaTeO_6	Pb1	1.771	8	2.422	0.256	3.068	3.324
	Pb2	1.637	7	2.503	0.349	2.666	3.015
Pb_2CoTeO_6	Pb1	2.026	**12**	**2.835**			
Pb_2MnTeO_6	Pb1	1.894	**12**	**2.868**			
Quaternary compounds							
Pb_6CdTeO_{10}	Pb1	1.852	6	2.410	**1.164**	2.742	3.906
	Pb2	1.951	4	**2.177**	**1.304**	2.507	3.811
	Pb3	1.854	5	2.213	0.642	3.260	3.902
	Pb4	1.663	5	2.219	0.445	2.881	3.326
$Pb_6Co_9Te_5O_{30}$	Pb1	1.856	8	2.417	0.432	2.727	3.159
	Pb2	1.624	4	2.385	**0.901**	2.425	3.326
$PbAl_8Ca_2TeO_{15}$	Pb1	1.617	5	2.293	0.589	2.446	3.035

Part VI

Appendix

Appendix A

Mathematical crystallography

This section is a listing of formulas used in this work. For more information it is hereby referred to the book *Mathematical Crystallography* by Boisen and Gibbs [73].

A.1 Cell transformations

D_1 and D_2 are two vector space bases. P is the transformation matrix from D_1 to D_2 according to A.1. It can be shown that P^{-1} is the transformation matrix from D_2 to D_1. C_1 and C_2 are the metric tensor of the original and transformed cell respectively. The general matrix of the tensor C is given in A.6.

$$P = \begin{pmatrix} p_{11} & p_{12} & p_{13} \\ p_{21} & p_{22} & p_{23} \\ p_{31} & p_{32} & p_{33} \end{pmatrix} \tag{A.1}$$

$$a_2 = p_{11}a_1 + p_{21}b_1 + p_{31}c_1 \tag{A.2}$$
$$b_2 = p_{12}a_1 + p_{22}b_1 + p_{32}c_1 \tag{A.3}$$
$$c_2 = p_{13}a_1 + p_{23}b_1 + p_{33}c_1 \tag{A.4}$$

To change the basis of a cell formula A.5 is applied.

$$C_2 = P^{-T} \cdot C_1 \cdot P^{-1} \tag{A.5}$$

$$C = \begin{pmatrix} a^2 & a \cdot b \cdot cos\gamma & a \cdot c \cdot cos\beta \\ a \cdot b \cdot cos\gamma & b^2 & b \cdot c \cdot cos\alpha \\ a \cdot c \cdot cos\beta & b \cdot c \cdot cos\alpha & c^2 \end{pmatrix} \tag{A.6}$$

A.2 Transformation of coordinates

Transformation of coordinates is calculated by equation A.7.

$$r_2 = P \cdot r_1 \tag{A.7}$$

Where r_1 and r_2 are the coordinates expressed as a column vector in D_1 and D_2 respectively.

A.3   Transformation into a Cartesian basis

For calculating angles and bond lengths it is sometimes necessary to transform the basis of the crystal into a Cartesian basis. This can be achieved by using transformation matrix A (A.8.

$$A = \begin{pmatrix} a & b \cdot cos\gamma & c \cdot cos\beta \\ 0 & b \cdot sin\gamma & -c \cdot cos\alpha^* \cdot sin\beta \\ 0 & 0 & c \cdot sin\beta \cdot sin\alpha^* \end{pmatrix} \tag{A.8}$$

a, b, c and α, β, γ are the cell parameters of the original cell. α^* is the reciprocal angle of α.

Appendix B

Tilt Angles Calculation

The tilt angle is defined as the angle which the octahedron is tilted from the perovskite main axis. It can be considered as the angle between two planes, spanned by the direction vector of the axis, along which the tilting is investigated and a cation-anion bond vector of the octahedra perpendicular to this direction, and by the corresponding ideal cation-anion bond vector, respectively. As all cation-anion bonds in an undistorted octahedron are equally tilted, it makes no difference which bond is chosen. For distorted octahedra it is more difficult to define the tilt angle. One approach is to calculate the angle of every single position and then build the mean value, this can only be done with angles differing only slightly from each other. For highly distorted octahedra this is not reasonable. In Fig. B.1 a schematic representation of an octahedron, spanned by cation B and six anions X is given.
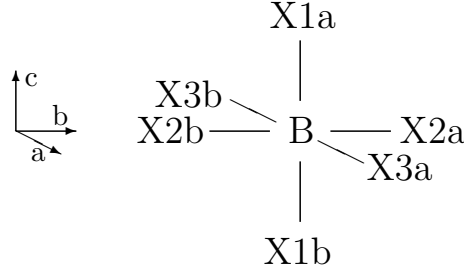
Figure B.1: Arrangement of the anions X in the $[BX_6]$- octahedron

A derivation of a formula for calculating tilt angles of ideal and slightly distorted octahedra is given below. A full derivation is only given for one bond, as the others can be calculated the same way. A full list of all formulas is given at the end of this chapter.

B.1   Calculation of angles in space

Given two planes $p_1 = \overline{ABC}$ and $p_2 = \overline{ABD}$. The angle between the two planes is the angle between its two normal vectors n_1 and n_2. Therefore it is only necessary to calculate the normal vectors. Those are obtained by calculating the cross product of two vectors of the plane. There are three points A, B and C of the planes given. One normal vector is the cross product of $\overrightarrow{AB}$ and $\overrightarrow{AC}$. The cross product is calculated by formula B.1.

$$\begin{pmatrix} x_1 \\ y_1 \\ z_1 \end{pmatrix} \times \begin{pmatrix} x_2 \\ y_2 \\ z_2 \end{pmatrix} = \begin{pmatrix} y_1 \cdot z_2 - y_2 \cdot z_1 \\ -(x_1 \cdot z_2 - x_2 \cdot z_1) \\ x_1 \cdot y_2 - x_2 \cdot y_1 \end{pmatrix} \tag{B.1}$$

The formula for calculating the angle φ between two vectors is given in B.2. This is the angle of n_2 to n_1 in a mathematical positive sense.

$$cos\varphi = \frac{n_1 \cdot n_2}{\mid n_1 \mid \cdot \mid n_2 \mid} \tag{B.2}$$

B.2   Calculation of tilt angles for one bond

The derivation of the formula for calculation the tilt angles in direction a of the perovskite cell is given below. The ideal positions are labelled with *.

Calculations for $X1$a

The tilt angle α_1 of bond B-$X1$a from axis a is equal to the angle ϕ between the two planes which are spanned by B, $X1$a*, $X3$a* and B, $X1$a, $X3$a respectively.

$$B = (0, 0, 0)$$
$$X1a* = (0, 0, 1)$$
$$X3a* = (1, 0, 0)$$
$$X1a = (x, y, z)$$

Normal vector n_1 of ideal plane.

$$n_1 = \overrightarrow{BX1a*} \times \overrightarrow{BX3a*} = \begin{pmatrix} 0 \\ 0 \\ 1 \end{pmatrix} \times \begin{pmatrix} 1 \\ 0 \\ 0 \end{pmatrix} = \begin{pmatrix} 0 \\ 1 \\ 0 \end{pmatrix}$$

Normal vector n_1 of plane $\overline{BX1aX3a*}$.

$$n_2 = \overrightarrow{BX1a} \times \overrightarrow{BX3a*} = \begin{pmatrix} x \\ y \\ z \end{pmatrix} \times \begin{pmatrix} 1 \\ 0 \\ 0 \end{pmatrix} = \begin{pmatrix} 0 \\ z \\ -y \end{pmatrix}$$

Insertion in formula B.2 gives

$$cos\varphi = \frac{n_1 \cdot n_2}{\mid n_1 \mid \cdot \mid n_2 \mid} = \frac{\begin{pmatrix} 0 \\ 1 \\ 0 \end{pmatrix} \cdot \begin{pmatrix} 0 \\ z \\ -y \end{pmatrix}}{1 \cdot \sqrt{y^2 + z^2}} = \frac{z}{\sqrt{y^2 + z^2}} \tag{B.3}$$

B.3   Formulas for calculating tilt angles

The other formulas are derived in a similar way. Where
$X1a* = (0, 0, 1)$
$X2a* = (0, 1, 0)$

$X3a* = (1, 0, 0)$

and $X1a, X1b, X2a, X2b, X3a, X3b$ are allocated at the general position (x, y, z). If B is not in the centre of the chosen coordinate system, the coordinates of the vectors $\overrightarrow{BX1}$ are used instead of the coordinates of X. The so derived formulas are given in Tab. B.1

Table B.1: Formulas for calculating bond tilt angles

Anion	Direction a	b	c
$X1a$	$\frac{z}{\sqrt{y^2+z^2}}$	$\frac{z}{\sqrt{x^2+z^2}}$	-
$X1b$	$\frac{-z}{\sqrt{y^2+z^2}}$	$\frac{-z}{\sqrt{x^2+z^2}}$	-
$X2a$	$\frac{y}{\sqrt{y^2+z^2}}$	-	$\frac{y}{\sqrt{x^2+y^2}}$
$X2b$	$\frac{-y}{\sqrt{y^2+z^2}}$	-	$\frac{-y}{\sqrt{x^2+y^2}}$
$X3a$	-	$\frac{x}{\sqrt{x^2+z^2}}$	$\frac{x}{\sqrt{x^2+y^2}}$
$X3b$	-	$\frac{-x}{\sqrt{x^2+z^2}}$	$\frac{-x}{\sqrt{x^2+y^2}}$

B.3.1 Sense of tilting

The above calculations of the angles give no information of the sense of tilting, as $cos\alpha = cos(-\alpha)$. The direction of the vector $\overrightarrow{BX}$ determines the arithmetic sign of the tilt angle. For example, if bond $BX1$ is tilted clockwise, coordinate y of vector $\overrightarrow{BX1}$ has to be positive. These considerations can be made for all directions. The conditions for every bond are summarised in Tab. B.2.

Table B.2: Conditions for clockwise tilt

Perovskite axis	$X1a$	$X1b$	$X2a$	$X2b$	$X3a$	$X3b$
a	y $+$	y $-$	z $-$	z $+$		
b	x $-$	x $+$			z $+$	z $-$
c			x $+$	x $-$	y $-$	y $+$

Appendix C

Parameters and details of data collection, refinement and structure solution

Table C.1: Crystal data, data collection parameters and refinement details for Pb_5TeO_8

Crystal data	
Chemical formula	Pb_5TeO_8
M_r	1291.55
Cell setting, space group	monoclinic, $P2_1/n$
Temperature (K)	296(2)
a, b, c (Å)	7.4426(2), 12.0107(3)
	10.6567(2)
$\beta(°)$	91.0400(10)
V (Å^3)	952.45(4)
Z	4
$D_x(Mg \cdot m^{-3})$	9.007
Radiation type	Mo $K\alpha$
$\mu(mm^{-1})$	91.099
Crystal form, colour	nearly isotropic, redish
Crystal size (mm)	0.12 x 0.070 x 0.014
Data collection	
Data collection	Bruker Apex II
Data collection method	ω and ϕ scans
Absorption correction	numerical
T_{min}, T_{max}	0.0263, 0.5223
No. of measured, independent and observed reflections	37384, 5910, 4506
Criterion for observed reflections	$I > 2\sigma(I)$
R_{int}	0.0754
$\Theta_{max}(°)$	45.568
Refinement	
Refinement on	F^2
$R[F^2 > 2\sigma(F)], \omega R(F^2), S$	0.0272, 0.0504, 0.986
No. of reflections	5910
No. of parameters	128
Weighting scheme	$\omega = 1/[\sigma^2(F_0^2) + (0.0145P)^2]$ where $P = (F_0^2 + 2F_c^2)/3$
$(\delta/\sigma)_{max}$	0.001
$\delta\rho_{max}, \delta\rho_{max}$ (e Å^{-3})	4.071, -5.161
Extinction method	SHELX
Extinction coefficient	0.000190(12)

Table C.2: Crystal data, data collection parameters and refinement details for Pb_2TeO_8

Crystal data	
Chemical formula	Pb_2TeO_8
M_r	621.98
Cell setting, space group	monoclinic, $C2/c$
Temperature (K)	293(2)
a, b, c (Å)	13.0853(6), 5.7071(3)
	7.5225(3)
$\beta(°)$	123.772(2)
V (Å^3)	466.98(4)
Z	4
$D_x(Mg \cdot m^{-3})$	8.847
Radiation type	Mo $K\alpha$
$\mu(mm^{-1})$	78.053
Crystal form, colour	plate, yellowish
Crystal size (mm)	0.036 x 0.012 x 0.011
Data collection	
Data collection	Bruker Apex II
Data collection method	ω and ϕ scans
Absorption correction	numerical
T_{min}, T_{max}	0.0101, 0.1843
No. of measured, independent and observed reflections	11504, 1927, 1539
Criterion for observed reflections	$I > 2\sigma(I)$
R_{int}	0.1077
$\Theta_{max}(°)$	45.04
Refinement	
Refinement on	F^2
$R[F^2 > 2\sigma(F)], \omega R(F^2), S$	0.0334, 0.0849, 0.989
No. of reflections	1927
No. of parameters	40
Weighting scheme	$\omega = 1/[\sigma^2(F_0^2) + (0.0467P)^2]$ where $P = (F_0^2 + 2F_c^2)/3$
$(\delta/\sigma)_{max}$	0.001
$\delta\rho_{max}, \delta\rho_{max}$ (e Å^{-3})	8.525, -3.992
Extinction method	SHELX
Extinction coefficient	0.0112(4)

Table C.3: Crystal data, data collection parameters and refinement details for Pb_2CdTeO_6

Crystal data	
Chemical formula	Pb_2CdTeO_6
M_r	750.38
Cell setting, space group	monoclinic, $C2/c$
Temperature (K)	296(2)
a, b, c (Å)	10.01716(3), 5.7197(2), 10.1577(3)
$\beta(°)$	107.528(2)
V (Å^3)	557.98(3)
Z	4
$D_x(Mg \cdot m^{-3})$	8.932
Radiation type	Mo $K\alpha$
$\mu(mm^{-1})$	69.06
Crystal form, colour	undefined habit, colourless
Crystal size (mm)	0.084 x 0.084 x 0.072
Data collection	
Data collection	Bruker Apex II
Data collection method	ω and ϕ scans
Absorption correction	multi-scan
T_{min}, T_{max}	0.0321, 0.4014
No. of measured, independent and observed reflections	11901, 1777, 1564
Criterion for observed reflections	$I > 2\sigma(I)$
R_{int}	0.0631
$\Theta_{max}(°)$	41.50
Refinement	
Refinement on	F^2
$R[F^2 > 2\sigma(F)], \omega R(F^2), S$	0.022, 0.046, 0.997
No. of reflections	1777
No. of parameters	49
Weighting scheme	$\omega = 1/[\sigma^2(F_0^2) + (0.0185P)^2]$ where $P = (F_0^2 + 2F_c^2)/3$
$(\delta/\sigma)_{max}$	0.002
$\delta\rho_{max}, \delta\rho_{max}$ (e Å^{-3})	4.515, -2.671
Extinction method	SHELXL
Extinction coefficient	0.00039(3)

Table C.4: Crystal data, data collection parameters and refinement details for Pb_2CaTeO_6

Crystal data	
Chemical formula	Pb_2CaTeO_6
M_r	678.1
Cell setting, space group	monoclinic, $P2_1/c$
Temperature (K)	296(2)
a, b, c (Å)	10.2293(3), 5.7926(2), 10.1698(3)
$\beta(°)$	108.6380(10)
V (Å^3)	571.00(3)
Z	4
$D_x(Mg \cdot m^{-3})$	7.885
Radiation type	Mo $K\alpha$
$\mu(mm^{-1})$	64.76
Crystal form, colour	fragment, colourless
Crystal size (mm)	0.072 x 0.060 x 0.060
Data collection	
Data collection	Bruker Apex II
Data collection method	ω and ϕ scans
Absorption correction	numerical
T_{min}, T_{max}	0.0556, 0.1316
No. of measured, independent and observed reflections	19109, 3504, 1323
Criterion for observed reflections	$I > 2\sigma(I)$
R_{int}	0.0938
$\Theta_{max}(°)$	41.47
Refinement	
Refinement on	F^2
$R[F^2 > 2\sigma(F)], \omega R(F^2), S$	0.041, 0.092, 0.990
No. of reflections	3504
No. of parameters	96
Weighting scheme	$\omega = 1/[\sigma^2(F_0^2) + (0.0257P)^2]$ where $P = (F_0^2 + 2F_c^2)/3$
$(\delta/\sigma)_{max}$	0.0223
$\delta\rho_{max}, \delta\rho_{max}$ (e Å^{-3})	5.562, -4.716
Extinction method	SHELX
Extinction coefficient	0.00033(5)

Table C.5: Crystal data, data collection parameters and refinement details for Pb_2CoTeO_6

Crystal data	
Chemical formula	Pb_2CoTeO_6
M_r	696.93
Cell setting, space group	cubic, $Fm\bar{3}m$
Temperature (K)	293(2)
a (Å)	8.01380(10)
V (Å^3)	514.654(11)
Z	2
$D_x(Mg \cdot m^{-3})$	8.994
Radiation type	Mo $K\alpha$
$\mu(mm^{-1})$	73.96
Crystal form, colour	brick, blue
Crystal size (mm)	0.072 x 0.072 x 0.048
Data collection	
Data collection	Bruker Apex II
Data collection method	ω and ϕ scans
Absorption correction	numerical
T_{min}, T_{max}	0.0512, 0.1295
No. of measured, independent and observed reflections	5750, 137, 124
Criterion for observed reflections	$I > 2\sigma(I)$
R_{int}	0.0479
$\Theta_{max}(°)$	43.84
Refinement	
Refinement on	F^2
$R[F^2 > 2\sigma(F)], \omega R(F^2), S$	0.0147, 0.0259, 1.061
No. of reflections	137
No. of parameters	8
Weighting scheme	$\omega = 1/[\sigma^2(F_0^2) + (0.0056P)^2 + 10.1519P]$ where $P = (F_0^2 + 2F_c^2)/3$
$(\delta/\sigma)_{max}$	0.000
$\delta\rho_{max}, \delta\rho_{max}$ (e Å^{-3})	2.764, -2.671
Extinction method	SHELX
Extinction coefficient	0.00018(3)

Table C.6: Crystal data, data collection parameters and refinement details for Pb_2MnTeO_6

Crystal data	
Chemical formula	Pb_2MnTeO_6
M_r	692.92
Cell setting, space group	cubic, $Fm\bar{3}m$
Temperature (K)	296(2)
a (Å)	8.10540(10)
V (Å^3)	532.505(11)
Z	4
$D_x(Mg \cdot m^{-3})$	8.643
Radiation type	Mo $K\alpha$
$\mu(mm^{-1})$	70.741
Crystal form, colour	isotropic, dark blue
Crystal size (mm)	0.048 x 0.036 x 0.036
Data collection	
Data collection	Bruker Apex II
Data collection method	ω and ϕ scans
Absorption correction	numerical
T_{min}, T_{max}	0.1125, 0.218
No. of measured, independent and observed reflections	5576, 143, 129
Criterion for observed reflections	$I > 2\sigma(I)$
R_{int}	0.0514
$\Theta_{max}(^{\circ})$	44.00
Refinement	
Refinement on	F^2
$R[F^2 > 2\sigma(F)], \omega R(F^2), S$	0.020, 0.0323, 1.214
No. of reflections	143
No. of parameters	8
Weighting scheme	$\omega = 1/[\sigma^2(F_0^2) + (0.0075P)^2 + 7.8344P]$ where $P = (F_0^2 + 2F_c^2)/3$
$(\delta/\sigma)_{max}$	0.000
$\delta\rho_{max}, \delta\rho_{max}$ (e Å^{-3})	3.283, -4.186
Extinction method	SHELX
Extinction coefficient	0.00017(5)

Table C.7: Crystal data, data collection parameters and refinement details for Pb_6CdTeO_{10}

Crystal data	
Chemical formula	Pb_6CdTeO_{10}
M_r	1643.14
Cell setting, space group	orthorhombic, $C222_1$
Temperature (K)	293(2)
a, b, c (Å)	9.1206(2), 11.5674(3), 11.3113(3)
V (Å^3)	1193.36(5)
Z	4
$D_x(Mg \cdot m^{-3})$	9.146
Radiation type	Mo $K\alpha$
$\mu(mm^{-1})$	88.511
Crystal form, colour	brick, yellowish
Crystal size (mm)	0.072 x 0.060 x 0.012
Data collection	
Data collection	Bruker Apex II
Data collection method	ω and ϕ scans
Absorption correction	Gaussian
T_{min}, T_{max}	0.0239, 0.3566
Flack parameter	0.004(5)
No. of measured, independent and observed reflections	24888, 2924, 2638
Criterion for observed reflections	$I > 2\sigma(I)$
R_{int}	0.0788
$\Theta_{max}(°)$	37.6
Refinement	
Refinement on	F^2
$R[F^2 > 2\sigma(F)], \omega R(F^2), S$	0.0234, 0.0461, 1.018
No. of reflections	2924
No. of parameters	85
Weighting scheme	$\omega = 1/[\sigma^2(F_0^2) + (0.0186P)^2]$ where $P = (F_0^2 + 2F_c^2)/3$
$(\delta/\sigma)_{max}$	0.000
$\delta\rho_{max}, \delta\rho_{max}$ (e Å^{-3})	3.036, -2.556
Extinction method	SHELX
Extinction coefficient	0.000401(13)

Table C.8: Crystal data, data collection parameters and refinement details for $Pb_6Co_9Te_5O_{30}$

Crystal data	
Chemical formula	$Pb_6Co_9Te_5O_{30}$
M_r	2891.51
Cell setting, space group	hexagonal, $P6_322$
Temperature (K)	293(2)
a, c (Å)	10.39150(10), 13.6273(2)
V (Å^3)	1274.37(3)
Z	2
$D_x (Mg \cdot m^{-3})$	7.535
Radiation type	Mo $K\alpha$
$\mu (mm^{-1})$	50.890
Crystal form, colour	brick, dark red
Crystal size (mm)	0.072 x 0.060 x 0.048
Data collection	
Data collection	Bruker Apex II
Data collection method	ω and ϕ scans
Absorption correction	numerical
T_{min}, T_{max}	0.1231, 0.2002
Flack parameter	0.134(10)
No. of measured, independent and observed reflections	45686, 2262, 1908
Criterion for observed reflections	$I > 2\sigma(I)$
R_{int}	0.0680
$\Theta_{max}(°)$	37.57
Refinement	
Refinement on	F^2
$R[F^2 > 2\sigma(F)], \omega R(F^2), S$	0.0246, 0.0559, 1.090
No. of reflections	2262
No. of parameters	81
Weighting scheme	$\omega = 1/[\sigma^2(F_0^2) + (0.0244P)^2]$ where $P = (F_0^2 + 2F_c^2)/3$
$(\delta/\sigma)_{max}$	0.001
$\delta\rho_{max}, \delta\rho_{max}$ (e Å^{-3})	3.785, -3.502
Extinction method	SHELX
Extinction coefficient	0.00019(3)

Table C.9: Crystal data, data collection parameters and refinement details for $PbAl_8Ca_2O_{15}$

Crystal data	
Chemical formula	$PbAl_8Ca_2O_{15}$
M_r	743.19
Cell setting, space group	orthorhombic, $Pnma$
Temperature (K)	296(2)
a, b, c (Å)	5.37020(10), 27.9903(4), 8.88110(10)
V (Å^3)	1334.95(3)
Z	4
$D_x(Mg \cdot m^{-3})$	3.698
Radiation type	Mo $K\alpha$
$\mu(mm^{-1})$	14.023
Crystal form, colour	brick, colourless
Crystal size (mm)	0.12 x 0.12 x 0.10
Data collection	
Data collection	Bruker Apex II
Data collection method	ω and ϕ scans
Absorption correction	numerical
T_{min}, T_{max}	0.2839, 0.3462
No. of measured, independent and observed reflections	39428, 5600, 5066
Criterion for observed reflections	$I > 2\sigma(I)$
R_{int}	0.0367
$\Theta_{max}(°)$	45.07
Refinement	
Refinement on	F^2
$R[F^2 > 2\sigma(F)], \omega R(F^2), S$	0.0241, 0.0577, 1.053
No. of reflections	5600
No. of parameters	122
Weighting scheme	$\omega = 1/[\sigma^2(F_0^2) + (0.0288P)^2 + 2.3587P]$ where $P = (F_0^2 + 2F_c^2)/3$
$(\delta/\sigma)_{max}$	0.001
$\delta\rho_{max}, \delta\rho_{max}$ (e Å^{-3})	4.013, -3.093
Extinction method	SHELX
Extinction coefficient	0.00017(10)

Table C.10: Crystal data, data collection parameters and refinement details for the preliminary solution of $PbCa_4Te_3O_{14}$

Crystal data	
Chemical formula	$PbCa_4Te_3O_{14}$
M_r	956.66
Cell setting, space group	monoclinic, $P2_1/n$
Temperature (K)	296(2)
a, b, $c(\text{Å})$	7.4514(7), 7.4457(7)
	10.4067(9)
$\beta(°)$	90.095(5)
V (Å^3)	577.37(9)
Z	1
$D_x(Mg \cdot m^{-3})$	2.802
Radiation type	Mo $K\alpha$
$\mu(mm^{-1})$	11.95
Crystal form, colour	fragment, colourless
Crystal size (mm)	0.052 x 0.040 x 0.039
Data collection	
Data collection	Bruker Apex II
Data collection method	ω and ϕ scans
Absorption correction	empirical
No. of measured, independent and observed reflections	20724, 5218, 2292
Criterion for observed reflections	$I > 2\sigma(I)$
R_{int}	0.1226
$\Theta_{max}(°)$	48.19
Refinement	
Refinement on	F^2
$R[F^2 > 2\sigma(F)], \omega R(F^2), S$	0.0725, 0.2578, 1.177
No. of reflections	4900
No. of parameters	297
Weighting scheme	$\omega = 1/[\sigma^2(F_0^2) + (0.0836P)^2]$ where $P = (F_0^2 + 2F_c^2)/3$
$(\delta/\sigma)_{max}$	0.265
$\delta\rho_{max}, \delta\rho_{max}$ (e Å^{-3})	13.290, -11.636
Extinction method	SHELX
Extinction coefficient	0.0013(3)

Table C.11: Crystal data, data collection parameters and refinement details for the preliminary solution of $PbCuTeO_5$

Crystal data	
Chemical formula	$PbCuTeO_5$
M_r	956.66
Cell setting, space group	triclinic, $P\bar{1}$
Temperature (K)	296(2)
a, b, c(Å)	6.4119(4), 11.2601(8)
	12.2686(8)
α, β, γ (°)	107.708, 90.939(5)
	90.452(5)
V (Å^3)	843.62(10)
Z	4
$D_x(Mg \cdot m^{-3})$	7.532
Radiation type	Mo $K\alpha$
$\mu(mm^{-1})$	51.590
Crystal form, colour	plate, turquoise
Crystal size (mm)	0.11 x 0.11 x 0.05
Data collection	
Data collection	Bruker Apex II
Data collection method	ω and ϕ scans
Absorption correction	empirical
No. of measured, independent and observed reflections	4900, , 4900, 4060
Criterion for observed reflections	$I > 2\sigma(I)$
R_{int}	0.0699
$\Theta_{max}(°)$	30.00
Refinement	
Refinement on	F^2
$R[F^2 > 2\sigma(F)], \omega R(F^2), S$	0.0599, 0.1571, 0.990
No. of reflections	4900
No. of parameters	297
Weighting scheme	$\omega = 1/[\sigma^2(F_0^2) + (0.0703P)^2 + 89.8601P]$ where $P = (F_0^2 + 2F_c^2)/3$
$(\delta/\sigma)_{max}$	0.021
$\delta\rho_{max}, \delta\rho_{max}$ (e Å^{-3})	6.586, -5.318
Extinction method	SHELX
Extinction coefficient	0.00060(9)

Table C.12: Crystal data, data collection parameters and refinement details for the preliminary solution of $Pb_{22}Te_7AlO_{44.5}$

Crystal data	
Chemical formula	$Pb_{22}Te_7AlO_{44.5}$
M_r	6190.36
Cell setting, space group	cubic, $Fm\bar{3}m$
Temperature (K)	293(2)
a (Å)	16.81540(10)
V (Å^3)	4754.68(5)
Z	4
$D_x(Mg \cdot m^{-3})$	8.648
Radiation type	Mo $K\alpha$
$\mu(mm^{-1})$	81.906
Crystal form, colour	plate-like, yellow
Crystal size (mm)	0.092 x 0.092 x 0.048
Data collection	
Data collection	Bruker Apex II
Data collection method	ω and ϕ scans
Absorption correction	empirical
No. of measured, independent and observed reflections	43289, 400, 367
Criterion for observed reflections	$I > 2\sigma(I)$
R_{int}	0.0875
$\Theta_{max}(°)$	29.89
Refinement	
Refinement on	F^2
$R[F^2 > 2\sigma(F)], \omega R(F^2), S$	0.0485, 0.1233, 1.111
No. of reflections	400
No. of parameters	26
Weighting scheme	$\omega = 1/[\sigma^2(F_0^2) + (0.0528P)^2 + 2170.6692]$ where $P = (F_0^2 + 2F_c^2)/3$
$(\delta/\sigma)_{max}$	0.000
$\delta\rho_{max}, \delta\rho_{max}$ (e Å^{-3})	4.769, -3.735
Extinction method	SHELX
Extinction coefficient	0.000056(8)

Glossary

Å	Ångström (10^{-10}m)
$a, b, c, \alpha, \beta, \gamma$	Unit cell parameters in direct space
$a^*, b^*, c^*, \alpha^*, \beta^*, \gamma^*$	Cell parameters in reciprocal space
V	Unit cell volume
C_n	Metric tensor
D_n	Vector space bases
r_n	Coordinates expressed as a column vector
n_n	normal vector of plane in space
p_n	plane in space spanned by three points
A	Transformation matrix
P	Transformation matrix
$[hkl]$	Miller indices describing a direction
$\langle hkl \rangle$	Miller indices describing a family of directions
(hkl)	Miller indices describing a plane
$\{hkl\}$	Miller indices describing a family of planes
S_{ij}	Experimental bond valence
V_i	Atomic valence
c.n.	Coordination number
vu	Valence units
BVS	Bond valence sum
BSI	Bond strain index
GII	Global instability index
RT	Room temperature
HT	High temperature
XRD	X-ray diffraction
XRPD	X-ray powder diffraction
θ	Angle of diffraction
DSC	Differential scanning calorimetry
TG	Thermo gravimetry
EDX	Energy-dispersive X-ray spectroscopy

t   Tolerance factor
Φ   Fitness factor
t *translationsgleich*
k *klassengleich*
i *isomorph*

References

[1] S. A. Larregola, J. A. Alonso, J. C. Pedregosa, M. J. Martinez-Lope, M. Alguero, V. De, la Pena-O'Shea, F. Porcher, and F. Illas. The role of the Pb^{2+} $6s$ lone pair in the structure of the double perovskite Pb_2ScSbO_6. *Dalton Transactions*, 28(28):5453–5459, 2009.

[2] R. H. Mitchell. *Perovskites: Modern and Ancient*. Thunder Bay, Ontario: Almaz Press, 2001.

[3] K. Ramesha, L. Sebastian, B. Eichhorn, and J. Gopalakrishnan. Perovskite and pyrochlore modifications of Pb_2MnReO_6: Synthesis, structure, and electronic properties. *Chemistry of Materials*, 15(3):668–674, 2003.

[4] K. Ramesha, L. Sebastian, B. Eichhorn, and J. Gopalakrishnan. Pb_2FeReO_6: new defect pyrochlore oxide with a geometrically frustrated Fe/Re sublattice. *Journal of Materials Chemistry*, 13(8):2011–2014, 2003.

[5] M. A. Pena and J. L. G. Fierro. Chemical structures and performance of perovskite oxides. *Chemical Reviews (Washington, D. C.)*, 101(7):1981–2017, 2001.

[6] Y. Uratani, T. Shishidou, F. Ishii, and T. Oguchi. First-principles exploration of ferromagnetic and ferroelectric double-perovskite transition-metal oxides. *Physica B: Condensed Matter (Amsterdam, Netherlands)*, 383(1):9–12, 2006.

[7] S. E. Lofland, S. M. Bhagat, K. Ghosh, R. L. Greene, S. G. Karabashev, D. A. Shulyatev, A. A. Arsenov, and Y. Mukovskii. Magnetic transition and electronic transport in colossal magnetoresistance perovskites. *Physical Review B: Condensed Matter*, 56(21):13705–13707, 1997.

[8] M. A. Subramanian, A. P. Ramirez, and G. H. Kwei. Colossal magnetoresistance behavior in manganese oxides: Pyrochlore versus perovskite. *Solid State Ionics*, 108(1-4):185–191, 1998.

[9] J. Y. Kim, Y. J. Kim, B. J. Park, B. W. Lee, C. S. Hwang, C. H. Choi, H. K. Chae, and C. S. Kim. Magnetoresistance in double perovskite Sr_2FeMoO_6. *Molecular Physics Reports*, 32(Physical Properties of Magnetic Materials):58–62, 2001.

[10] I. Grinberg, V. R. Cooper, and A. M. Rappe. Relationship between local structure and phase transitions of a disordered solid solution. *Nature (London, United Kingdom)*, 419(6910):909–911, 2002.

[11] I. Grinberg, V. R. Cooper, and A. M. Rappe. Oxide chemistry and local structure of $PbZr_xTi_{1-x}O_3$ studied by density-functional theory supercell calculations. *Physical Review B: Condensed Matter and Materials Physics*, 69(14):144118/1–144118/17, 2004.

[12] I. Grinberg and A. M. Rappe. First principles calculations, crystal chemistry and properties of ferroelectric perovskites. *Phase Transitions*, 80(4-5):351–368, 2007.

[13] Y.-H. Shin, I. Grinberg, I-W. Chen, and A. M. Rappe. Nucleation and growth mechanism of ferroelectric domain-wall motion. *Nature (London, United Kingdom)*, 449(7164):881–884, 2007.

[14] G. Bayer. The crystal chemistry of tellurium, tellurium oxide and tellurium-containing oxide compounds. *Fortschritte der Mineralogie*, 46(1):41–72, 1969.

[15] G. Bayer. New perovskite-type compounds A_2BTeO$_6$. *Journal of the American Ceramic Society*, 46(12):604–5, 1963.

[16] E. D. Politova and Y. N. Venevtsev. New tellurium-containing ferro- and antiferroelectrics with a perovskite structure. *Doklady Akademii Nauk SSSR*, 209(4):838–41, 1973.

[17] Y. N. Venevtsev, E. D. Politova, and G. S. Zhdanov. Tellurium containing ferroelectrics. X-ray data, dielectric properties, phase transitions. *Ferroelectrics*, 8(1-2):489–90, 1974.

[18] E. D. Politova and Y. N. Venevtsev. Ferroelectricity and antiferroelectricity in tellurium-containing compounds with perovskite structure. *Materials Research Bulletin*, 10(4):319–25, 1975.

[19] L. I. Kosse, E. D. Politova, A. A. Bush, S. Yu. Stefanovich, and Yu. N. Venevtsev. Crystal growth and properties of lead orthotellurate (Pb$_3$TeO$_6$) single crystals. *Kristallografiya*, 28(3):514–17, 1983.

[20] G. Baldinozzi, P. Sciau, and A. Bulou. Analysis of the phase transition sequence of the elpasolite (ordered perovskite) Pb$_2$MgTeO$_6$. *Journal of Physics: Condensed Matter*, 9(47):10531–10544, 1997.

[21] G. Baldinozzi, D. Grebille, P. Sciau, J-M. Kiat, J. Moret, and J-F. Berar. Rietveld refinement of the incommensurate structure of the elpasolite (ordered perovskite) Pb$_2$MgTeO$_6$. *Journal of Physics: Condensed Matter*, 10(29):6461–6472, 1998.

[22] G. Baldinozzi, G. Calvarin, P. Sciau, D. Grebille, and E. Suard. Neutron rietveld refinement of the incommensurate phase of the ordered perovskite Pb$_2$CoWO$_6$. *Acta Crystallographica, Section B: Structural Science*, B56(4):570–576, 2000.

[23] R. Caracas and X. Gonze. First-principles study of Pb$_2$MgTeO$_6$: High-T cubic phase and average low-T rhombohedral phase. *Physical Review B: Condensed Matter and Materials Physics*, 65(18):184103/1–184103/7, 2002.

[24] R. Caracas and X. Gonze. First-principles determination of the dynamical properties of Pb$_2$MgTeO$_6$. *Physical Review B: Condensed Matter and Materials Physics*, 71(5):054101/1–054101/9, 2005.

[25] G. Baldinozzi, P. Sciau, M. Pinot, and D. Grebille. Crystal structure of the antiferroelectric perovskite Pb$_2$MgWO$_6$. *Acta Crystallographica, Section B: Structural Science*, B51(5):668–73, 1995.

[26] A. Kania, E. Jahfel, G. E. Kugel, K. Roleder, and M. Hafid. A Raman investigation of the ordered complex perovskite PbMg$_{0.5}$W$_{0.5}$O$_3$. *Journal of Physics: Condensed Matter*, 8(24):4441–4453, 1996.

[27] B. Wedel, L. Wulff, and H. Müller-Buschbaum. Isolated $\infty [\, TeO_5]$ chains of octahedra in the lead tellurate Pb_2TeO_5. *Zeitschrift für Naturforschung, B: Chemical Sciences*, 53(3):287–290, 1998.

[28] B. Wedel and H. Müller-Buschbaum. On the crystal structure of the tellurates $Pb_3Fe_2Te_2O_{12}$ and Pb_2CoTeO_6. *Zeitschrift für Naturforschung, B: Chemical Sciences*, 52(1):35–39, 1997.

[29] L. Wulff, B. Wedel, and H. Müller-Buschbaum. On the crystal chemistry of tellurates containing Mn^{2+} in the cationic and anionic part of the crystal structure $(Mn_{2.4}Cu_{0.6})TeO_6$, Ba_2MnTeO_6, and $Pb(Mn_{0.5}Te_{0.5})O_3$. *Zeitschrift für Naturforschung, B: Chemical Sciences*, 53(1):49–52, 1998.

[30] B. Wedel, K. Sugiyama, and H. Müller-Buschbaum. Connection of $(TeO_6)_6$ and $(TeO_6)_3(NiO_6)_3$ hexagons by $TeNiO_9$ octahedra double in $Pb_3Ni_{4.5}Te_{2.5}O_{15}$. *Zeitschrift für Naturforschung, B: Chemical Sciences*, 53(5/6):527–531, 1998.

[31] B. Wedel and H. Müller-Buschbaum. Lead copper tellurate $PbCu_3TeO_7$ containing Cu^{2+} in distorted square pyramidal and tetrahedral oxygen coordination. *Zeitschrift für Naturforschung, B: Chemical Sciences*, 51(11):1587–1590, 1996.

[32] I. D. Brown. *The Chemical Bond in Inorganic Chemistry: The Bond Valence Model*. IUCR Monographs in Crystallography 12. Oxford University Press, 2002.

[33] I. D. Brown. Recent developments in the methods and applications of the bond valence model. *Chemical Reviews (Washington, DC, United States)*, 109(12):6858–6919, 2009.

[34] I.D. Brown. Accumulated table of bond valence parameters. `http://www.ccp14.ac.uk/ccp/web-mirrors/i_d_brown/`, Aug. 2009.

[35] C. Preiser, J. Losel, I. D. Brown, M. Kunz, and A. Skowron. Long-range coulomb forces and localized bonds. *Acta Crystallographica, Section B: Structural Science*, B55(5):698–711, 1999.

[36] N. W. Alcock. Secondary bonding to nonmetallic elements. *Advances in Inorganic Chemistry and Radiochemistry*, 15:1–58, 1972.

[37] G. M. Sheldrick. SADABS. 2001.

[38] W. Herrendorf. HABITUS. 1997.

[39] George M. Sheldrick. A short history of SHELX. *Acta Crystallographica, Section A: Foundations of Crystallography*, A64(1):112–122, 2008.

[40] A. L. Spek. Single-crystal structure validation with the program PLATON. *Journal of Applied Crystallography*, 36(1):7–13, 2003.

[41] E. Dowty. ATOMS for windows: Version 6.3. 2006.

[42] P. Boher, P. Garnier, J. R. Gavarri, and A. W. Hewat. Quadratic α-lead monoxide (i): Description of the ferroelastic structural transition. *Journal of Solid State Chemistry*, 57(3):343–50, 1985.

[43] M. C. Knapp and P. M. Woodward. A-site cation ordering in $AA'BB'O_6$ perovskites. *Journal of Solid State Chemistry*, 179(4):1076–1085, 2006.

[44] C. J. Howard, B. J. Kennedy, and P. M. Woodward. Ordered double perovskites - a group-theoretical analysis. *Acta Crystallographica, Section B: Structural Science*, B59(4):463–471, 2003.

[45] Lester R. Morss. Crystal structure of dipotassium sodium fluoroaluminate (elpasolite). *Journal of Inorganic and Nuclear Chemistry*, 36(12):3876–8, 1974.

[46] V. M. Goldschmidt. Laws of crystal chemistry. *Naturwissenschaften*, 14:477–85, 1926.

[47] R. D. Shannon. Revised effective ionic radii and systematic studies of interatomic distances in halides and chalcogenides. *Acta Crystallographica, Section A: Crystal Physics, Diffraction, Theoretical and General Crystallography*, A32(5):751–67, 1976.

[48] Y. Teraoka, M.-D. Wei, and S.. Kagawa. Double perovskites containing hexavalent molybdenum and tungsten: Synthesis, structural investigation and proposal of a fitness factor to discriminate the crystal symmetry. *Journal of Materials Chemistry*, 8(11):2323–2325, 1998.

[49] I. M. Reaney. Effect of octahedral tilt transitions on the properties of perovskites and related materials. *Ferroelectrics*, 222(1-4):401–410, 1999.

[50] P. M. Woodward. Octahedral tilting in perovskites. i. Geometrical considerations. *Acta Crystallographica, Section B: Structural Science*, B53(1):32–43, 1997.

[51] P. M. Woodward. Octahedral tilting in perovskites. ii. Structure stabilizing forces. *Acta Crystallographica, Section B: Structural Science*, B53(1):44–66, 1997.

[52] A. M. Glazer. Classification of tilted octahedra in perovskites. *Acta Crystallographica, Section B: Structural Crystallography and Crystal Chemistry*, 28(Pt. 11):3384–92, 1972.

[53] A. M. Glazer. Simple ways of determining perovskite structures. *Acta Crystallographica, Section A: Crystal Physics, Diffraction, Theoretical and General Crystallography*, A31(6):756–62, 1975.

[54] J. Blasco, R. I. Merino, J. Garcia, and M. C. Sanchez. Properties and phase transition of the ordered perovskite Pb_2MnWO_6. *Journal of Physics: Condensed Matter*, 18(7):2261–2271, 2006.

[55] G. Baldinozzi, P. Sciau, and J. Lapasset. Crystal structure of lead cobalt tungsten oxide (Pb_2CoWO_6) in the cubic phase. *Physica Status Solidi A: Applied Research*, 133(1):17–23, 1992.

[56] C. J. Howard and M. A. Carpenter. Octahedral tilting in cation-ordered Jahn-Teller distorted perovskites - a group-theoretical analysis. *Acta Crystallographica, Section B: Structural Science*, B66(1):40–50, 2010.

[57] Th. Hahn, editor. *International Tables for Crystallography. Volume A: Space-group symmetry*. D. Reidel Publishing company, 2009.

[58] U. Müller. Crystallographic group-subgroup relations and their use in crystal chemistry. *Zeitschrift für Anorganische und Allgemeine Chemie*, 630(11):1519–1537, 2004.

[59] O. Bock and U. Müller. Symmetry relationships by variation of perovskite-type structures. *Acta Crystallographica, Section B: Structural Science*, B58(4):594–606, 2002.

[60] L. Ortega-San, M., J. P. Chapman, G. Cuello, J. Gonzalez-Calbet, M. I. Arriortua, and T. Rojo. Crystal structure of the ordered double perovskite, Sr_2NiTeO_6. *Zeitschrift fürAnorganische und Allgemeine Chemie*, 631(11):2127–2130, 2005.

[61] W. D. Townes, Jen-Ho Fang, and Anthony J. Perrotta. Crystal structure and refinement of ferrimagnetic barium ferrite, $BaFe_{12}O_{19}$. *Zeitschrift für Kristallographie, Kristallgeometrie, Kristallphysik, Kristallchemie*, 125(1/6):437–49, 1967.

[62] C. Brosset. The crystal structure of chiolite. *Zeitschrift für Anorganische und Allgemeine Chemie*, 238:201–8, 1938.

[63] C. Jacoboni, A. Leble, and J. J. Rousseau. Accurate determination of the structure of chiolite, $Na_5Al_3F_{14}$, and EPR study of chromium(3+)-doped chiolite. *Journal of Solid State Chemistry*, 36(3):297–304, 1981.

[64] W. T. Fu and D. J. W. Ildo. Chiolite-like $Ca_5Te_3O_{14}$: An x-ray and neutron diffraction study. *Journal of Solid State Chemistry*, 181(5):1236–1239, 2008.

[65] A. Le Bail and A.-M. Mercier. Distorted chiolite crystal structures of $Na_5M_3F_{14}$ (M = Cr,Fe,Ga) studied by X-ray powder diffraction. *Powder Diffraction*, 18(2):128–134, 2003.

[66] Holleman Wiberg. *Lehrbuch der Anorganischen Chemie*. Walter de Gruyter Berlin, New York, 2009.

[67] W. T. Fu, Y. S. Au, S. Akerboom, and D. J. W. IJdo. Crystal structures and chemistry of double perovskites $Ba_2M(II)M'(VI)O_6$ (M = Ca, Sr, M' = Te, W, U). *Journal of Solid State Chemistry*, 181(9):2523–2529, 2008.

[68] P. Koehl and D. Reinen. Structural and spectroscopic investigations of barium copper tellurate Ba_2CuTeO_6. *Zeitschrift fuer Anorganische und Allgemeine Chemie*, 409(3):257–72, 1974.

[69] Sergey V. Krivovichev. Encapsulation effect and its influence on bond-valence parameters. *Zeitschrift fuer Kristallographie*, 214(7):371–372, 1999.

[70] V. Sidey. On the correlations between the polyhedron eccentricity parameters and the bond-valence sums for the cations with one lone electron pair. *Acta Crystallographica, Section B: Structural Science*, B64(4):515–518, 2008.

[71] V. Sidey. Alternative presentation of the brown-wu bond-valence parameters for some s^2 cation/O_2- ion pairs. *Acta Crystallographica, Section B: Structural Science*, B65(1):99–101, 2009.

[72] S. V. Krivovichev and I. D. Brown. Are the compressive effects of encapsulation an artifact of the bond valence parameters?. *Zeitschrift für Kristallographie*, 216:245–247, 2001.

[73] M. B. Boisen Jr and G. V. Gibbs. *Reviews in Mineralogy Volume 15: Mathematical Crystallography*. Mineralogical Society of America, 1990.

[74] M. Bonin, W. Paciorek, K. J. Schenk, and G. Chapuis. X-ray study of and structural approach to the incommensurate perovskite Pb_2CoWO_6. *Acta Crystallographica, Section B: Structural Science*, B51(1):48–54, 1995.

[75] J.-W. Choi, K. H. Yoon, and R. B. van, Dover. Effect of the octahedral bond valence on microwave dielectric properties of $(1\text{-}x)\text{Al}_{0.5}\text{Ta}_{0.5}\text{O}_{2-x}\text{Mg}_{0.33}\text{Ta}_{0.67}\text{O}_2$ ceramics. *Journal of the American Ceramic Society*, 89(3):1083–1086, 2006.

[76] V. R. Cooper, I. Grinberg, and A. M. Rappe. Extending first principles modeling with crystal chemistry: A bond-valence based classical potential. *AIP Conference Proceedings*, 677(Fundamental Physics of Ferroelectrics 2003):220–230, 2003.

[77] M. Kunz and I. D. Brown. Out-of-center distortions around octahedrally coordinated d^0 transition metals. *Journal of Solid State Chemistry*, 115(2):395–406, 1995.

[78] Ulrich Müller. *Anorganische Strukturchemie*. B.G. Teubner Verlag, 2004.

[79] J. P. Miranday, G. Ferey, C. Jacoboni, J. M. Dance, A. Tressaud, and R. De, Pape. Crystal growth, polymorphism, and magnetic properties of pentasodium tetradecafluorotrichromate. *Revue de Chimie Minerale*, 12(2):187–92, 1975.

[80] H. S. Park, K. H. Yoon, and E. S. Kim. Effect of bond valence on microwave dielectric properties of $(\text{Pb}_{1-x}\text{Ca}_x)(\text{Mg}_{0.33}\text{Ta}_{0.67})\text{O}_3$ ceramics. *Journal of Materials Research*, 16(3):817–821, 2001.

[81] N. Rivezzi and Ph. Sciau. Study of the solid solution between magnesium tungstate and tellurate: $\text{Pb}_2\text{MgW}_x\text{Te}_{(1-x)}\text{O}_6$. *Journal of Solid State Chemistry*, 139(2):332–341, 1998.

[82] M. Schwarten and D. Babel. Chromium hexacyano complexes. the crystal structures of the cyano elpasolites $(\text{NMe}_4)_2 A\text{Cr}(\text{CN})_6$ (A = K, Cs) and of the cubic barium compound $\text{Ba}_3[\text{Cr}(\text{CN})_6]_{2.20}\text{H}_2\text{O}$. *Zeitschrift für Anorganische und Allgemeine Chemie*, 626(9):1921–1928, 2000.

[83] Y.-H. Shin, V. R. Cooper, I. Grinberg, and A. M. Rappe. Development of a bond-valence molecular-dynamics model for complex oxides. *Physical Review B: Condensed Matter and Materials Physics*, 71(5):054104/1–054104/4, 2005.

[84] A. Teichert and H. Müller-Buschbaum. Crystal structure of calcium lead oxide, Ca_2PbO_4. *Zeitschrift für Anorganische und Allgemeine Chemie*, 607:128–30, 1992.